การตรวจสอบการแยกเฟสแบบชั้นของพอลิอิมิดผสมระหว่างพอลิอิมิดที่มีซิลิคอนเป็นองค์ประกอบ
กับพอลิอิมิดที่มีความยืดหยุ่นของสายโซ่ที่ต่างกัน

นาย สุนันท์ ทิพย์ทิพากร

AN INVESTIGATION ON THE LAYERED PHASE SEPARATION OF POLYIMIDE BLENDS

BETWEEN SILICON-CONTAINING POLYIMIDE

AND POLYIMIDES OF DIFFERENT CHAIN FLEXIBILITY

Mr. Sunan Tiptipakorn

A Dissertation Submitted in Partial Fulfillment of the Requirements

for the Degree of Doctor of Engineering Program in Chemical Engineering

Department of Chemical Engineering

Faculty of Engineering

Chulalongkorn University

Academic year 2007

|	
Thesis Title	AN INVESTIGATION ON THE LAYERED PHASE SEPARATION OF POLYIMIDE BLENDS BETWEEN SILICON-CONTAINING POLYIMIDE AND POLYIMIDES OF DIFFERENT CHAIN FLEXIBILITY
By	Mr. Sunan Tiptipakorn
Field of Study	Chemical Engineering
Thesis Advisor	Assistant Professor Sarawut Rimdusit, Ph.D.
Thesis Co-advisor	Professor Shinji Ando, Ph.D.

Accepted by the Faculty of Engineering, Chulalongkorn University in Partial Fulfillment of the Requirements for the Doctoral Degree
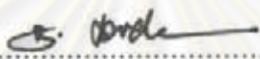
.... Dean of the Faculty of Engineering
(Associate Professor Boonsom Lerdhirunwong, Dr. Ing.)

THESIS COMMITTEE
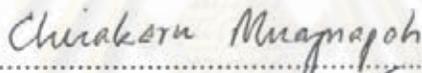
.... Chairman
(Associate Professor Chirakarn Muangnapoh, Dr. Ing.)
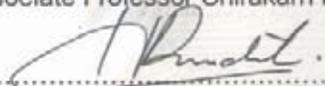
.... Thesis Advisor
(Assistant Professor Sarawut Rimdusit, Ph.D.)
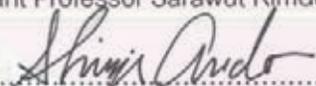
.... Thesis Co-advisor
(Professor Shinji Ando, Ph.D.)

.... Member
(Sirijutaratana Covavisaruch, Ph.D.)

.... Member
(Assistant Professor Varong Pavarajarn, Ph.D.)

.... Member
(Phiriyatorn Suwanmala, Ph.D.)

นายสุนันท์ ทิพย์ทิพากร : การตรวจสอบการแยกเฟสแบบชั้นของพอลิอิมิดผสมระหว่างพอลิอิมิดที่มีซิลิคอน
เป็นองค์ประกอบกับพอลิอิมิดที่มีความยืดหยุ่นของสายโซ่ที่ต่างกัน (AN INVESTIGATION ON THE
LAYERED PHASE SEPARATION OF POLYIMIDE BLENDS BETWEEN SILICON-
CONTAINING POLYIMIDE AND POLYIMIDES OF DIFFERENT CHAIN FLEXIBILITY)
อ. ที่ปรึกษา : ผศ.ดร. ศราวุธ ริมดุสิต, อ. ที่ปรึกษาร่วม : PROF. SHINJI ANDO, 101 หน้า.

งานวิจัยนี้ได้มุ่งศึกษาพฤติกรรมการแยกเฟสของพอลิอิมิดผสมระหว่างบล็อกโคพอลิอิมิดที่มีซิลิคอนเป็น
องค์ประกอบ (BSF30) กับ พอลิอิมิดมีที่ความยืดหยุ่นของสายโซ่ที่ต่างกันสามชนิด นั่นคือ 3,3',4,4'-oxydiphthalic
anhydride (ODPA)/ 4,4'- diaminodiphenyl ether (4,4'-ODA); 3,3',4,4'-biphyltetracarboxylic dianhydride
(s-BPDA)/ 4,4'- diaminodiphenyl ether (ODA) และ 1,2,4,5-benzenetetracarboxylic dianhydride (PMDA)/ 4,4'-
diaminodiphenyl ether (ODA) พอลิอิมิดสังเคราะห์ได้จากกระบวนการสองขั้นตอนซึ่งในขั้นตอนแรกจะได้พอลิเอมิก
แอซิด (PAA) ซึ่งเป็นพอลิเมอร์ที่อยู่ในตัวทำละลาย N-methyl-2-pyrrolidinone (NMP) ในการผสมพอลิเอมิกแอซิดกับ
บล็อกโคพอลิอิมิดที่มีซิลิคอนเป็นองค์ประกอบจะทำการเปลี่ยนแปลงปริมาณของบล็อกโคพอลิอิมิดที่มีซิลิคอนเป็น
องค์ประกอบและทำการขึ้นรูปเป็นฟิล์มโดยใช้กระบวนการสร้างหมู่อิไมด์ด้วยความร้อน โดยนำฟิล์มตัวอย่างที่มีความ
หนา 50 ไมครอน ไปทดสอบลักษณะที่ผิวของฟิล์มผสมโดยใช้เทคนิคการวัดมุมสัมผัส (Contact angle measurement),
เครื่อง Surface Profilometer, Attenuated total reflection Fourier transform infrared (ATR-FTIR) และเครื่อง ATR
microscope จากผลการทดลองด้วยเครื่องมือดังกล่าวพบว่าพอลิอิมิดทั้งสามชนิดกับบล็อกโคพอลิอิมิดที่มีซิลิคอนเป็น
องค์ประกอบเกิดการแยกตัวที่ผิวหน้าขึ้นโดยซิลิคอนในส่วนของบล็อกโคพอลิอิมิดที่มีซิลิคอนเป็นองค์ประกอบซึ่งมี
ความเป็นขั้วต่ำ จะเคลื่อนตัวขึ้นไปอยู่ที่ผิวหน้าด้านที่สัมผัสกับอากาศ และ พอลิอิมิดทั้งสามชนิดจะอยู่ด้านที่ติดกับ
กระจกเนื่องจากมีความเป็นขั้วสูงว่าบล็อกโคพอลิอิมิดที่มีซิลิคอนเป็นองค์ประกอบ   พฤติกรรมการแยกตัวที่ผิวหน้านี้
สามารถเห็นได้ชัดเจนด้วยเทคนิค ATR-FTIR เมื่ออัตราส่วนของบล็อกโคพอลิอิมิดที่มีซิลิคอนเป็นองค์ประกอบมากพอ
เช่นในกรณีที่มี BSF30 เท่ากับ 30 phr ผิวฟิล์มที่ส่วนสัมผัสกับอากาศจะประกอบด้วยสองส่วน คือส่วนที่มีลักษณะเป็น
เนินเขา (hill) และ แอ่ง (valley) โดยจากการศึกษาด้วย ATR microscope พบว่าปริมาณ ซิลิคอนในส่วนที่เป็นเนินเขา
ของฟิล์มทั้งสามชนิด ไม่ต่างกันมากนักคือประมาณ 75 % แต่จะเห็นความแตกต่างในส่วนปริมาณซิลิคอนบริเวณเป็น
แอ่งของพอลิอิมิดผสมของ BSF30 กับ ODPA/ODA, s-BPDA/ODA และ PMDA/ODA ซึ่งมีค่าประมาณ 62%, 54%
และ 5 % ตามลำดับ ซึ่งเชื่อว่าน่าจะเป็นตัวบ่งบอกว่าการแยกเฟสของระบบ PMDA/ODA กับ BSF30 มากที่สุด ซึ่ง
สัมพันธ์กับโครงสร้างของสายโซ่โมเลกุลของพอลิอิมิดที่มีค่าน้อยที่สุด

ภาควิชา............วิศวกรรมเคมี.................   ลายมือชื่อนิสิต...

สาขาวิชา...........วิศวกรรมเคมี.................   ลายมือชื่ออาจารย์ที่ปรึกษา..........................

ปีการศึกษา........2550........................   ลายมือชื่ออาจารย์ที่ปรึกษาร่วม....................
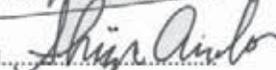
#4671852721: MAJOR CHEMICAL ENGINEERING

KEY WORD: POLYIMIDE/ IMMISCIBLE BLENDS/ SURFACE SEGREGATION/

PHASE SEPARATION/ CHAIN FLEXIBILITY

SUNAN TIPTIPAKORN: AN INVESTIGATION ON THE LAYERED PHASE SEPARATION OF POLYIMIDE BLENDS BETWEEN SILICON-CONTAINING POLYIMIDE AND POLYIMIDES OF DIFFERENT CHAIN FLEXIBILITY THESIS ADVISOR: ASST. PROF. SARAWUT RIMDUSIT, Ph.D., THESIS CO-ADVISOR: PROF. SHINJI ANDO, Ph.D., 101 pp.

In this research, surface segregation behaviors of polyimide blends between polysiloxane-block-polyimide (BSF30) and three polyimides of different chain flexibility [3,3',4,4'-oxydiphthalic anhydride (ODPA)/ 4,4'- diaminodiphenyl ether (4,4'-ODA); 3,3',4,4'-biphyltetracarboxylic dianhydride (s-BPDA)/ 4,4'-diaminodiphenyl ether (ODA), and 1,2,4,5-benzenetetracarboxylic dianhydride (PMDA)/ 4,4'-diaminodiphenyl ether (ODA)] have been investigated. The polyimides were synthesized by a conventional two-step method via poly(amic acid) (PAA) precursor in N-methyl-2-pyrrolidinone (NMP) solvent. These polyimide blends, having various compositions of the silicon-containing block copolyimide, were processed by the solution casting method then undergone thermal imidization to yield the solid films. All film samples with 50 μm thickness were characterized by contact angle measurement, surface profilometer, Attenuated total reflection Fourier transform infrared (ATR-FTIR), and ATR microscope. These techniques revealed that the surface segregation typed phase separation occurred between the two polymers for all three types of polyimide blends. In this study, the films at various BSF30 contents were processed on a glass substrate. At low concentration of BSF30 (less than 10 phr), three types of the polyimides tended to migrate to the glass-side surface, while BSF30 component tended to migrate to the air-exposed surface. For high concentration of BSF30 (i.e. 30 phr), the glass-side surface was covered with the polyimides whereas the air-side surface showed two different areas on the air-exposed surface of the films, i.e. hill area and valley area. With ATR microscope, the differences of % Si-C content on the valley area of three polyimide blends revealed the %Si-C content PMDA/ODA blending system exhibited the highest segregation level. That is believed to be related with the lowest chain flexibility of PMDA/ODA.

Department...Chemical Engineering...... Student's signature.....S. Tiptipakorn.....

Field of study....Chemical Engineering... Advisor's signature...........

Academic year ......2007..................... Co-advisor's signature..........

ACKNOWLEDGEMENTS

TABLE OF CONTENTS

LIST OF FIGURES

LIST OF TABLES

TABLE   **PAGE**

ศูนย์วิทยทรัพยากร

จุฬาลงกรณ์มหาวิทยาลัย

CHAPTER I

INTRODUCTION

Since the first commercialization of polyimides in the late 1960s by Du Pont, the advancement in the science and technology of the polymers, particularly in the field of aromatic polyimides, has led to a wide range of their utilization among which the most relevant are in the microelectronic industries (as optical components or dielectric and passivation layers) [Licari and Hughes, 1990; Ghosh and Mittal, 1996; Cho et al., 2005], in the membrane industries [Ohya, 1996], as well as in the space application field [Tsujita, 2003; Rimdusit and Yokota, 2003; Silverman, 1995; Yokota, 1999]. Nowadays, s-BPDA/ODA (Upilex-R trademark from Ube Industries), and PMDA/ODA (Kapton trademark from DuPont), and ODPA/ODA are widely used in many applications such as microelectronic, and filtration fields. These three kinds of polyimide has been a dramatic increase in demand of polyimides. Therefore, PMDA/ODA, s-BPDA/ODA, and ODPA/ODA were chosen as a major component of polyimide blends in this study.

In order to modify the properties of polyimides, the blends of polyimides and other chemicals (such as TiO_2, SiO_2, and etc.) have been an interesting topic to be studied recently. [Arnold et al., 1989; Arnold et al., 1997; Tiwari et al., 2004; Banks and Denko, 2002]. Silicon-containing polymers such as poly(dimethyl siloxane), copolymer of poly(dimethyl siloxane) and polyimide, or polysilsesquioxane is one of the chemicals that was have been reported to possess high UV stability, enhanced solubility, high impact resistance, modified surface properties, etc. [Rimdusit, 2007; Tiwari and Nema, 2003; Yamada, 1998]. It has been well known that the blends of polyimide and Silicon-containing block copolyimide polymers are immiscible. Rimdusit *et al.* [2007] studied the segregation behaviour of the blends between s-BPDA/ODA and silicon-containing block copolyimide, and reported that the behavior of the blend confirms the surface segregation of gradient structure.

As mentioned before, three types of polyimide, i.e. PMDA/ODA, s-BPDA/ODA, and ODPA/ODA have been used in this study because of their different chain structures. PMDA/ODA includes only one benzene ring in each repeating unit; the structure of s-BPDA/ODA includes two benzene rings, and that of

ODPA/ODA includes ether group linked between two benzene rings. The conformation of ODPA/ODA is the most, while that of PMDA/ODA is the least. The differences of internal structures of these polyimides in the blends possibly lead to interesting different behavior of segregation. Due to the differences of the chain flexibilities among three polyimides (major component), the segregation degrees of the blends are expected to be different.

The aim of this research is to study the surface-segregation of polyimide blend between silicon-containing block copolyimide (BSF30) and the three types of polyimides. In this study, the degree of segregation of the polyimide blends was determined via surface profilometer, Attenuated total reflectance Fourier transform infrared spectroscopy (ATR), and ATR microscope. Furthermore, the dynamic mechanical properties, thermal stability, and tensile properties of the blends were investigated in this study as well.
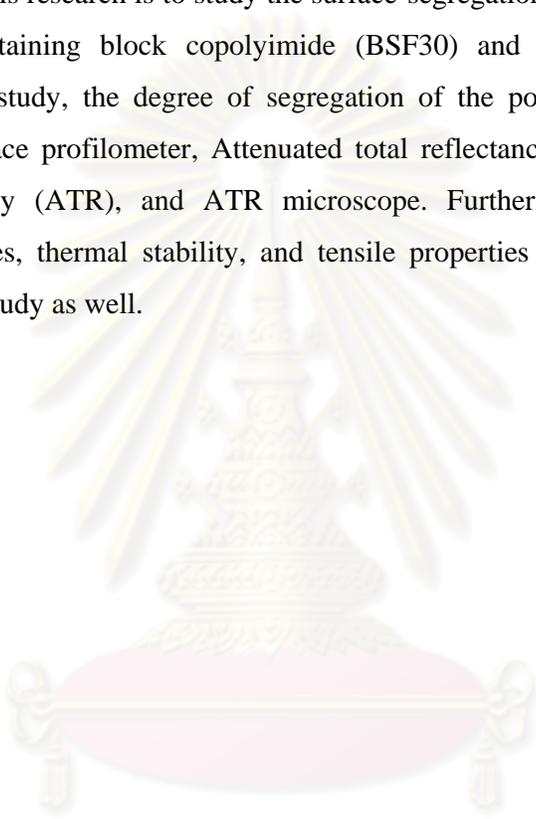
CHAPTER II

THEORY

2.1 Polyimides

Polyimides have become one of the most important and versatile classes of high performance materials, which are a type of polymers with imide groups as shown in Figure 2.1.

$$R'-\overset{\overset{O}{\|}}{C}-\underset{\underset{R}{|}}{N}-\overset{\overset{O}{\|}}{C}-R''$$
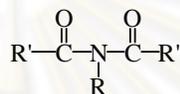
Figure 2.1: Imide Monomer

Polyimides usually take one of two forms. The first of these is an aliphatic structure where the atoms of the imide group are part of a linear chain. The second one is a heterocyclic structure where the imide group is part of a cyclic unit in the polymer chain. The main chain of these polymers contains, as the principal component, five- or six-membered heteroaromatic rings, i.e., imides which are usually presented as condensed aromatic systems, such as with benzene and naphthalene rings.

$$\left(R'-\overset{\overset{O}{\|}}{C}-\underset{\underset{R}{|}}{N}-\overset{\overset{O}{\|}}{C}\right)_n$$
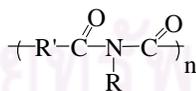
Aliphatic Polyimide
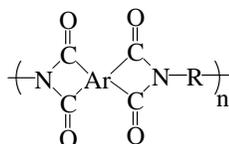
Aromatic Polyimide

Figure 2.2: Schematic representation of aliphatic polyimide and aromatic polyimide
repeating unit (Dunson, 2000)

Aromatic heterocyclic polyimides are typical of most commercial polyimides, such as Ultem from G.E. and DuPont's Kapton. These polymers have such incredible mechanical and thermal properties that they are used in place of metals and glass in many high performance applications in the electronics, automotive, and even the aerospace industries. These properties come from strong intermolecular forces between the polymer chains.

Polyimides can be produced by a variety of synthetic routes. Typically, the most widely used synthetic route is a two-step method. This method consists of the formation of the poly(amic acid) precursor, and the dehydration of this prepolymer to yield the final polyimide.

2.1.1 Synthetic Methods: Two-step Method via Poly(amic acid)

The two-step method for the preparation of polyimides consists of polymerization of a soluble poly(amic acid) intermediate, followed by dehydration of this prepolymer to yield the final polyimide. As illustrated in Figure 2.3, this approach is based on the reaction of a diamine with a tetracarboxylic acid dianhydride in a polar, aprotic solvent such as dimethylacetamide (DMAC), dimethylformamide (DMF), or N-methylpyrolidone (NMP), at temperatures between 15 and 75°C (Willson, Stenzenberger, and Hergenrother, 1990). The resultant poly(amic acid) is then cyclized either thermally or chemically in a subsequent step to produce the desired polyimide.

Poly(amic acid)s are shaped into articles such as films and fibers by removing a solvent. The shaped poly(amic acid) films, for example, are thermally or chemically converted to the final polyimide products. The conversion produces water as a by-product. Because water must be removed during this in-situ imidization, the process is generally suitable only for the preparation of thin object such as films.

Step 1

Dianhydride

H_2N—Ar'—NH_2

Diamine

$\triangle$, Solvent

poly(amic acid)

Step 2

Heat $-H_2O$

Polyimide   + H_2O

Figure 2.3 Schematic of a two-step synthesis of polyimide from diamine and dianhydride.

2.1.2 Formation of Poly(amic acid)

The most important aspect of this process is that it is an equilibrium reaction. Often it appears to be an irreversible reaction because a high-molecular-weight poly (amic acid) is readily formed in most cases as long as pure reagents are used. This is because the forward reaction is much faster than the reverse reaction, usually by several orders of magnitude. If the large reaction rate difference is not met, the high-molecular-weight poly(amic acid) is not formed. Therefore, it is important to examine the driving forces that favor the forward reaction over the reverse reaction. It should also be noted that the acylation reaction of amines is an exothermic reaction and that the equilibrium is favored at lower temperatures. The forward reaction in dipolar solvents is a second-order-reaction and the reverse reaction is a first-order reaction. Therefore, the equilibrium is favored at high monomer concentrations to form higher molecular-weight poly (amic acids).

2.1.3 Thermal Imidization of Poly(amic acid)

Conversion of poly(amic acid)s to the corresponding polyimides is most commonly performed thermally in "solid state". This method is suitable for preparation of thin objects such as films, coatings, fibers, and powders in order to allow the diffusion of by-product and solvent without forming brittles and voids in the final polyimide products. The cast films are dried and heated gradually up to 250-350°C, depending upon the stability and glass transition temperature (T_g) of the polymer. Too rapid heating may cause the formation of bubbles in the sample. When a DMAc solution of poly(amic acid) is cast and dried at ambient temperature to a nontacky state, the resulting film still contains a substantial amount of the solvent (typically up to 25% by weight, depending on the drying conditions). In the subsequent heating, imidization reaction takes place not in a true solid state but rather in a very concentrated viscous solution, at least during the initial and the intermediate stages of thermal imidization. The presence of residual solvent plays an important role in the film forming behaviors. The imidization precedes faster in the presence of dipolar amide solvents. The observation is attributed to the specific solvation to allow the favorable conformation of amic acid group to cyclize. It may also be explained by

the plasticizing effect of the solvent to increase the mobility of the reacting functional groups. The favorable property of amide solvent also suggests that its basicity to accept protons may be responsible for the specific effect. The proton of the carboxylic group is strongly hydrogen-bonded to the carbonyl group of the amide solvent. The cyclization of o-carboxyamide group results in dehydrogen bonding and release of the solvent molecules along with water of condensation.

The most common method of converting the poly(amic acid) to the polyimide is by bulk (or melt) imidization (Bowens, 1999). Films of the poly(amic acid)s are often cast from polar aprotic solvents and subsequently dried and imidized. A typical imidization cycle may proceed by the following schedule: 100°C, 200°C, followed by 300°C. Complete cyclization is accomplished at imidization temperatures above the T_g of the material to ensure chain mobility. Imidization temperatures close to or below the T_g of the material greatly affects the % conversion of the poly(amic acid) moieties.

2.1.4 Properties of polyimides

The properties of polyimides depend on many factors, i.e. the used chemicals (aromatic dianhydride, diamine monomer and a dipolar aprotic solvent). The conditions to produce polyimides are one of the factors. UPILEX®, KAPTON® are the examples of commercial polyimide films from different aromatic dianhydride and the same diamines. The properties of these commercial polymers are presented as follows:-

UPILEX® (a trademark of Ube Industries) is the ultra-high heat-resistant polyimide film, produced from the polycondensation reaction between biphenyltetracarbonxylic dianhydride (BPDA), and ODA. UPILEX® has been the subject of much attention as a new material for use in the electronics and other leading-edge industries. Most notable of these characteristics is UPILEX's unbeatable physical, mechanical, electrical, and chemical properties under high-temperature conditions.

Kapton (a trademark of Dupont) is the trademark polyimide of the polycondensation reaction between Pyromellitic dianhydride (PMDA), and diamines (ODA).

The properties of the commercial films of BPDA/ODA and PMDA/ODA are presented as Table2.1.

Table 2.1: Properties of BPDA/ODA and PMDA/ODA films. (Willson et al., 1990)

Property	Upilex R (BPDA/ODA)	Kapton (PMDA/ODA)
Mechanical properties		
Tensile strength (MPa)	241	172
Tensile modulus (GPa)	3.7	3.0
Elongation (%)	130	70
Thermal properties		
Glass transition temperature, T_g (°C)	285	385
Chemical properties		
Gas permeability		
O_2	100	25
N_2	30	6
CO_2	115	45
He	2200	415
Solvent resistance	Excellent	Excellent
Electrical properties		
Dielectric constant at 10^3 Hz	3.5	3.5

The properties of ODPA/ODA film, which were examined at Occidental Petroleum Corporation and at NASA, are presented in Table 2.2:

Table 2.2: Typical Properties of ODPA/ODA Polyimide Film, 25 microns [Wilson et.al.1990]

Property	Typical Value of , ODPA/ODA polyimide film, 23°C
Tensile Strength, MPa	172
Ultimate Elongation %	16.7
Density g/cm^3	1.39[a]
Glass Transition Temperature (^{o}C)	270

[a] Source: Jeffrey et al., 1999

2.2 Silicone-Containing Block Copolyimides

Linear polysiloxanes (silicon) are prepared by either polycondensation of bifunctional silanes or by ring-opening polymerization of cyclic oligosiloxanes. Linear polydimethylsiloxanes (PDMS) (Figure 2.4) are found in a wide range of commercial applications due to their excellent properties. These properties include good adhesive property, an extremely low glass temperature (-123°C), high thermal and oxidative stability, UV resistance, low surface energy and hydrophobicity, good electrical properties, high permeability to many gases, and low toxicity.

$$\left(\begin{array}{c} CH_3 \\ | \\ Si-O \\ | \\ CH_3 \end{array}\right)_n$$
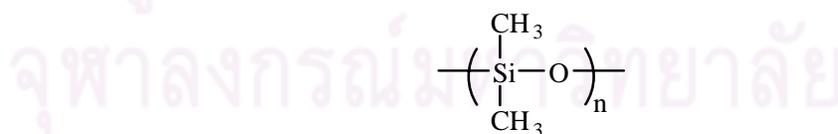
Figure 2.4: Structure for polydimethylsiloxane. (Bowens, 1999)

Silicon-containing polyimides were developed by General Electric since 1993. They come in two variations: random copolymers and block-copolymers. In random copolymers relatively low molecular weight siloxane-containing diamines are

mixed with other diamines and dianhydrides in the correct stochiometric ratio. The chemical structure is comparable to polyisocyanates with randomly distributed hard and soft segment. In siloxane-containing block-copolyimides the hard-block is a polyimide and the soft-block is a polysiloxane. Block and graft copolymers containing relatively long siloxane units have also been synthesized (Ghosh and Mittal, 1996).

In microelectronic applications, silicon-containing polyimides are used primarily as adhesives and encapsulants. With the combined properties of the polyimide and silicon-containing polyimides copolymers have increased solubility and flexibility as compared to the polyimide homopolymer, leading to increased overall processability. The introduction of the siloxane component allows increased impact resistance, excellent adhesion, reduced water absorption, decreased dielectric constants, and increased gas permeability, while maintaining the thermal and mechanical stability that is adequate for most microelectronic applications (Furukawa et al., 1997). Silicon-containing polyimides; however, are much more complicated than the polyimide homopolymers in that there are two involved components, which have a low mixing entropy. This low mixing entropy results in microphase separation of the polymer, with a domain size that varies with block length and percentage of PDMS. Also, in copolymer systems, the low surface energy component (in this case PDMS) tends to migrate to the surface in order to minimize the total free energy of the system. Numerous studies have shown that the PDMS is likely to microphase separate and segregate to the surface in copolymer systems. PDMS has been shown to predominate in the surface of such block copolymers PS-PDMS (Chen, Gardella, and Kumler, 1993; Chen and Gardella., 1994), PMMA-PDMS (Smith et al., 1992) and nylon-6-PDMS (Polk, 2001). This phenomenon has also been shown to occur in silicon-containing polyimides copolymer systems. The extent to which this segregation occurs; however, depends on numerous variables including bulk composition, block length, processing conditions (such as annealing and casting solvent), and the block sequence distribution.

2.3. Factors Affecting Polymer Blend Film Morphology

The surface morphology of polymer blend films have become a very important subject, both experimentally and theoretically, because of their associated industrial applications such as adhesion, friction, and wetting properties, etc. To particular requirements, such as surface coatings, how to create and control films with different properties is very important. In general, phase morphology depends on polymer molecular structures, composition ratio, molecular weights, solvent selection and the method of blend preparation and can also be influenced by a suitable selection of the substrate surface free energy.

2.3.1 Molecular weight of polymers

High molecular weight induces metastable structure due to less mobility. For immiscible polymer blends, many studies on the surface morphology formation had been reported. Li, Han, and An [2003] investigated the effects of the molecular weights on the surface morphologies of PS/PMMA blend films. For the spin-coated films, three different kinds of surface morphologies (a nanophase-separated morphology, a PMMA cellular or network-like morphology whose meshes filled with PS, a sea-island like morphology) were observed when molecular weight was varied. The results indicate that the surface morphology of the polymer blend films can be controlled by the polymer molecular weight.

2.3.2 Composition ratio

In bulk materials, major component tends to form continuous phase. In thin film, interface and surface energies are important factors determining the segregation of blend components, and the component with the lower surface energy is generally enriched in the surface region in order to minimize the air-polymer interfacial free energy. Tanaka, Takahara and Kajiyama (1996) reported the PS/PMMA blend films, the air-polymer interfacial region was covered with a PS rich over layer due to its

lower surface free energy compared with that of PMMA and a well-defined macroscopic phase separated structure was formed in the bulk phase.

2.3.3 Substrate surface free energy

A component with the greater affinity for the substrate is more prevalent at the substrate interface. Many groups studied the effects of substrate surface free energy on the morphology. Kano et al. (1998) investigated the effect of the substrate on the gradient domain morphology for immiscible blends of poly(2-ethylhexyl acrylate-co-acrylicacid-co-vinylacetate) [P(2EHA-AA-VAc)] and poly(vinylidend fluoride-co-hexafluoro acetone) [P(2VDF-HFA)]. They concluded that the affinity between P(2VDF-HFA) and substrate influenced the formation of the gradient domain morphology and the surface segregation of P(2EHA-AA-VAc). Walheim et al. (1997) studied the morphology formation of PS/PMMA blends onto SiO_x, Au and ODM substrate. They revealed that on the polar SiO_x and Au surface, the more polar PMMA forms a homogenous layer on the substrate. On top of this continuous layer, a characteristic phase segregated domain structure is formed. On the hydrophobic ODM surface a PS/PMMA bilayer is observed, with PS next to the substrate. The PMMA layer is punctured by holes that are partially filled by the PS-rich phase. These results showed that the substrate surface energy also played an important role. The blend surface structure was governed by the preferential orientation of one phase to the substrate. Winesett et al. (2000) observed similar features for the same system under similar condition.

2.3.4 Choice of solvent

Solvent also plays an important role in influencing the surface morphology of a polymer blend. It controls evaporation characteristics and relative solubility. Walheim et al. (1997) studied the solvent effects on the surface structure of PS/PMMA blend films. The degree of solubility and swelling of PS and PMMA in toluene, tetrahydrofuran (THF) and methyl ethyl ketone (MEK), as well as the solvent evaporation rate, controlled the final surface structure. Toluene and THF are better solvents for PS than PMMA; therefore, the PS rich phase contains more toluene or

THF than the PMMA phase. As more solvent evaporates, a characteristic time is passed where there is practically no toluene or THF left in the PMMA phase, while the other phase is still swollen with toluene or THF. Further evaporation collapses the swollen PS phase to level that lies much below the interface of the higher PMMA structures. Inversely, MEK preferentially dissolves PMMA and accumulates in the PMMA-rich phase, which leads to protruding PS domains.

2.3.5 Temperature of substrate

Temperature of substrate can affect evaporation rate of solvent and solubility of polymers. Kano et al. (1998) reported the rate of solvent evaporation as the other factor correlating the segregation towards the surface of P(2EHA-AA-VAc) because the blend film was prepared by coating from THF solution. When the rate of solvent evaporation was very fast, no segregation of P(2EHA-AA-VAc) occurred in the blend film because the polymer chains were quickly frozen before the start of the segregation towards the surface side of P(2EHA-AA-VAc). In this report, since the preparation of blend films was performed at 23°C, the rate of solvent evaporation was presumably very slow. Therefore, they presume that the segregation towards the surface side of P(2EHA-AA-VAc) was caused by the affinity between PTFE and P(VDF-HFA) and by the slow solvent evaporation rate.

2.3.6 Heat treatment procedure

Temperature above glass transition (T_g) allows significant chain mobility. Polymers are cured beyond the T_g because the molecular motion above the T_g allows tenaciously held molecules (e.g. solvent) to depart more easily and induces molecular packing. Ton-That et al. (2000) reported the effect of annealing temperature above glass transition temperature of PS/PMMA blend, the polymers behave like viscous liquids, and polymer segment movements on large scale are attainable.

2.3.7 Contaminants

Impurities can act as surfactants or compatibilizers which change phase morphology. Hayashi et al. (1998) reported the morphology of thin films casted on glass slides of a pure blend of PSU and PA. The result showed strong phase separation although the structure formation is strongly influenced by the interaction with the glass and air interface, i.e. wetting. When adding a small amount of a reactive component (a modified PSU) to the blend, the phase separation process can be suppressed completely.

2.4. Surface Segregation in Polymer Blends

Surface segregation is a phenomenon of redistribution of the components of a binary polymer blend in the solution or melt state near the interface with a solid. This effect is connected to the different thermodynamic affinity of the blend components to the surface and relates also to the disparities in the surface tension of polymer components. The phenomenon takes place when the melt or solution of polymer blends contacts with the surface. As a result, in the direction normal to the surface there arises the transition layer with the concentration gradient that determines the properties of the layer near the interface. The effect has a thermodynamic origin and is considered in the framework of modern thermodynamic theories of polymer blends.

The blending of silicons with organic polymers is of particular interest since small bulk concentrations of polydimethylsiloxane (PDMS) polymers can result in rather dramatic surface enrichment. The unique surface behavior rendered by the addition of the low surface energy PDMS component is a direct result of the structural properties of the polymer. The characteristic surface properties of PDMS are low surface tension, moderate interfacial tension against water, high water repellency (hydrophobic), no surface shear viscosity, good lubrication of plastics and elastomers, good wetting, spreading, flow-out aid, and soft feel (Owen et al., 1993).

The combined effects of the low intermolecular forces between the methyl groups and the flexibility of the siloxane backbone have been used as the basis for understanding the surface properties. From a surface tension viewpoint, the more flexible the backbone, the more readily the lowest surface energy configuration will be adopted.

Since the surface tension of PDMS is very low ($\approx$20 dyne/cm) when compared to most organic polymers, the siloxane segments are expected to migrate to the more hydrophobic top (air) surface to form a silicon enriched layer. Surface energetic and molecular mobility of the PDMS component govern the surface/bulk compositional differences can be observed. This yields such properties as reduced friction, improved gloss and feel, aid in release from molds, and increased electrical properties.

2.5. General Principles for Polymer-Polymer Miscibility

The basic thermodynamic equation that is able to describe the miscibility of two polymers is the Gibbs free energy equation:

$$\Delta G_m = \Delta H_m - T \Delta S_m \quad \ldots\ldots\ldots\ldots\ldots (2.1)$$

where ΔG_m is the Gibbs free energy mixing, ΔH_m is the enthalpy of mixing, ΔS_m is the entropy of mixing, and T is the temperature in Kelvin.

Equation 2.1 can predict whether a blend is miscible, immiscible, or partially miscible by taking into account the sign of ΔG_m as seen in Figure 2.5. With the negative sign of Gibbs free energy, the blend is miscible, whereas the positive sign can see in an immiscible blend. Nevertheless, some can represent partially miscible, even with the negative sign of ΔG_m. Thus, the sign of the second derivative of ΔG_m is required to identify the difference between miscibility and partially miscibility. Systems always exhibit miscibility if the satisfy this following condition:

$$\frac{\partial^2 \Delta G_m}{\partial \phi_i^2} > 0 \quad \ldots\ldots\ldots\ldots\ldots\ldots\ldots (2.2)$$
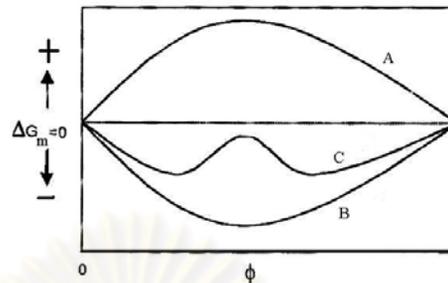
Figure 2.5 Plots of Gibbs free energy of mixing as a function of composition for a binary mixing exhibiting three types of mixing behaviors; immiscibility (A), complete miscibility (B) and partial miscibility (C).

For the partially miscible blend, the homogenous systems phase separate if temperature becomes higher demonstrating the LCST (Lower Critical Solution Temperature) behavior, while some change from being inhomogeneous at higher temperature called the UCST (Upper Critical Solution Temperature) behaviors. Not only can Equation 2.1 explain the miscibility of mixture, it can also demonstrate what kind of phase diagram the blend should exhibit. Polymer blends generally exhibit the UCST behavior since, as temperature decreases, TDS term should also decrease. Consequently, the free energy term becomes positive and phase separation then takes place indicating the UCST behavior. On the other hand, some blends appear to show the LCST behavior, this might be as the result of the enthalpy of mixing increase as temperature increases, causing the free energy to be positive and phase separation occurs. There are two explanations for such behavior [Strobl 1997, Cowie 1988]. First, once mixing two polymers, there are two type of interaction competing with each other, i.e., the repulsive interaction and the attractive force between specific groups incorporated in the two polymers. With increasing temperature the fraction of closed bonds decreases and the repulsive forces eventually dominate. This may induce the enthalpy of mixing to change from being negative at low temperature to being positive at higher one. The second explanation is that, as temperature increases, the free volume for the local motion of monomer decreases. Hence the mobility is reduced, leading to lowering of the entropy.

In polymer blends, it appears that not only do the UCST and LCST phase diagrams have been found; other types of phase diagrams can also be observed. Figure 2.6 presents a schematic representation of various types of phase diagrams for polymer mixture, and for the sake of clarity, the discussion here will be restricted to monodisperse binary mixture. As can be seen from Figure2.6a, there is no instability regime indicating that the blend appears completely miscible. Figure 2.6b and 2.6c present that the UCST and the LCST exist separately, whereas in Figure 2.6d-f, the UCST merges with the LCST.
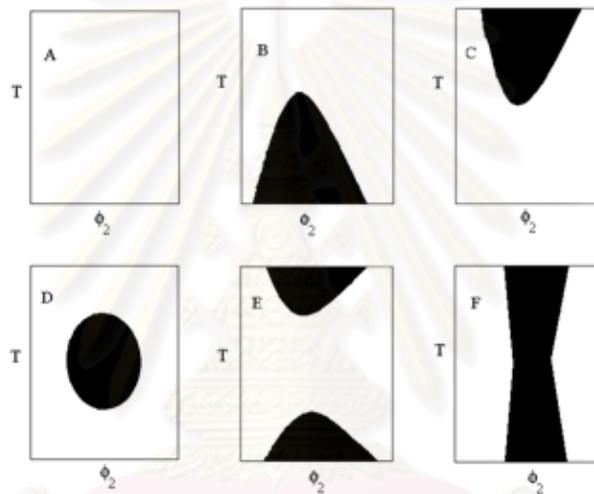
Figure 2.6 Schematic of liquid-liquid temperature-composition phase diagrams. Shade areas show the temperature-composition regimes of solution instability where phase separation occurs [Olabisi et. al.1979].

2.6 The Flory-Huggins Theory [Painter and Coleman, 1994]

The equation for the free energy of polymer solutions obtained independently and almost simultaneously by Flory and Huggins uses many of the assumptions of regular solution theory and has a similar form to the regular solution result as follows:-

$$\frac{\Delta G_m}{RT} = n_s ln\varphi_s + n_p ln\varphi_p + n_s \varphi_p \chi \quad ......(2.3)$$

The subscript s and p refer to solvent and polymer, respectively. The first two terms are the combinatorial entropy. It can be seen that the symbols ϕ_s and ϕ_p, which represent the volume fractions of the solvent and polymer, replace the mole fractions used in regular solution theory. The third term uses the parameter χ to describe the interactions between components and, as in the regular solution model, it is related to the change in energy when solvent/solvent and polymer/polymer contacts and hence interactions are replaced by solvent/ polymer interactions.

Side of the above equation can be divided by V/V_r to obtain equation (2.4). V is the total (molar) of the system and V_r is reference (molar) volume.

$$\frac{\Delta G_m'}{RT} = \left[\frac{\Delta G_m}{RT}\right] \cdot \left[\frac{V_r}{V}\right] = \frac{\phi_A}{M_A} \ln \phi_A + \frac{\phi_B}{M_B} \ln \phi_B + \phi_A \phi_B \chi_{AB} ...(2.4)$$

where we have reverted to more general subscript A and B, rather than the s and p, which are used to designate solvent and polymer, respectively. Equation (2.4) exhibits the free energy of mixing per mole of lattice sites and this form of the free energy equation is informative because it immediately makes plain some of the points concerning the entropy of mixing.

The quantities M_A and M_B can be thought of as the "degree of polymerization" of A and B.

In case of polymer and polymer mixing, we can let V_r be equal to the molar volume of one of the chemical repeat units, then both M_A and M_B would both be large and the entropy of mixing would be very small. In case of most hydrocarbon (non-polar) molecule, χ is positive, that make the positive value of ΔG.

Flory-Huggins interaction parameter or Solubility parameter (χ_{AB}) can be obtained from the equation (2.5)

$$\chi_{AB} = \frac{V_r}{RT}\left(\delta_A - \delta_B\right)^2 \quad \ldots\ldots\ldots(2.5)$$

, where the subscript A and B indicates A and B segments (or molecules)

$$\delta = \frac{\sum_i F_i^*}{\sum_i V_i^*} \ (cal \ .cm^{-3})^{0.5} \quad \ldots\ldots\ldots\ldots(2.6)$$

, where F^* is the molar attraction constant of the ith group, while V^* is the corresponding molar volume constant of this group. The value of F^* and V^* are shown in Table 2.1.

Table 2.3 Molar Volume and Attraction Constants [Painter and Coleman, 1994]

Group	Molar Volume Constant V^* (cm^3 mole^{-1})	Molar Attraction Constant F^* ((cal. cm^3)$^{0.5}$ mole^{-1})
-CH$_3$	31.8	218
-CH$_2$-	16.5	132
>CH-	1.9	23
>C<	- 14.8	- 97
C$_6$H$_3$	41.4	562
C$_6$H$_4$	58.5	652
C$_6$H$_5$	75.5	735
CH$_2$=	29.7	203
-CH=	13.7	113
>C=	-2.4	18
-OCO-	19.6	298
-CO-	10.7	262
-O-	5.1	95
-Cl	23.9	264
-CN	23.6	426
-NH$_2$	18.6	275
>NH	8.5	143
>N-	- 5.0	- 3

CHAPTER III

LITERATURE REVIEWS

Currently, polyimides are widely used for advanced applications, e.g., interlayer dielectrics in thin film microelectronic packaging. Since they are based on a mature technology and satisfy the requisite properties to survive thermal, chemical, and mechanical stresses associated with microelectronic fabrication processes. There are many studies about this engineering polymer. For example, Hergenrother et al. (2002) studied the series of new polyimides prepared from the reaction of 3,3',4,4'-biphenyltetracarboxylic dianhydride (s-BPDA) with the various aromatic diamines. s-BPDA polyimide films were cured in air tend to darken slightly in color. Near colorless films turned pale yellow while yellow films often became more intense yellow to orange. Higher curing temperatures generally improved the tensile properties at the sacrifice of color. Curing in a nitrogen atmosphere would have been desired and probably would have helped reduce color intensity of films. Hsiao and Chen (2002) investigated a series of aromatic diamines polymerized with two aromatic dianhydrides, pyromellitic dianhydride (PMDA) and 3,3',4,4'-biphenyltetracarboxylic dianhydride (s-BPDA). The resulting poly(amic acids) was thermally cyclodehydrated to yield aromatic polyimides. The polyimides were characterized by determining their glass transition temperatures (T_g). The PMDA-based (325°C) polyimides generally exhibited a higher T_g than the corresponding s-BPDA-based (270°C) analogues, but s-BPDA-based polyimides have shown much higher elongation than PMDA-based one. Currently, polyimides are widely used for advanced applications, e.g., interlayer dielectrics in thin film microelectronic packaging. Since they are based on a mature technology and satisfy the requisite properties to survive thermal, chemical, and mechanical stresses associated with microelectronic fabrication processes.

Polysiloxane-block-polyimide becomes increasingly important materials for microelectronic applications, aerospace, and printed circuit industries due to their excellent adhesive properties, low dielectric constants, distinguished properties of

oxidative stability, and good overall thermal and mechanical properties (Yamada, 1998 and Andre et al., 2001). With the combined properties of the polyimide and poly(dimethylsiloxane) (PDMS) components, polysiloxane-block-polyimide can increase solubility and flexibility as compared to the polyimide homopolymer, leading to increase overall process ability. An introduction of siloxane component offers increased impact resistance, excellent adhesion, and decreased dielectric constants (Tiwari and Nema, 2003), while maintaining the thermal and mechanical stability that is adequate for most microelectronic applications.

Yamada (1998) studied systematic thermal, mechanical, electrical, adhesive and coating properties of siloxane-modified polyimide. Based on experimental results, it can be seen that all of polyimides showed excellent thermal, mechanical, electrical, adhesive and coating properties, which are suitable for use in microelectronics coating applications. The polysiloxane block polyimides, which have the good stress relaxation properties due to their low tensile moduli, microphase separated structures possess two different glass transition temperatures. One is arising from the siloxane phase at lower temperature (T_{g1}) and the other one caused by the polyimide phase at higher temperature (T_{g2}). Polysiloxane-block-polyimides exhibited lower tensile strengths, moduli and larger elongations because the polysiloxane component incorporated into the polymer backbone. In addition, tensile modulus and strength of the polysiloxane-block-polyimides become lower.

The surface properties of poly(dimethylsiloxane) (PDMS) containing polymer blends have been investigated by several groups. Zisman et al. (1964) was the first group which reported polymer surface modification using siloxane containing copolymers, and show that the key property of PDMS is its low surface tension, which results in surface segregation of PDMS in most polymer blend systems. This property is often desirable for many applications regarding low surface energy such as antifouling coatings (Owen, 1993). Water contact angle analyses of PDMS containing block copolymer film has been used to confirm the presence of the siloxane enriched surface. This analytical technique was used to measure the yields of the relative surface tension of the material. A higher water contact angle indicated a low energy hydrophobic surface. PDMS showed a reported water contact angle of

approximately 101°. Phase separated PDMS containing block copolymer films showed that water contact angle values were very close to that of pure PDMS, indicating a siloxane enriched surface. One of the key properties is its low surface energy, which results in surface segregation of siloxane at the micro- or nano-level in most polymer blend systems. This attractive feature enables one to achieve a low energy surface when added even in small amounts to the corresponding homopolymeric system.

Furukawa et al. (1997) investigated the surface properties of the polyimide, polysiloxane-block-polyimides, and their blend. They found that the addition of 10 wt% PDMS the contact angle increased by 25° over the homopolymer. Moreover, additional incorporation of PDMS did not contribute to an increase in water contact angle. Further investigation indicated that the surface tension of the block copolymers was almost identical with that of the PDMS homopolymer. The polar component of surface tension was decreased with polysiloxane composition, while the dispersion component of surface tension was gradually increased.

Chen and Gardellar (1994) and Spanos et al. (2003) were summarized the two generic ways for modifying the surface properties of polymeric materials. The first one case called the external methods, including gas plasma treatment, plasma coating deposition, surface grafting, and photochemistry. The second method was base on, surface segregation from within the material bulk can e.g., polymer blend systems, which consisted of blending two homopolymers (A) and (B) or mixing a block copolymer (AB) with a homopolymer (A). If polymer/polymer segment (B) has a lower surface energy than that of the homopolymer/block (A), a net lowering of the surface energy of their blend system will lead to the surface enrichment of B relative to its bulk concentration. The overall driving force in this case is a net lowering of the surface energy for the polymer blend system leading to the surface enrichment of B relative to its bulk concentration. The small amounts of block copolymers behave like a surfactant and segregates to the surface region; changing the properties of this region whereas the bulk properties remain the same as the homopolymer.

Poly(dimethylsiloxane) is a low surface energy polymer ($\gamma_{PDMS} \approx 21$ Dyne/cm) and is often found to be incompatible with other polymer systems. Therefore, PDMS can be chosen as a homopolymer or included as a segment in block copolymers for mixing into polymeric materials. Typically, this leads to surface enrichment of the PDMS component. For instance, numerous poly(dimethylsiloxane) copolymer/homopolymer blend mixtures have been studied in the past; examples include PDMS-co-poly(methyl methacrylate)/poly(methyl methacrylate) (Inoue et al., 1990), PDMS-co-polystyrene/polystyrene (Chen and Gardella, 1998), PDMS-co-polyurethane/phenoxy (Wen et al., 1997), polycarbonate-polydimethylsiloxane block copolymer/polycarbonate (Kim et al., 2002), and polyethylene-poly(dimethylsiloxane) copolymer/polyethylene (Spanos et al., 2003)

Inoue at al. (1990) investigates the surface segregation of PDMS-co-poly(methyl methacrylate)/poly(methyl methacrylate). They reported that the polysiloxane segments of PDMS-PMMA block copolymer and their PMMA blends were accumulated on the air side surfaces of solution-cast film and surface segregation was significantly affected by siloxane chain length in block copolymers.

Consequently, blending of PDMS containing block copolymers with organic polymers can have a dramatic effect on the surface properties. Chen and Gardella (1994) investigated the surface segregation of blends prepared with PDMS block copolymers and homopolymers of polystyrene, poly(methylstyrene), and bisphenol A polycarbonate. Because of the low surface tension of the PDMS blocks, surface segregation of the PDMS blocks is found in all these AB/B blends. The authors concluded that the amount of the block copolymer in the blend, the molecular weight of the homopolymer A, and the block copolymer architecture were contributing factors that affected the surface compositions of the AB/B blends. When the PDMS was incorporated into the blends at 6% or less by weight, the surface PDMS concentrations of the blends would be as high as 95%. The PDMS surface concentrations did not change substantially when the bulk concentration the block copolymer in the blend increased form 10 to 100%.

Spanos et al. (2003) studies surface segregation blend system between polyethylene-poly(dimethylsiloxane) copolymer and homopolymer of polyethylene. They revealed that the poly(dimethylsiloxane) copolymer is found to readily undergo surface segregation during annealing to produce a well-adhered polysiloxane-rich layer. On the basis of the lower surface energy PDMS segment contained in the polyethylene-co-poly(dimethylsiloxane)-co-polyethylene block copolymer ($\gamma_{PDMS} = 21$ Dyne/cm and $\gamma_{PE} = 36$ Dyne/cm), one would expect this additive to migrate toward the air-polymer interface.

Rimdusit (2007) studied surface segregation in polymer blend systems between 3,3´,4,4´-biphenyltetracarboxylic dianhydride/4,4´-diaminodiphenyl ether (s-BPDA/ODA) polyimide and block copolymer based on polysiloxane-*block*-polyimide (SPI). These polyimide blends, having various compositions of the SPI, were processed by a solution casting method. The glass substrate used in the film-casting process shows significant effect on the migration of surface segregated species to enrich the air-exposed surface, whereas the more polar s-BPDA/ODA tends to remain close to the polar glass substrate. Contact angle measurement evidently indicates an enrichment of the hydrophobic siloxane fraction on the blend film surface. The average water contact angle of glass side surface is 77° whereas that of the air side is about 102° in every blend ratio. This behavior confirms the surface segregation phase separation in these polymer blends.

CHAPTER IV

EXPERIMENT

4.1 Materials

4,4'- diaminodiphenyl ether (4,4'-ODA) was purchased from Tokyo Kasei Kogyo Co., Ltd. 3,3',4,4'-biphyltetracarboxylic dianhydride (s-BPDA) was obtained from Ube Chemical Co., Ltd. 1,2,4,5-benzenetetracarboxylic dianhydride (PMDA) was bought from Tokyo Kasei Kogyo Co., Ltd. 3,3',4,4'-oxydiphthalic anhydride (ODPA) was supplied by Shanghai Research Institute of Synthetic Resins (Figure 4.1). N-methyl-2-pyrrolidinone (NMP), the solvent for poly(amic acid) synthesis, was purchased from Fluka. Tetrahydrofuran (THF), the cosolvent for polyimide blend, was purchased from Merck Company. All chemicals were used as received without any further purification. As shown in Figure 4.2, polysiloxane-block-polyimide (BSF30) under the trademark of "BSF30" with molecular weight of 167,720 was obtained from Nippon Steel Chemical Co., Ltd. The ratio of the block components (polysiloxane/polyimide) is 36.8 mol%. Glass petri dishes were used as substrate for polymer blend processing.
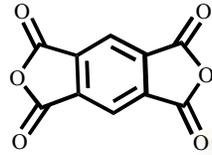
1,2,4,5-benzenetetracarboxylic dianhydride (PMDA)
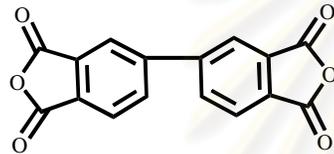
3,3',4,4'-biphyltetracarboxylic dianhydride (s-BPDA)
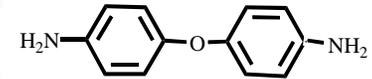
4,4'-diaminodiphenyl ether (ODA)
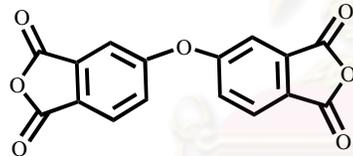
3,3',4,4'-oxydiphthalic anhydride (ODPA)

Figure 4.1: Chemical structures of dianhydrides and diamine
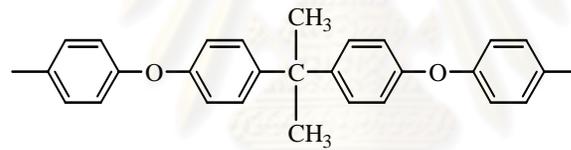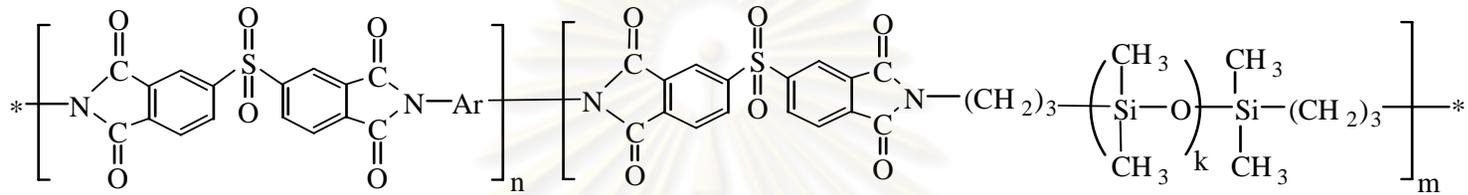
Silicon-containing polyimides (BSF30) and the corresponding Ar group

Figure 4.2: Chemical structures of silicon-containing polyimide

4.2 Poly(amic acid) Preparation

Generally, polyimide was synthesized by the condensation polymerization via two-step method, consisting of polymerization of a soluble poly(amic acid) intermediate. As illustrated in Figure 4.3, this approach is based on the reaction of a diamine i.e. 4,4'-diaminodiphenylether (ODA) with a tetracarboxylic acid dianhydride i.e. 1,2,4,5-benzenetetracarboxylic dianhydride (PMDA), 3,3',4,4'-biphenyltetracarboxylic dianhydride (s-BPDA), and 3,3',4,4'-oxydiphthalic anhydride (ODPA) in a polar aprotic solvent such as N-methyl-2-pyrrolidinone (NMP) at room temperature. The resultant poly(amic acid) is then cyclized by thermal imidization in a subsequent step to produce the desired polyimide.

Dianhydride   Diamine
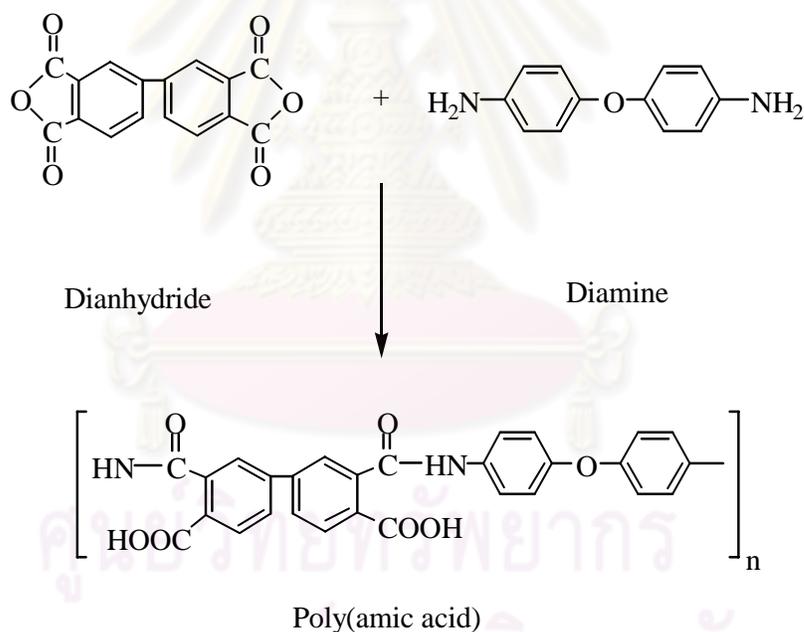
Poly(amic acid)

Figure 4.3: Synthetic scheme for the preparation of poly(amic acid).

4.3 Polyimide Blend Preparation and Imidization Condition

Poly(amic acid) (PAA) was prepared under the conventional two-step method, whereas polysiloxane-block-polyimide solution was made by dissolving calculated

amounts of the dried copolymer film in THF solution to yield the solution having desirable concentrations. Solution mixture of the polymer blend was prepared by measuring equal mass of PAA solution and the copolymer solution and, then, thoroughly mixed using a vortex mixer. The measured amounts of the resulting clear solution mixtures were then poured onto petri dish. The mixtures were dried in an air-circulated chamber at room temperature for 1 hour and at 60°C for 8 hours. The imidization was performed stepwise using the heating program at 150°C for 1 hour, 200°C for 1 hour and at 300°C for 1 hour in a vacuum oven. Polyimide blend films obtained were cooled to room temperature and removed from the glass plates. These blend films were kept separately in sealed containers for further surface and bulk characterizations.

4.4 Characterization Methods

4.4.1 Contact Angle Measurement

Contact angle measurement was performed at room temperature using a Contact Angle Meter Model CAM-PLUS MICCRO equipped with an optical microscope from TANTEC INC. The measured liquids were deionized water and ethylene glycol droplets with a radius of 10 μm. Sample's contact angle was averaged from 6-10 measured values.
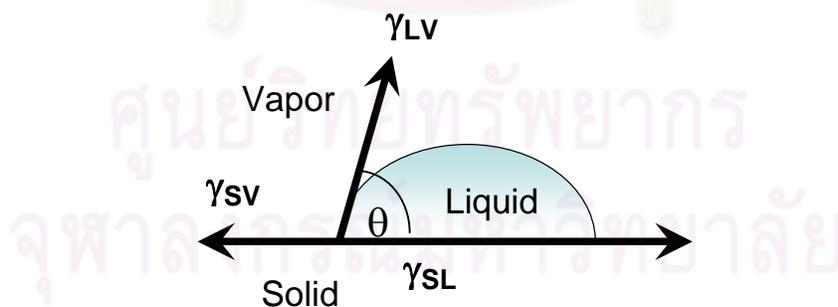
Figure 4.4: Equilibrium sessile drop system; γ_{LV} is of the liquid-vapor, γ_{SV} of the solid-vapor, and γ_{SL} is the solid-liquid interfacial tension, respectively and θ is the measured angle with respect to the surface.

The surface tension of polymer film was calculated from the obtained contact angles. As shown in Figure 4.4, their check relationship is given by Young's equation (Eq. 4.1) and Fowke's equation (Eq. 4.2) (Wu, 1982).

$$\gamma_S = \gamma_{SL} + \gamma_L cos\theta \tag{4.1}$$

$$\gamma = \gamma^d + \gamma^p \tag{4.2}$$

Where γ_S, γ_L, γ_{SL}, θ, γ, γ^d, and γ^p are surface tensions of solid, and liquid, a surface tension between solid and liquid, a contact angle, a total surface tension, as well as dispersive and a polar components of the surface tension, respectively. The relationships between the surface tensions of solid and liquid are given by

$$\gamma_s = \gamma_s^d + \gamma_s^P \tag{4.3}$$

$$\gamma_L = \gamma_L^d + \gamma_L^P \tag{4.4}$$

$$\gamma_{SL} = \gamma_S + \gamma_L - 2(\gamma_S^d \, \gamma_L^d)^{1/2} + 2(\gamma_S^p \, \gamma_L^p)^{1/2} \tag{4.5}$$

$$(1+cos\theta) \, \gamma_L = 2(\gamma_S^d \, \gamma_L^d)^{1/2} + 2(\gamma_S^p \, \gamma_L^p)^{1/2} \tag{4.6}$$

where γ_S^p, γ_S^d, γ_L^d, γ_L^p are polar and dispersion components of surface tensions of solid and liquid, respectively. The surface tension of solid can be calculated from the data of two different liquids used in the measurement as follows:

$$(1+cos\theta_1) \, \gamma_{L1} = 2 \, [(\gamma_S^d \, \gamma_{L1}^d)^{1/2} + (\gamma_S^p \, \gamma_{L1}^p))^{1/2}] \tag{4.7}$$

$$(1+cos\theta_2) \, \gamma_{L2} = 2[(\gamma_S^d \, \gamma_{L2}^d)^{1/2} + (\gamma_S^p \, \gamma_{L2}^p)^{1/2}] \tag{4.8}$$

where θ_i, γ_{Li} and γ_{Li}^p are a contact angle, a surface tension and a polar component of surface tension of liquid i ($i = 1$ or 2).

By measuring the contact angles of two different liquids with known surface energies, the surface energy of the solid can be obtained by solving Eqs. (4.7) and (4.8). Water and ethylene glycol were used and their surface energies are listed in Table 4.1.

Table 4.1: Surface energy for water and ethylene glycol (Kealbe et al., 1971; Kinloch, 1987)

Liquid	γ_L^p (dyne/cm)	γ_L^d (dyne/cm)	γ_L (dyne/cm)
Water	51.0	21.8	72.8
Ethylene Glycol	19.0	29.0	48.0

4.4.2 Surface Profilometer

The surface profile was assessed with the Sloan DEKTAK III stylus profilometer. In comparison on the effect of polyimide type, the scan track was 10 mm. To depict the contour on the surface for hill and valley areas, the scan tract was 800 μm for determining the effect of BSF30 contents.

4.4.3 Attenuated Total Reflectance Fourier Transform Infrared Spectroscopy (ATR-FTIR)

Infrared spectrum of the air side and the glass side surface, of polyimide blend films were measured using a Perkin Elmer Spectrum GX FTIR spectrophotometer. Attenuated total reflection Fourier transform infrared (ATR-FTIR) spectra were acquired using ZnSe as a prism at an incidence angle of 45°. The scan number and the spectral resolution were 64 and 8 cm^{-1}, respectively.

4.4.4 ATR Microscope

For higher depth profile, ATR microscope with Germanium tip was used to detect the functional groups on the hill and valley surface of the 30 phr blends in comparison with those on the surface of pure polyimides and pure BSF30. The scan number and the spectral resolution were 64 and 8 cm^{-1}, respectively.

4.4.5 Dynamic Mechanical Analysis (DMA)

Dynamic mechanical properties of the polyimide blend systems were tested using the NETZSCH Model DMA 242. The experiment is done in a tension mode using the dimension of the specimen of approximately $23.7\times5\times0.05$ mm^3 (L$\times$W$\times$T). The applied strain amplitude was 0.3% at the deformation frequency of 1 Hz. The specimen was heated using a temperature ramp rate of 3°C/min from 40°C to 300°C for ODPA/ODA blends, to 320°C for s-BPDA/ODA blends, and to 420°C for PMDA/ODA blends.

4.4.6 Tensile Property Measurement

Tensile modulus and tensile strength of polyimide blend films were determined utilizing a universal testing machine (model 5567) from Instron Instrument. The test method used was a tension mode with a specimen dimension of 8.0 cm in length, 0.50 cm in width, and 50 microns in thickness. The tensile properties were obtained following the general procedure in ASTM D882 using five specimens per test condition.

4.4.7 Thermogravimetric Analysis (TGA)

The decomposition temperature (T_d) and char yield of the blends were studied using TGA Instruments (model TGA/SDTA 851^e). The experiments were performed using a heating rate of 20°C/min from 40 to 1000°C under nitrogen atmosphere. The flow of purging nitrogen was kept at 80 ml/min. The sample mass was approximately 20 mg.

4.4.8 Scanning Electron Microscope (SEM)

The surface appearance of the polyimide-BSF30 blend films in microscale were investigated using a scanning electron microscope (JEOL, model ISM-5800LV) at an acceleration voltage of 15 kV.

CHAPTER V

RESULTS AND DISCUSSION

5.1 Contact Angle Measurement

In general, high water contact angle is indicative of a hydrophobic low energy surface. Figure 5.1, 5.2, and 5.3 respectively show a change in water contact angles of the ODPA/ODA, s-BPDA/ODA, and PMDA/ODA polyimide including BSF30 blend films casted on a glass substrate as a function of the BSF30 content. From the experiment, the water contact angles of the neat ODPA/ODA polyimide film on the air-exposed surface and on the glass-contacted surface were measured to be 81° and 74°, while those of the pure s-BPDA/ODA film were 83° and 76°. Additionally, those of the pristine PMDA/ODA film were 83°, and 71°, whereas those of the BSF30 film were 106°, and 96°. Interestingly for all three types of all blend films systems, the water contact angles on the air-exposed surface were about the same as the values of 102°. The contact angles of all blend films on the air-exposed surface were found to be almost constant at 101°-102° even at the presence of only small amount of the BSF30 (i.e. 1 phr). Further incorporation of BSF30 into all three types of polyimide would not contribute to the increase in water contact angle on the air-exposed surface beyond this value. The values reaching 102° for these polyimide blends were comparable to the water contact angle on the air side of the neat BSF30 itself. In the literatures, polydimethylsiloxane (PDMS) was reported to possess an average water contact angle value of approximately 101°-103° (Owen, 1993; Bowens, 1999). It can be implied that on the surface of the BSF30 and of the blends containing BSF30, siloxane species tended to migrate to the air-exposed surface, thus giving the contact angle approaching that of siloxane moieties.

The above results indicate that surface segregation occurred in all three types of polyimides and BSF30 blend films. Surface segregation of this blend films on the air-exposed surface provided the water contact angle very close to that of pure PDMS. The glass side surface, on the other hand, was enriched with all three polyimide

fractions thus it shows smaller values of water contact angle of 74°, 76°, 71° which are the signature values of those on the glass-contacted surface of ODPA/ODA, s-BPDA/ODA, and PMDA/ODA polyimide species, respectively. All three polyimides are more hydrophilic than BSF30; therefore, the polyimide tends to migrate to the more polar glass substrate to yield this surface segregation phase separation.

Figures 5.4, 5.5, and 5.6 exhibit the similar results on the change in contact angles based on ethylene glycol droplets. The increase of the contact angle values was also observed even at a small BSF30 fraction in blends although the values were smaller than the contact angles against water. The surface tension and its polar and dispersion components of the blend films were calculated by substituting the contact angle data into Eq. (4.7) and (4.8). For the air side surface, the results were plotted against the BSF30 composition in Figure 5.7, 5.8, and 5.9. It was obvious that the polar component of the surface tension decreased with increasing the BSF30 composition while the dispersion component showed an opposite trend. The sum of both components, which is the surface tension of the film, was the lowest at the presence of the BSF30 even at the content as low as 1 phr in the blends. The values of surface tension on the air-exposed surface for all three polyimide blends for all BSF30 content are close to that of PDMS (21.8 dyne/cm) reported in the literature (Owen, 1993). Therefore, the air-exposed surface of the blend films was believed to be covered with polysiloxane segments of the BSF30 block copolymer. This result is consistent with those reported by Furukawa et al. on the surface characteristics of the poly(imide siloxane) block copolymer (Furukawa et al., 1997). Therefore, the polysiloxane moieties in BSF30 are expected to migrate to the air-exposed surface of the blend films to form a silicone-enriched layer.

In comparison among the surface tension values on glass-exposed surface of the blends, the ODPA/ODA system renders the lowest value (29.3 dyne/cm) which is close to that of the s-BPDA/ODA blend (29.9 dyne/cm), while the PMDA/ODA blend possesses the highest values (32.8 dyne/cm). It is known that the lower surface tension indicates the greater hydrophobic behaviors. That means ODPA/ODA shows the greatest hydrophobic behavior, while PMDA/ODA has the highest hydrophilic

behavior. Therefore, the difference between the surface tension of BSF30 and PMDA/ODA is greater than those of BSF30 and other two polyimides. It is believed that the system of PMDA/ODA and BSF30 tends to provide the greatest segregation among the other ones.

5.2 Attenuated Total Reflectance - Fourier Transform Infrared (ATR-FTIR)

Attenuated total reflectance Fourier transform infrared (ATR-FTIR) technique was used to confirm the surface segregation phase separation characteristics of these blend systems. This technique could be used to explore molecular species on the surface through their vibration states and to render information on chemical bonds including molecular orientation as well. Figures 5.10, 5.11, and 5.12 present the spectra at 0 phr, 1 phr, 3 phr, 10 phr, 30 phr and pure BSF30 for the blends of ODPA/ODA blends, s-BPDA/ODA blends, and PMDA/ODA blends, respectively.

The results of ATR-FTIR spectra for glass-side surface of polyimide blend for ODPA/ODA polyimides are presented in Figure 5.10a. It can be observed that the spectra of the polyimide blend on glass side surface does not present the peaks of 1060 cm^{-1}, and 1015 cm^{-1}, which represented the Si-O-Si stretching vibration and 795 cm^{-1} of Si-C stretching. These are important vibrational signatures of siloxane group in BSF30. Furthermore, the spectra of glass side surface of the blends presented the same appearance as those of pure polyimide. That means the BSF30 component did not appear on the glass side, and the glass-side surface is covered with polyimide. Figure 5.10b shows the spectra for air-exposed surface of three types of polyimide blends. The spectra of the blends at 30 phr exhibit the Si-O-Si stretching vibration and 795 cm^{-1} of Si-C stretching of BSF30, which indicated that the air-side surface is covered with BSF30. This phenomenon does not occur in case of the blends of the lower BSF30 content, i.e. 3 phr or less, at highly diluted blend compositions (i.e. 1-3 phr) which yield a submicron layer of the BSF30 domain, the ATR technique is not sensitive enough to acquire the siloxane vibration on the surface. This is due to the fact that ATR-FTIR technique is sensitive to the chemical species with sufficient depth depending on the type of the crystal used. In this case, a ZnSe crystal used

provide a depth profile in the range of 2-4 microns. This phenomenon exhibits the segregation behavior of the polyimide moiety on the glass side surface and BSF30 moiety on the air side surface.

Figure 5.11a and 5.12a exhibit the spectra on the glass-exposed surface of the s-BPDA and PMDA blends. The result shows the same behavior as that occurs on the glass-exposed surface of ODPA/ODA blend. That means the BSF30 component did not present on the glass-exposed surface for all three polyimide blending systems. Figure 5.11b and 5.12b present the spectra on the air-exposed surface of the s-BPDA and PMDA blends. The result shows the presence of BSF30 component on the air-exposed surface for all three polyimide blending systems.

5.3 Surface Profilometry

Figure 5.13 exhibits the profiles of three blending systems at 30 phr. The different patterns of contours were observed. It can be observed that PMDA/ODA blend renders the greatest roughness, while ODPA/ODA blend possesses slightly less roughness than s-BPDA/ODA blend. It can be observed that the blend films at 30 phr for all polyimide blends provide two major zones, i.e. hills and valleys. From this figure, it can be observed that PMDA/ODA blend provides the highest difference between the height of hill and valley zones, while those of s-BPDA/ODA and ODPA/ODA are rather similar to each other. It can be hypothesized that the PMDA/ODA blend has the highest degree of segregation, whereas the ODPA/ODA blend possesses the lowest one.

Figures 5.14a to 5.14c show the profiles of three polyimide blends in comparison between 10 phr and 30 phr (air side surface). The results reveal that the increase of BSF30 content has the effect on the increase of roughness. This phenomenon is clearly observed in the PMDA/ODA blends. That could indicate the PMDA/ODA provide the greatest roughness among three polyimide-BSF30 blends.

5.4 Attenuated Total Reflectance (ATR) Microscopy

From the results of the surface profilometer, it can be observed that two zones (hills and valleys) are observed on the air-exposed surface of the films at high BSF30 content i.e. 30 phr for all three polyimide blends. For further investigation about the degree of segregation, the ATR microscope was applied to analyze the chemical structure at each zone of polyimide blends to provide both quantitative and qualitative information.   Figures 5.15 and 5.16 illustrate the IR spectra of the OPDA/ODA blends and s-BPDA/ODA blends for both hill area and valley area. It can be seen that the hill area on the film could exhibit BSF30 spectra, while the valley one could show the combination spectra of BSF30 and polyimide. Figure 5.17 presents the spectra of PMDA/ODA blends. It can be observed that the hill area shows BSF30 spectra, but the valley one exhibits only peak indicating polyimide character.

The Beer-Lambert law, which states that absorbance increases linearly with concentration, was used for quantitative analysis of mixture surfaces by measuring absorbance peak heights. From the calculation of intensity at wavenumber 795 cm^{-1} is summarized in Figure 5.18. The calculation of Si-C content of the film was performed by used the equation (5.1)

$$\% \, Si\text{-}C \, content = \frac{Intensity \, at \, 795 \, cm^{-1} \, on \, specific \, area}{Intensity \, at \, 795 \, cm^{-1} \, of \, pure \, BSF30} \qquad (5.1)$$

In comparison between the BSF30 content (estimated from the percentage of Si-C content at the wavenumber of 795 cm^{-1}) at the valley zone of each polyimide blend, it informs that there was some difference between the Si-C content on valley area between the ODPA/ODA blend (62%) and the s-BPDA/ODA blend (54%). Obviously, it can be observed that the Si-C content of the PMDA/ODA blend at 30 phr on the valley area presents was quite low (about 5%), whereas the Si-C contents on the hill area for all three types of polyimide blends were about 75 %. It can confirm that PMDA/ODA blend trends to possess the highest segregation behavior, while the segregation of s-BPDA/ODA blend tends to be slightly greater than that of the ODPA/ODA blend.

5.5 Dynamic Mechanical Analysis (DMA)

Figures 5.19a to 5.19c illustrate storage modulus of ODPA/ODA blends, s-BPDA/ODA blends and PMDA/ODA blends at various BSF30 compositions. As reported at 40°C, the thermograms revealed the glassy state moduli of the ODPA/ODA film to be 3.06 GPa (Figure 5.19a), s-BPDA/ODA film to be 2.99 GPa (Figure 5.19b), PMDA/ODA film to be 2.70 GPa (Figure 5.19c), and that of BSF30 to be 1.21 GPa. The BSF30 is, therefore, much less stiff than all three pure polyimide film due to the presence of the soft silicone segments in its molecular structure as seen in Figure 4.2. Thermal stability of polymers can also be obtained from the slope of the glassy state modulus in the DMA thermograms. The lower slope of the glassy state modulus indicates the greater thermal stability of the polymer. As a result, the DMA thermograms in Figures 5.19a to 5.19c clearly suggested that all three polyimide films were significantly more stable than the BSF30 polyimide. The large decrease in the storage modulus in the thermograms at elevated temperature indicated the corresponding glass transition region of each specimen. The storage modulus of the blend film at a large BSF30 content of 30 phr clearly showed the mixed characteristics of the two parent polyimides. The blend film displayed two successive drops in its storage modulus. However, when the amount of the BSF30 in the blend films was kept to be in low BSF30 concentration, the decrease of their storage moduli, at about 180°C, due to the presence of BSF30, was suppressed and hardly detected. The resulting thermograms emphasized the requirement to use a relatively small amount of the BSF30 in the blend systems in order to maintain the overall thermal and mechanical integrity of the resulting films.

Figure 5.20a present the glass transition temperature of pure BSF30, pure ODPA/ODA polyimides, the blends at 10 phr, and 30 phr of BSF30. The results present that the glass transition temperatures of pure BSF30 and pure ODPA/ODA are reported to be 176°C and 282°C, respectively. The blend at 30 phr presents two glass transition temperatures. The first Tg situated in the lower temperature range about 180°C belonged to the BSF30 fraction. The second Tg appeared at higher temperature of about 280°C was obviously the characteristic of glass transition temperature for the ODPA/ODA polyimide fraction. Additionally, the Tg of the blend at 10 phr was not

changed from that value at 30 phr. This phenomenon confirmed the immiscibility of the systems and the two domains clearly exhibited their own thermal characteristics.

This behavior can be observed in the s-BPDA/ODA-BSF30 blends and PMDA/ODA-BSF30 blends as shown in Figure 5.20b and 5.20c.

5.6 Tensile Property Test

Tensile properties of three polyimide blends are presented in Figure 5.21a-5.21c. In Figure 5.21a, the pure ODPA/ODA film rendered the tensile strength of 93 MPa and the tensile modulus of 2.52 GPa. In Figure 5.21b, the tensile strength and tensile modulus of the pure s-BPDA/ODA film were 130 MPa and 3.22 GPa respectively. In Figure 5.21c, the ones of the pure PMDA/ODA film were 89 MPa and 2.82 GPa, respectively. It can be observed that the values of tensile strength and tensile modulus were decreased with increasing BSF30 content. That is due to the low tensile strength of BSF30 (52 MPa) and the low tensile modulus of BSF30 (1.30 GPa). The stress-strain curves of the PMDA/ODA blending system are presented in Figure 5.22.

5.7 Thermogravimetric Analysis (TGA)

Thermal stability of the polyimide blends for ODPA/ODA blends, s-BPDA/ODA blends, and PMDA/ODA blends with various compositions of BSF30 was examined and presented in Figure 5.23a–5.23c, respectively. It was clearly seen that when relatively large amount of the BSF30, i.e. 10 phr and 30 phr, was shown in the blend films, the degradation temperature of the film was substantially sacrificed due to the inherently lower degradation temperature of the BSF30 portion in the blend films. All polyimide blends exhibit two-step changes, which corresponds to those of pure BSF30 and pure polyimides, respectively.

On the other hand, no significant change in degradation temperature of the blend films was observed within the composition range of 1 and 3 phr of the blends, obviously due to the small quantity of the BSF30 presented. For all three types of polyimide blends, it can be observed that the char yield of the blends tended to

decrease with increasing the BSF30 content. In this study, the char yield of BSF30 (at $900^{o}C$, $10^{o}C/min$) was 36 %, which was similar to our previous TGA study in the literature [Tiptipakorn, 2007].

5.8 Appearance of the Blend Films

Figure 5.24a to 5.24c show the appearance of three blend films at various BSF30 contents. It can be observed that all three blend films were clear at low BSF30 content such as 1 phr. When the BSF30 content was increased to 3 phr, the films were opaque. At 10 phr, the surfaces of the film were slightly rough. The surfaces of the films were more rough at high BSF30 content i.e. 30 phr.; two colors were observed on the surfaces of the films.

5.9 SEM Micrographs of the Blend Films

Figures 5.25 a to c show the SEM micrographs on the hill area of the blend films at 30 phr. From the figures, it was found that there are some small pits (a diameter of smaller than 1 micron) on both ODPA/ODA blend and s-BPDA/ODA blend, but big pits (a diameter of larger than 1 micron) are found in the PMDA/ODA blend. In comparison among the blend films, the roughness of the s-BPDA/ODA blend is slightly greater than that of ODPA/ODA blend. Additionally, the big pits of PMDA/ODA blends lead to roughness on the surface of the blends. These micrographs are able to confirm the result from the surface profilometer.
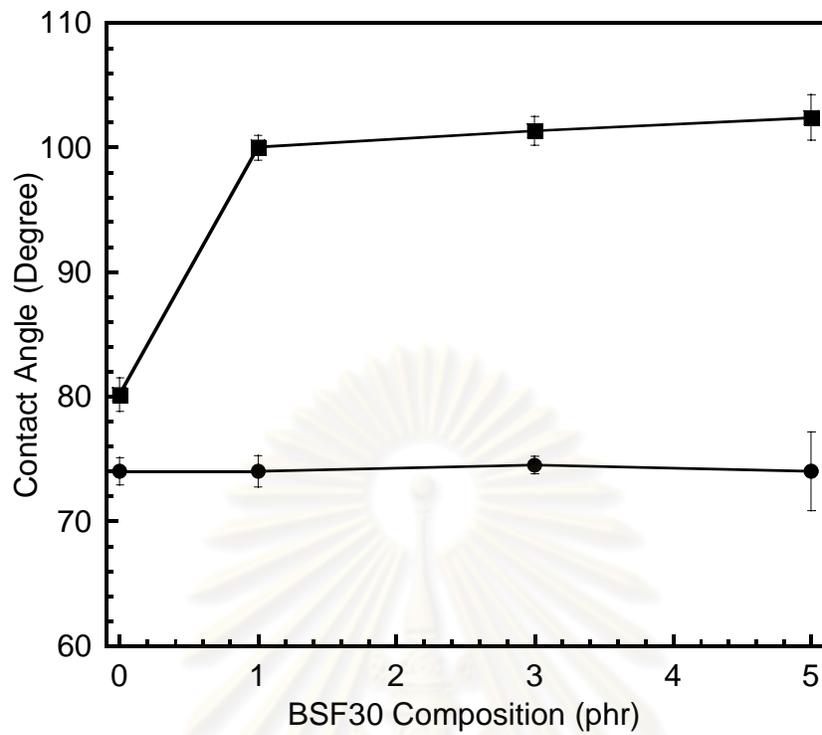
Figure 5.1: Water contact angles of ODPA/ODA polyimide-BSF30 blends as a
function of the BSF30 content: (■) Air side, and (●) Glass side.
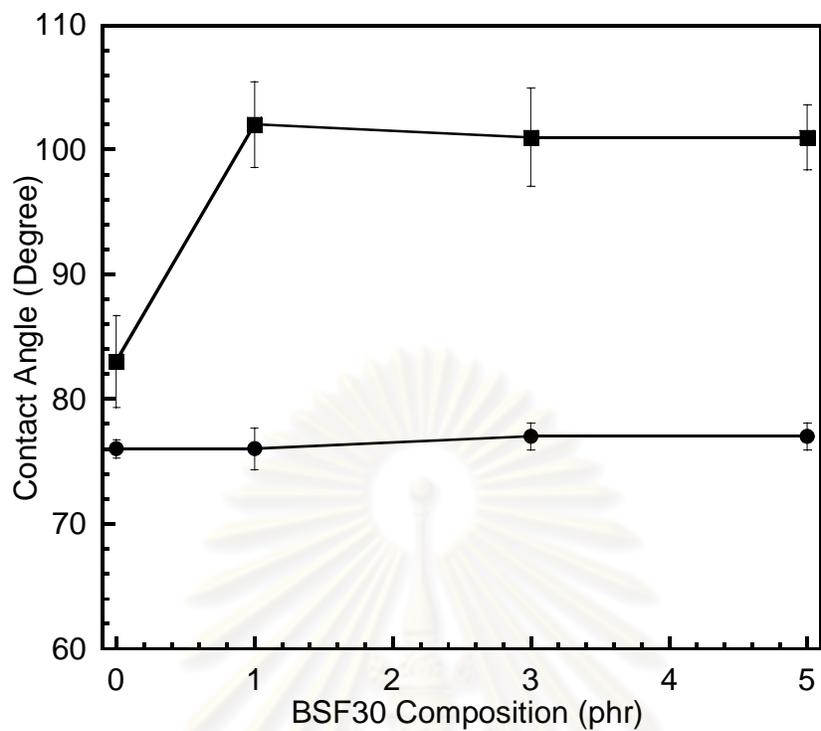
Figure 5.2: Water contact angles of s-BPDA/ODA polyimide-BSF30 blends as a
function of the BSF30 content: (■) Air side, and (●) Glass side.
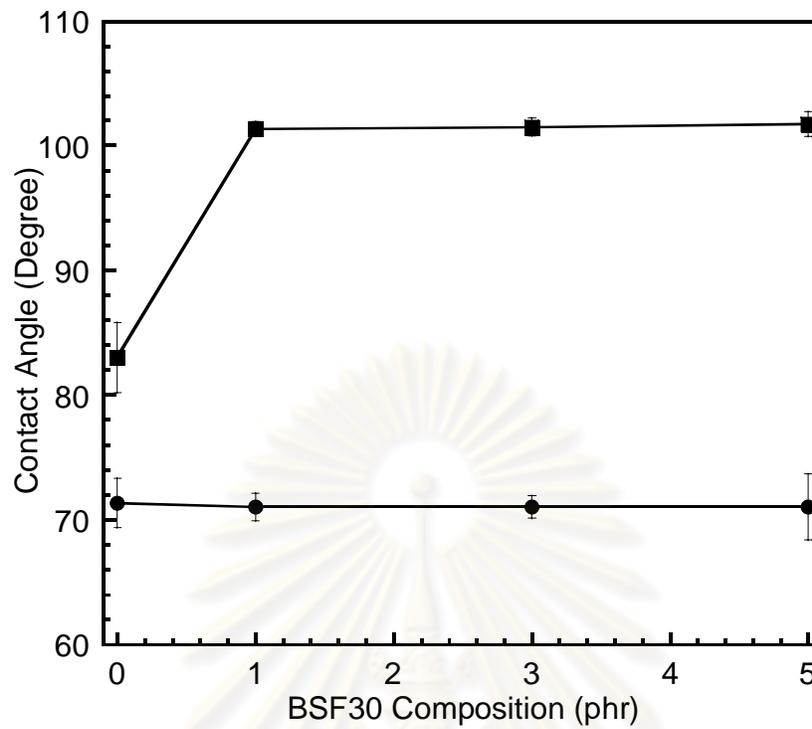
**Figure 5.3**: Water contact angles of PMDA/ODA polyimide-BSF30 blends as a
function of the BSF30 content: (■) Air side, and (●) Glass side.
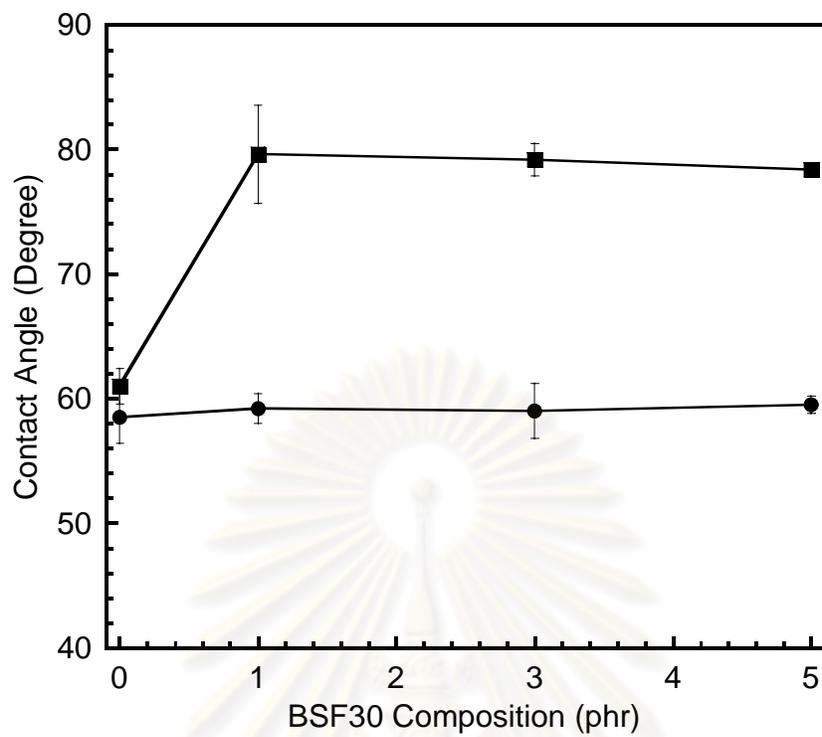
Figure 5.4: Contact angle measurements obtained from ethylene glycol drop on
ODPA/ODA polyimide-BSF30 blends as a function of BSF30 content:
(■) Air side, and (●) Glass side.
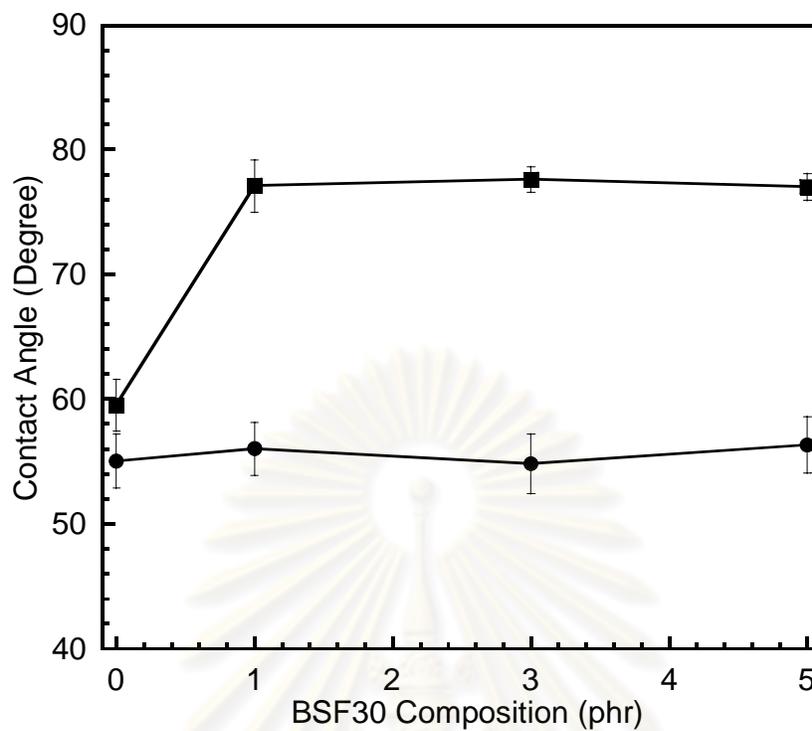
Figure 5.5: Contact angle measurements obtained from ethylene glycol drop on
s-BPDA/ODA polyimide-BSF30 blends as a function of BSF30 content:
(■) Air side, and (●) Glass side.
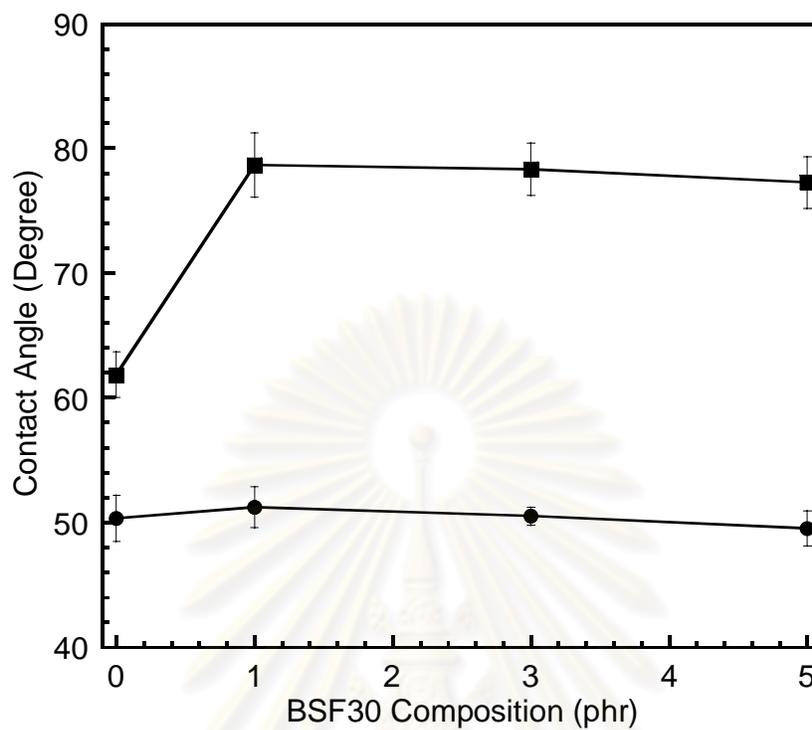
Figure 5.6: Contact angle measurements obtained from ethylene glycol drop on
PMDA/ODA polyimide-BSF30 blends as a function of BSF30 content:
(■) Air side, and (●) Glass side.
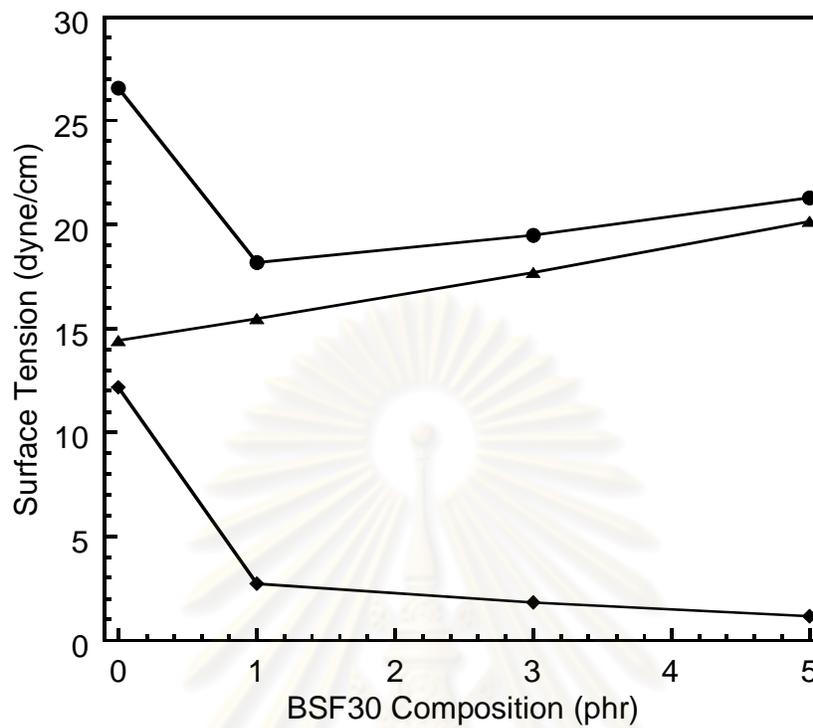
Figure 5.7: Surface tension of ODPA/ODA polyimide-BSF30 blends as a function of BSF30 content: (■) Surface Tension, (▲) Dispersion component of surface tension, and (●) Polar component of surface tension.
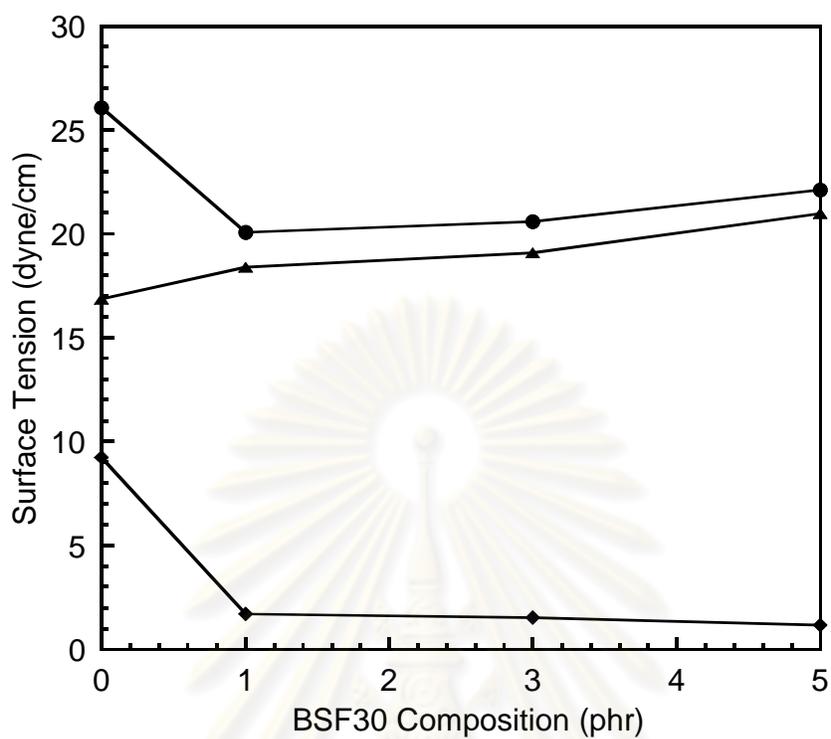
Figure 5.8: Surface tension of s-BPDA/ODA polyimide-BSF30 blends as a function of BSF30 content: (■) Surface Tension, (▲) Dispersion component of surface tension, and (●) Polar component of surface tension.
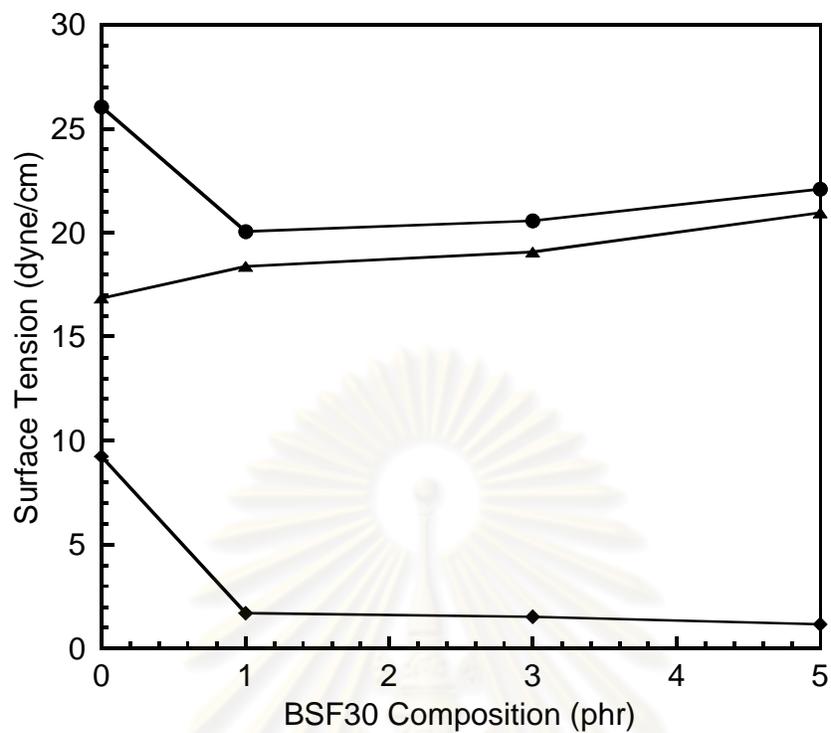
Figure 5.9: Surface tension of PMDA/ODA polyimide-BSF30 blends as a function of BSF30 content: (■) Surface Tension, (▲) Dispersion component of surface tension, and (●) Polar component of surface tension.
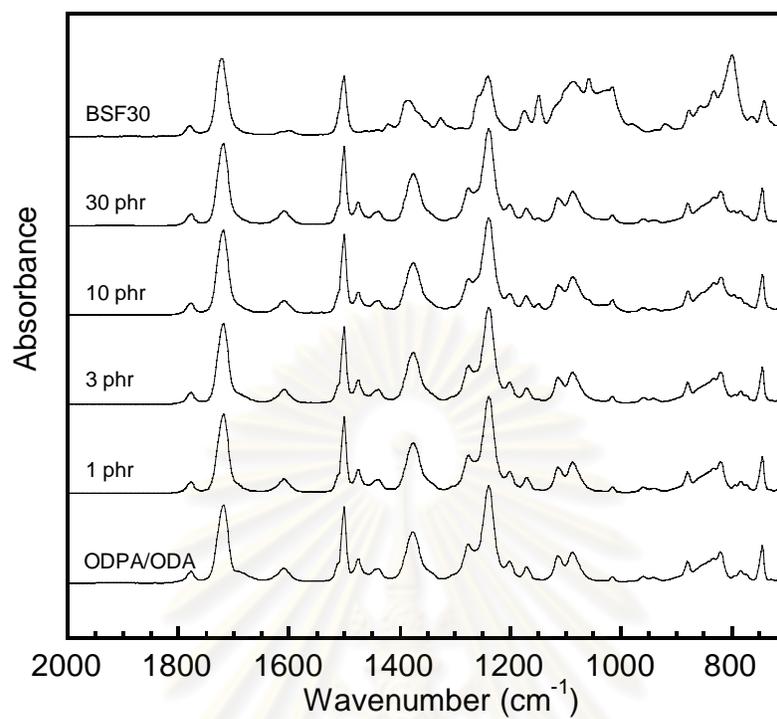
Figure 5.10a: ATR-FTIR spectra of ODPA/ODA polyimide-BSF30 blends as a
function of the BSF30 composition (Glass-exposed side).
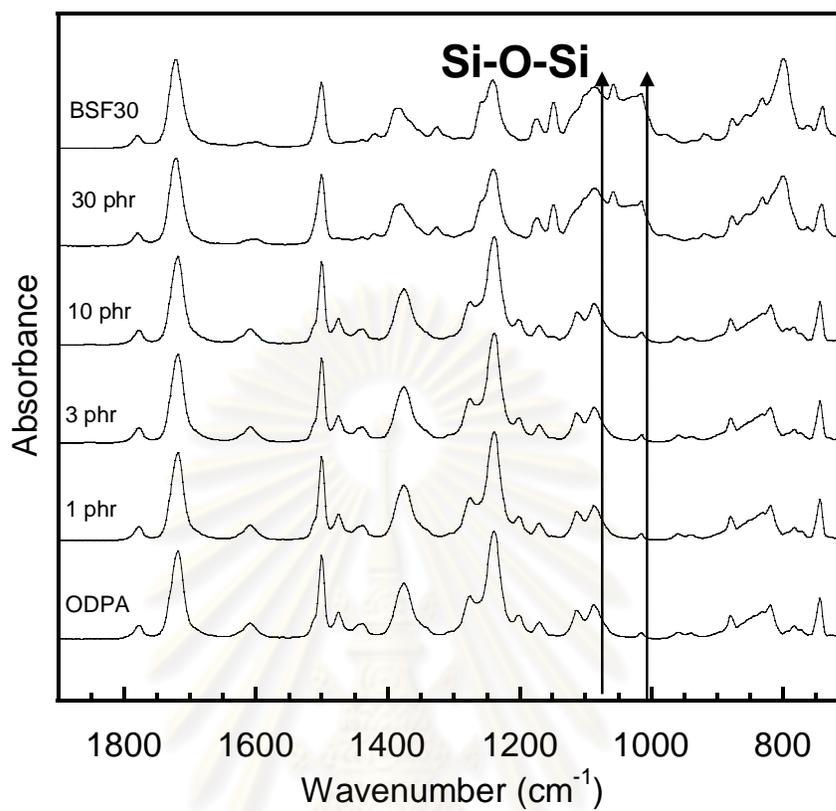
Figure 5.10b: ATR-FTIR spectra of ODPA/ODA polyimide-BSF30 blends as a function of the BSF30 composition (Air-exposed side).
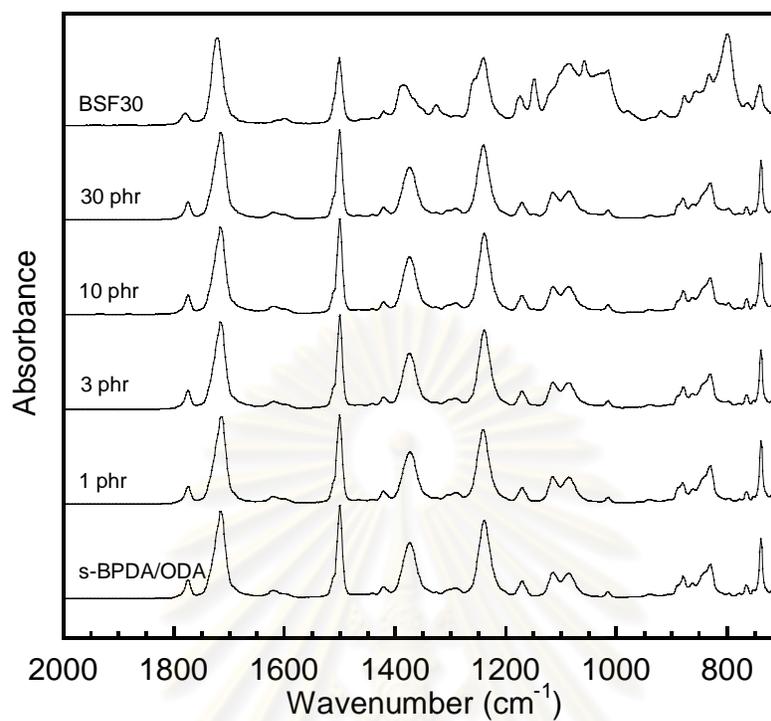
Figure 5.11a: ATR-FTIR spectra of s-BPDA/ODA polyimide-BSF30 blends as a
function of the BSF30 composition (Glass-exposed side).
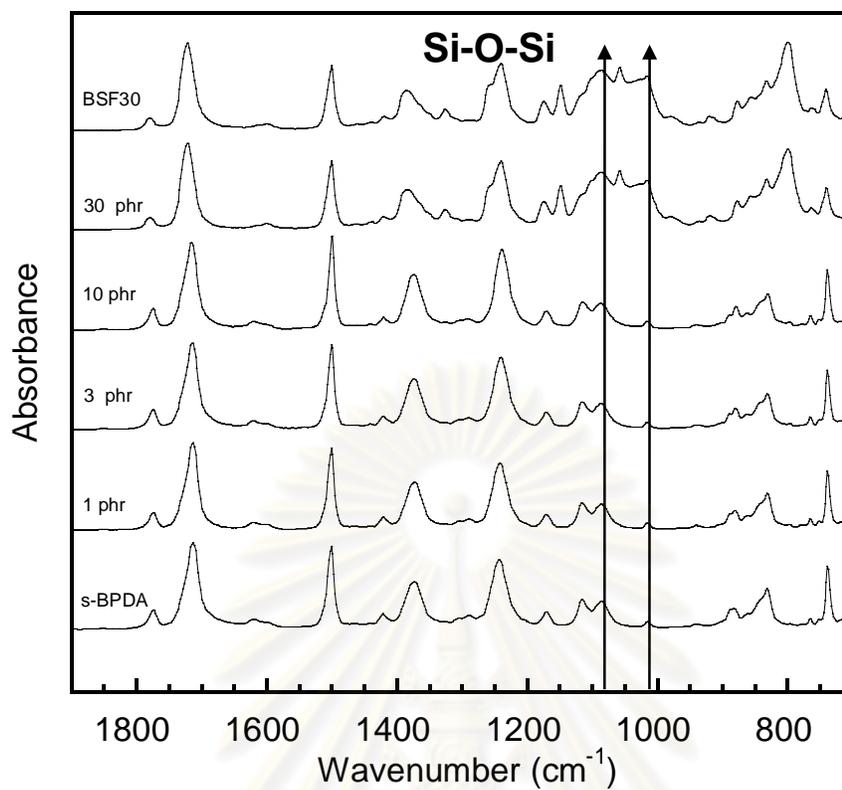
Figure 5.11b: ATR-FTIR spectra of s-BPDA/ODA polyimide-BSF30 blends as a function of the BSF30 composition (Air-exposed side).
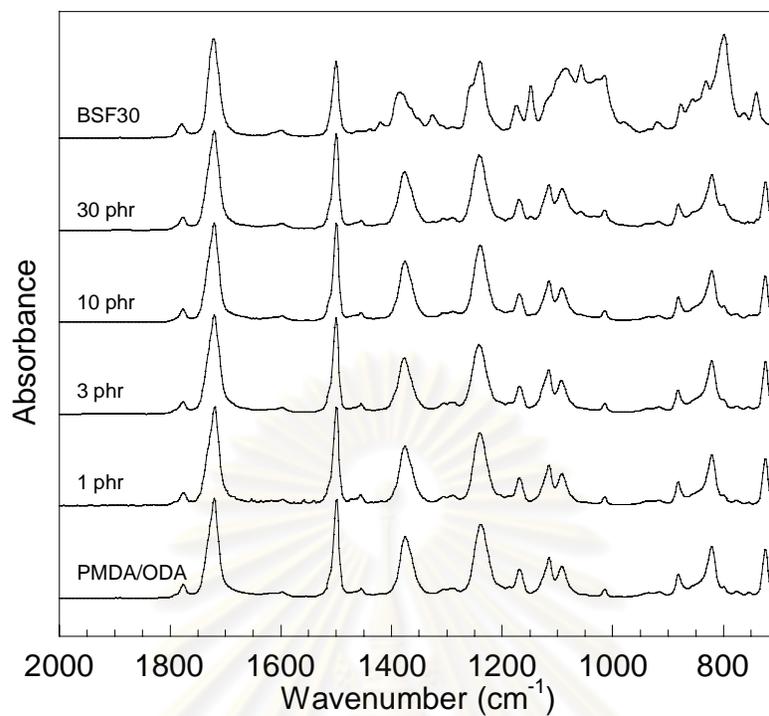
Figure 5.12a: ATR-FTIR spectra of PMDA/ODA polyimide-BSF30 blends as a function of the BSF30 composition (Glass-exposed side).
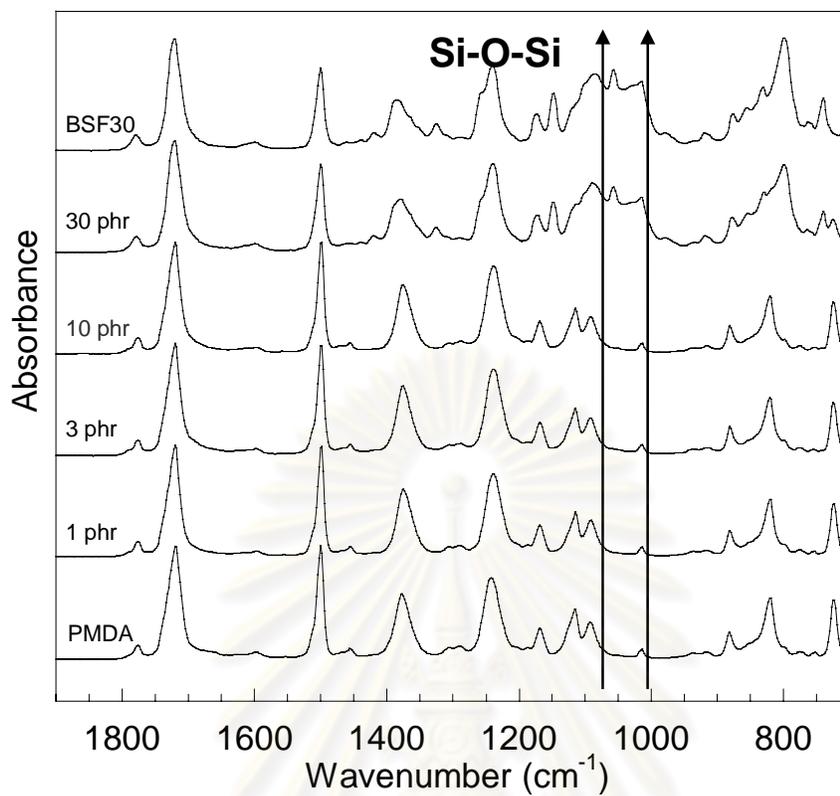
Figure 5.12b: ATR-FTIR spectra of PMDA/ODA polyimide-BSF30 blends as a function of the BSF30 composition (Air-exposed side).
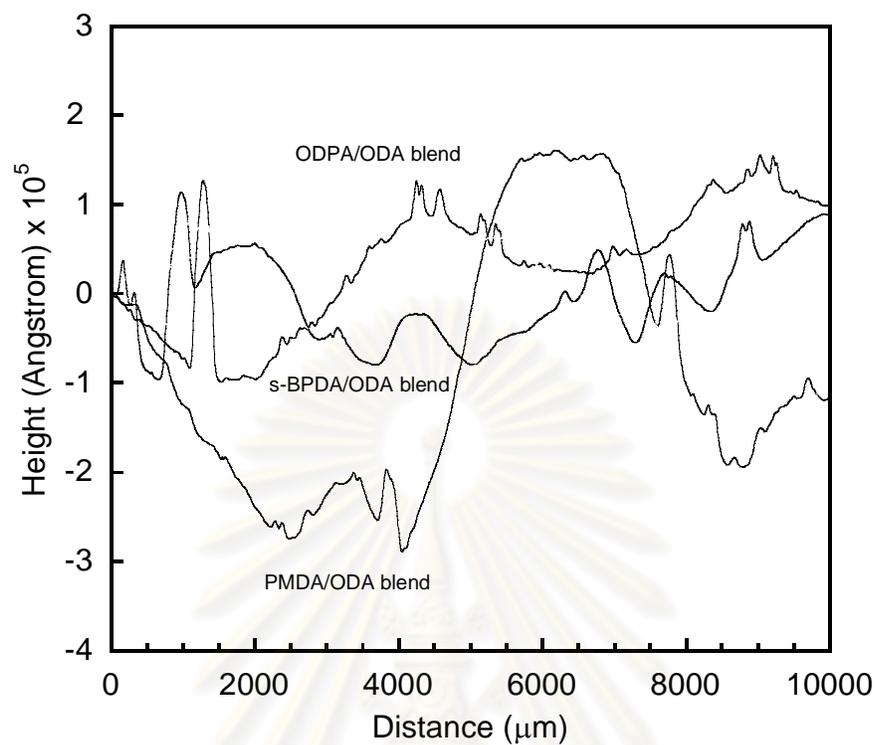
Figure 5.13: Surface profile of three types of polyimide-BSF30 blends at 30 phr
on the air-exposed surface.
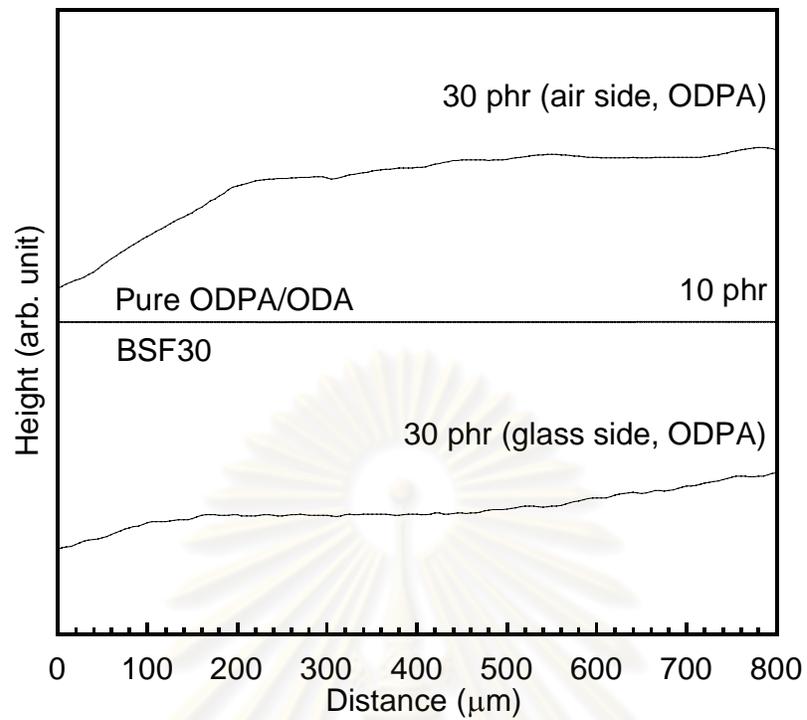
Figure 5.14a: Surface profile of ODPA/ODA polyimide-BSF30 blends at 10phr
and 30 phr in comparison with those of pure polyimide and BSF30.
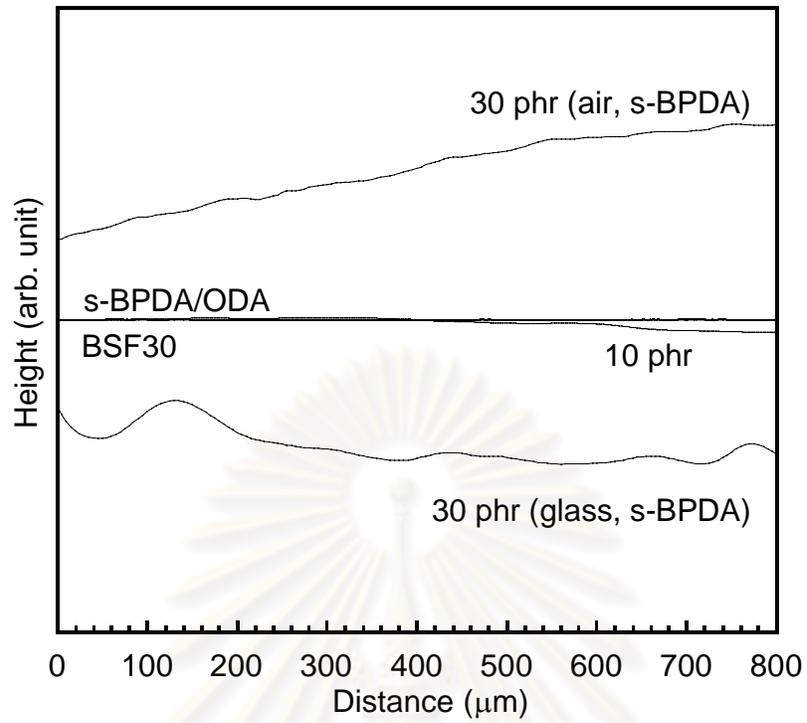
Figure 5.14b: Surface profile of s-BPDA/ODA polyimide-BSF30 blends at 10phr
and 30 phr in comparison with those of pure polyimide and BSF30.
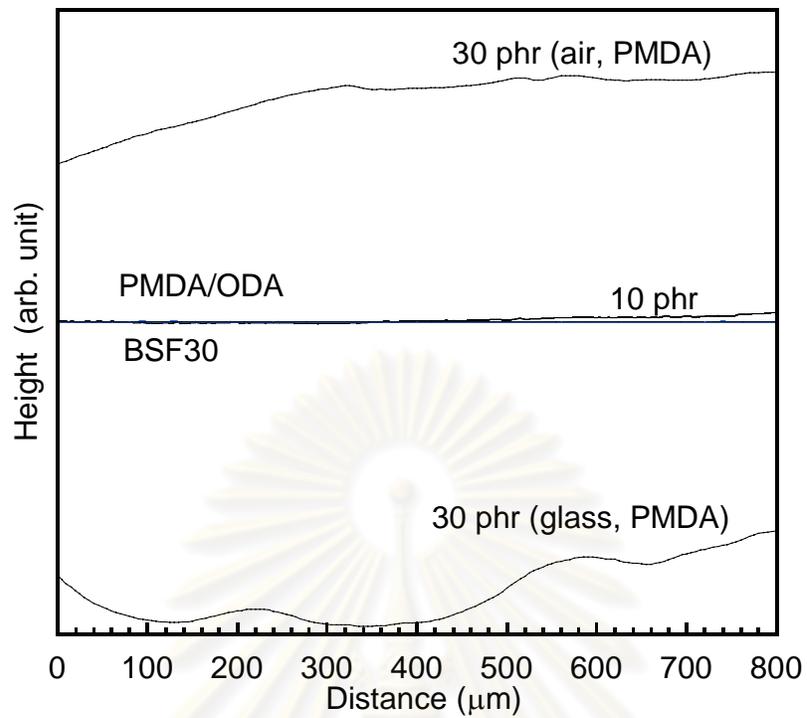
Figure 5.14c: Surface profile of PMDA/ODA polyimide-BSF30 blends at 10phr
and 30 phr in comparison with those of pure polyimide and BSF30.
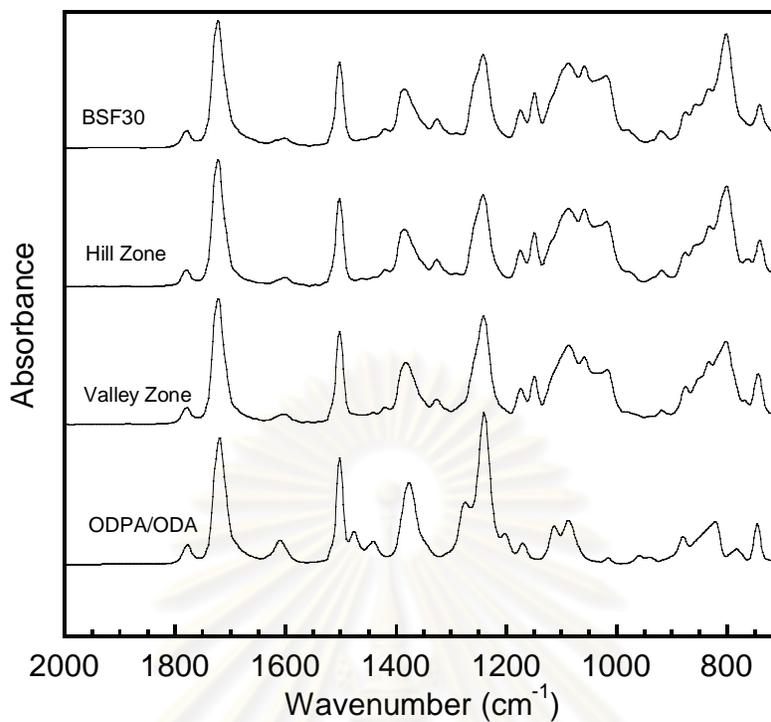
Figure 5.15: Infrared spectra of hill area and valley area on the air-exposed surface of ODPA/ODA-BSF30 blends at 30 phr in comparison with those of pure polyimide and BSF30.
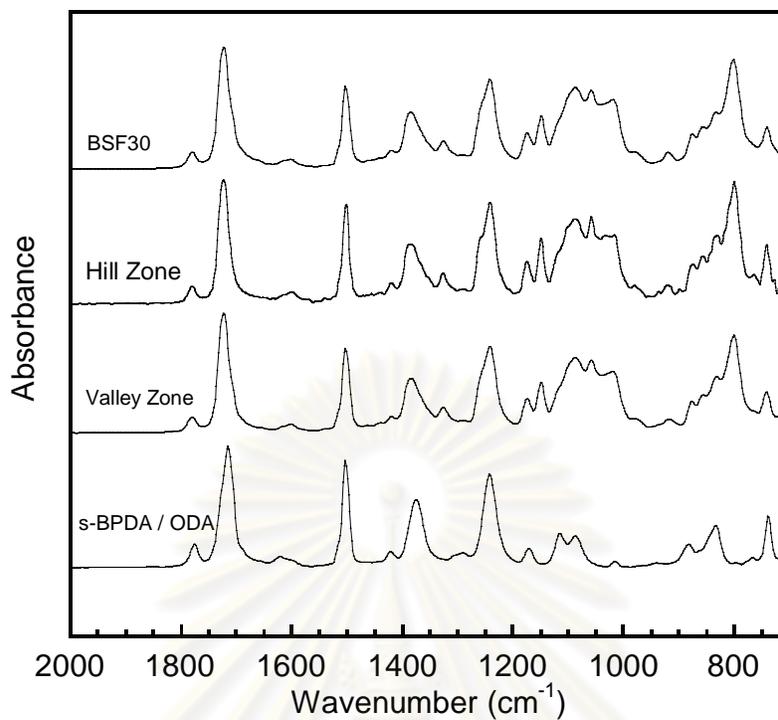
Figure 5.16: Infrared spectra of hill area and valley area on the air-exposed surface
of s-BPDA/ODA-BSF30 blends at 30 phr in comparison with those
of pure polyimide and BSF30.
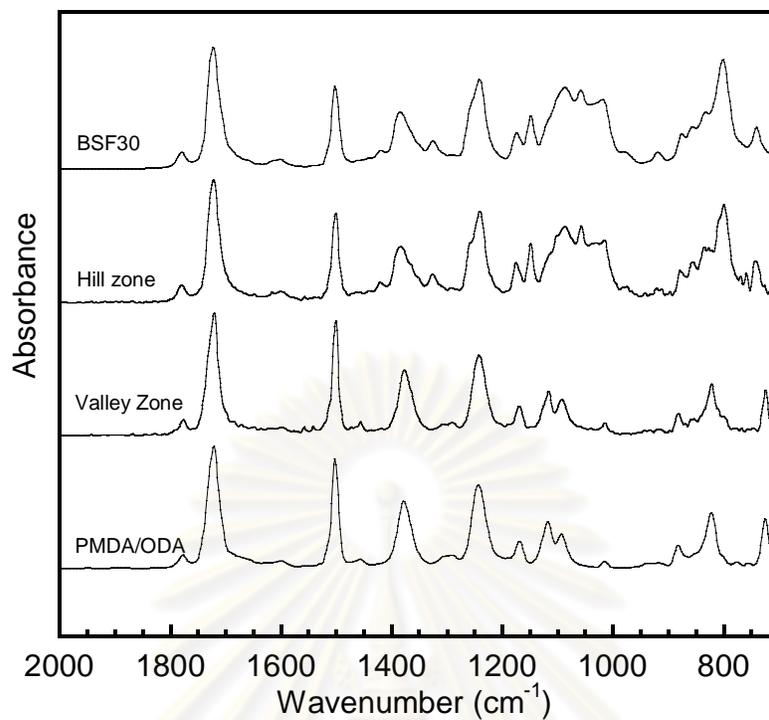
Figure 5.17: Infrared spectra of hill area and valley area on the air-exposed surface of PMDA/ODA-BSF30 blends at 30 phr in comparison with those of pure polyimide and BSF30.
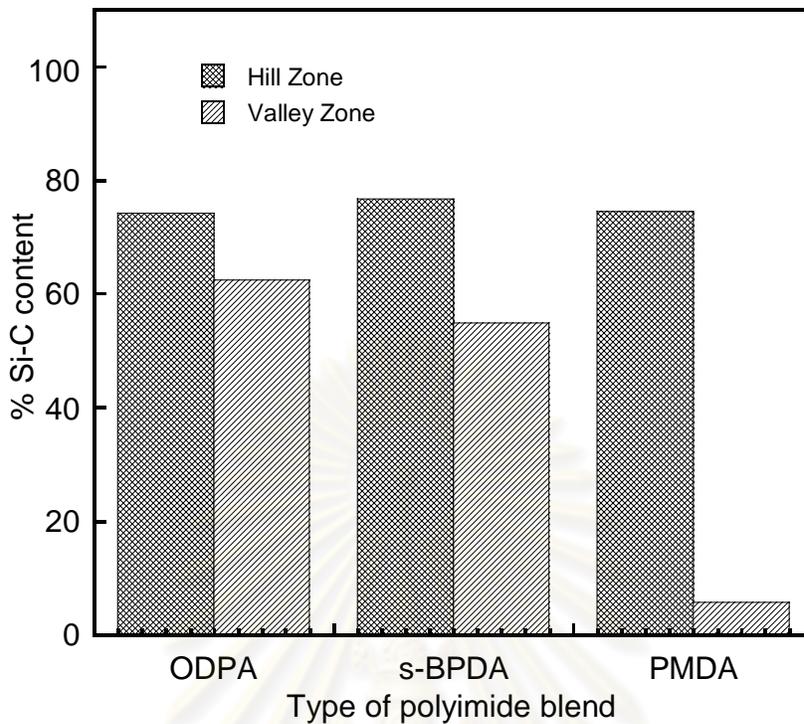
Figure 5.18: Comparison of %Si-C content on the hill area and valley area of
polyimide-BSF30 blends at 30 phr.
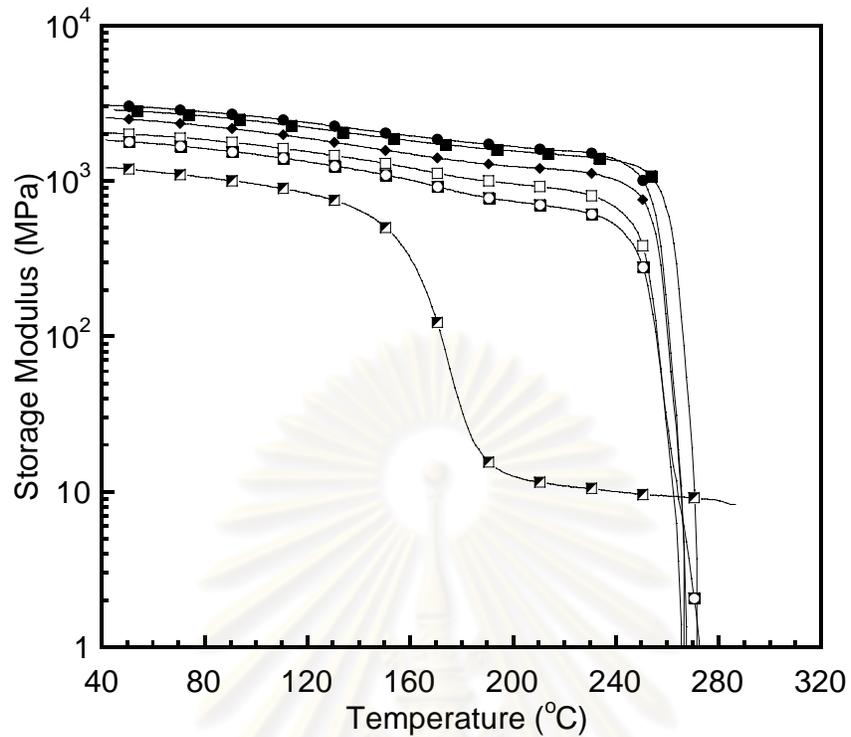
Figure 5.19a: Storage modulus of ODPA/ODA blends at various

BSF30 contents: (●) ODPA/ODA, (■) 1 phr, (♦) 3 phr,

(□) 10 phr, (◨) 30 phr, (◩) BSF30.

ศูนย์วิทยทรัพยากร

จุฬาลงกรณ์มหาวิทยาลัย
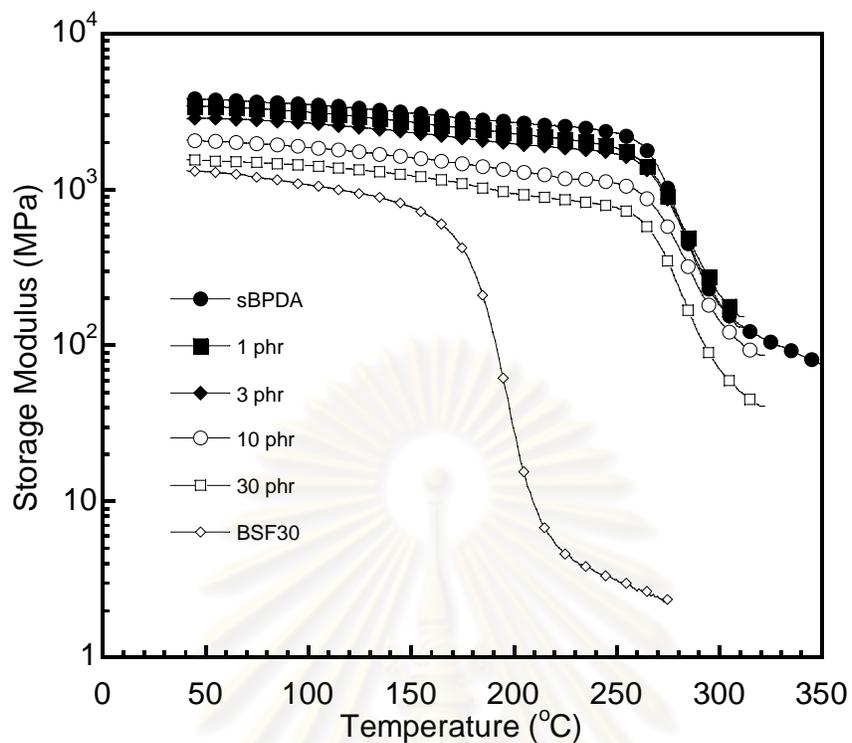
Figure 5.19b: Storage modulus of s-BPDA/ODA blends at various
BSF30 contents: (●) s-BPDA/ODA, (■) 1 phr, (♦) 3 phr,
(○) 10 phr, (□) 30 phr, (◊) BSF30.
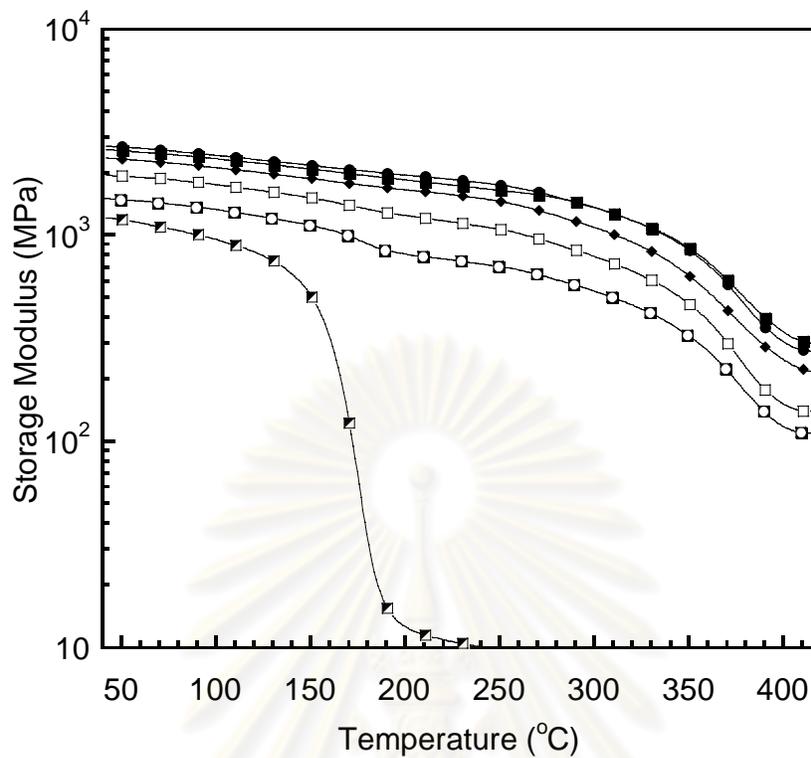
Figure 5.19c: Storage modulus of PMDA/ODA blends at various BSF30
contents: (●) PMDA/ODA, (■) 1 phr, (♦) 3 phr, (□) 10 phr, (▣) 30 phr,
(◪) BSF30.
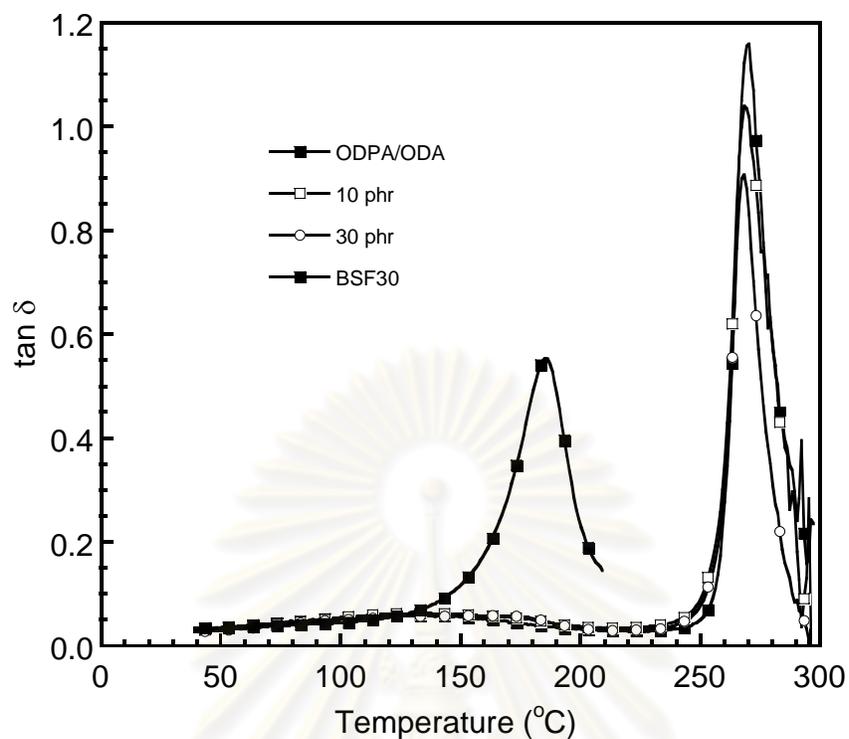
Figure 5.20a: Loss tangent of ODPA/ODA blends at various BSF30 contents.
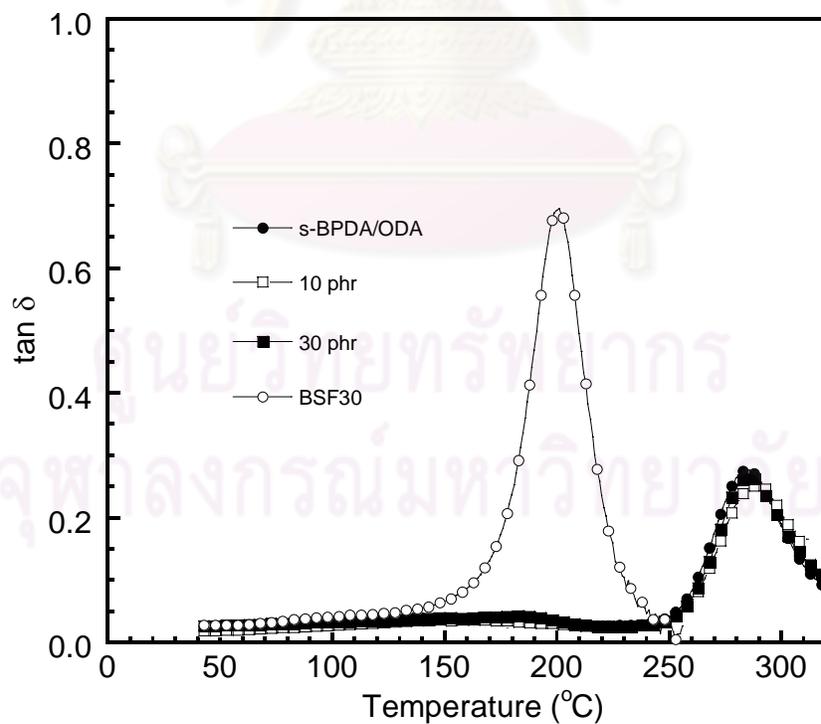
Figure 5.20b: Loss tangent of s-BPDA/ODA blends at various BSF30 contents.
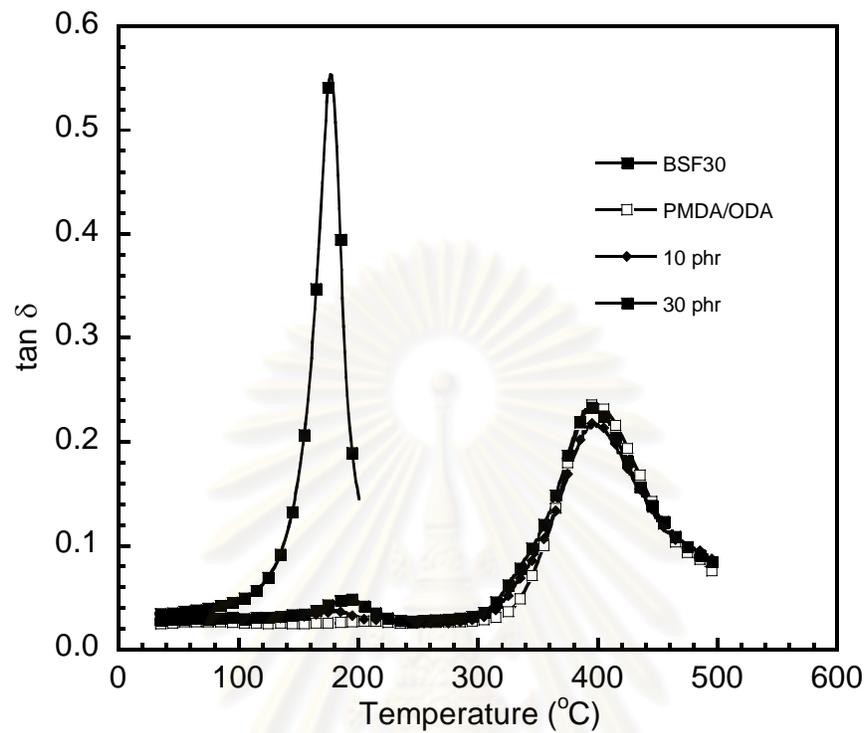
Figure 5.20c: Loss tangent of PMDA/ODA blends at various BSF30 contents.

ศูนย์วิทยทรัพยากร
จุฬาลงกรณ์มหาวิทยาลัย
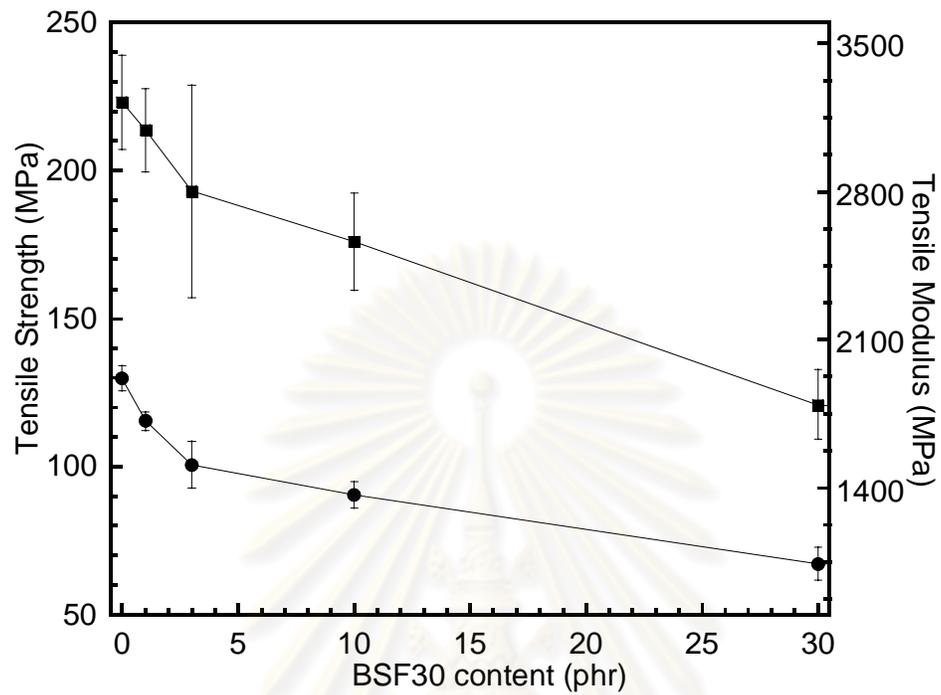
Figure 5.21a: Tensile properties of ODPA/ODA-BSF30 blends: (■) Tensile

Modulus, (●) Tensile Strength; (●) Tensile Strength; Modulus of pure

BSF30 = 1.30 GPa, Strength of pure BSF30 = 52 MPa.
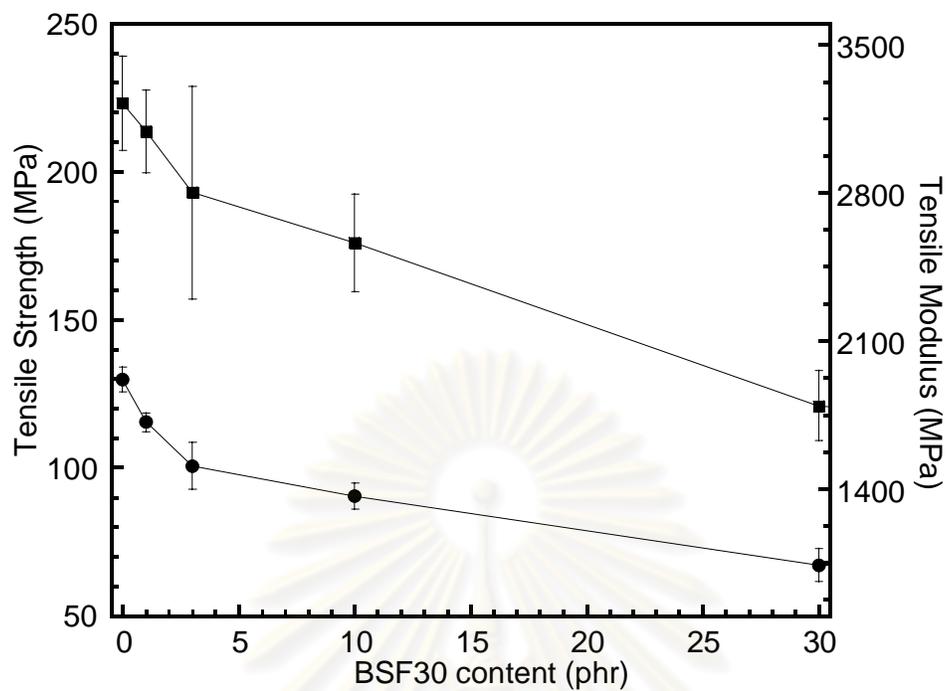
Figure 5.21b: Tensile properties of the s-BPDA/ODA blends: (■) Tensile Modulus, (●) Tensile Strength; (●) Tensile Strength; Modulus of pure BSF30 = 1.30 GPa, Strength of pure BSF30 = 52 MPa.
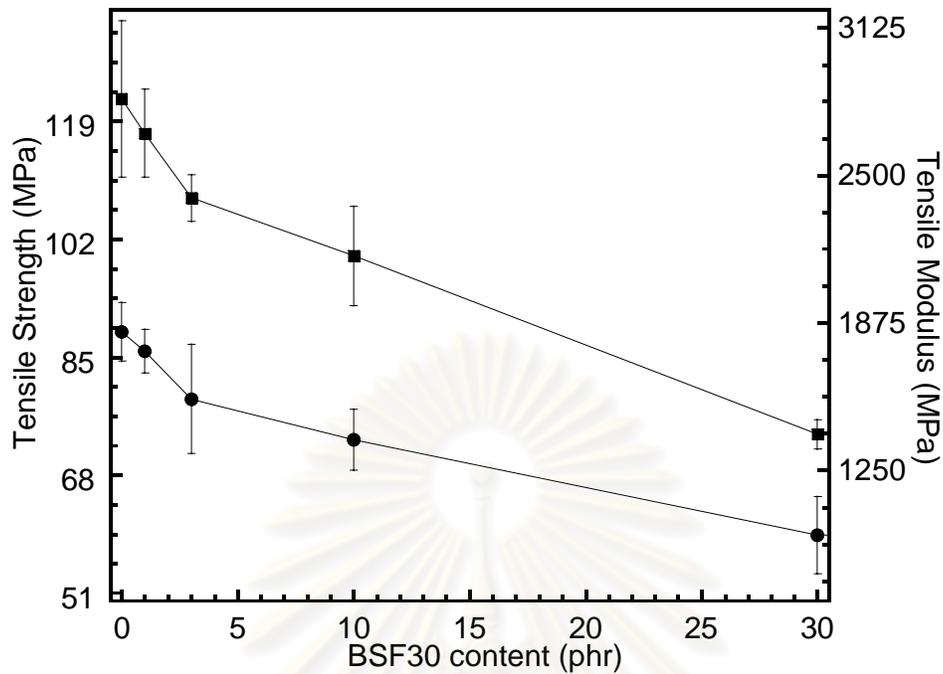
Figure 5.21c: Tensile properties of the PMDA/ODA blends: (■) Tensile Modulus,

(●) Tensile Strength; Modulus of pure BSF30 = 1.30 GPa, Strength of

pure BSF30 = 52 MPa.
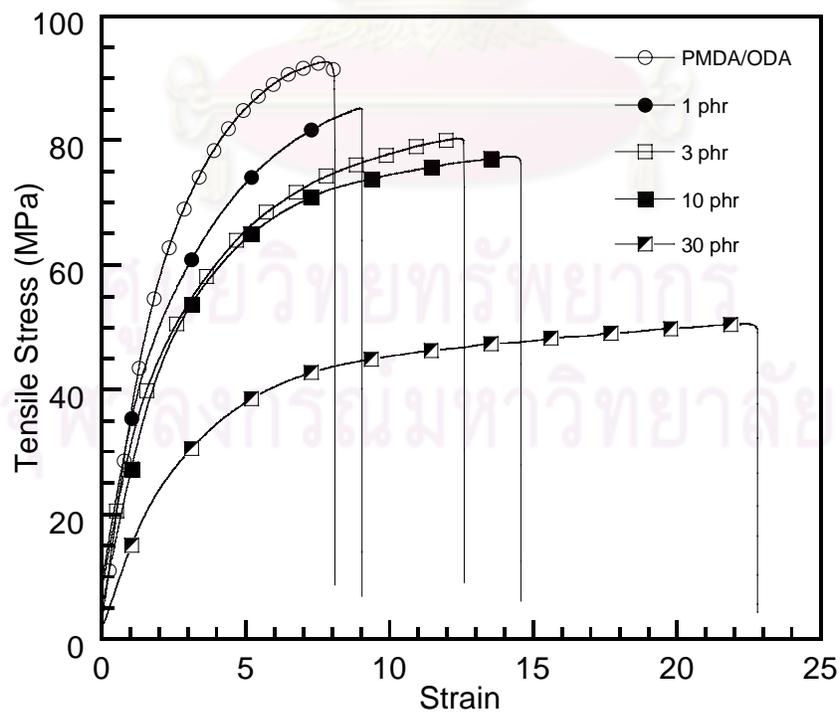
Figure 5.22: Stress-strain curves of the PMDA/ODA blends.
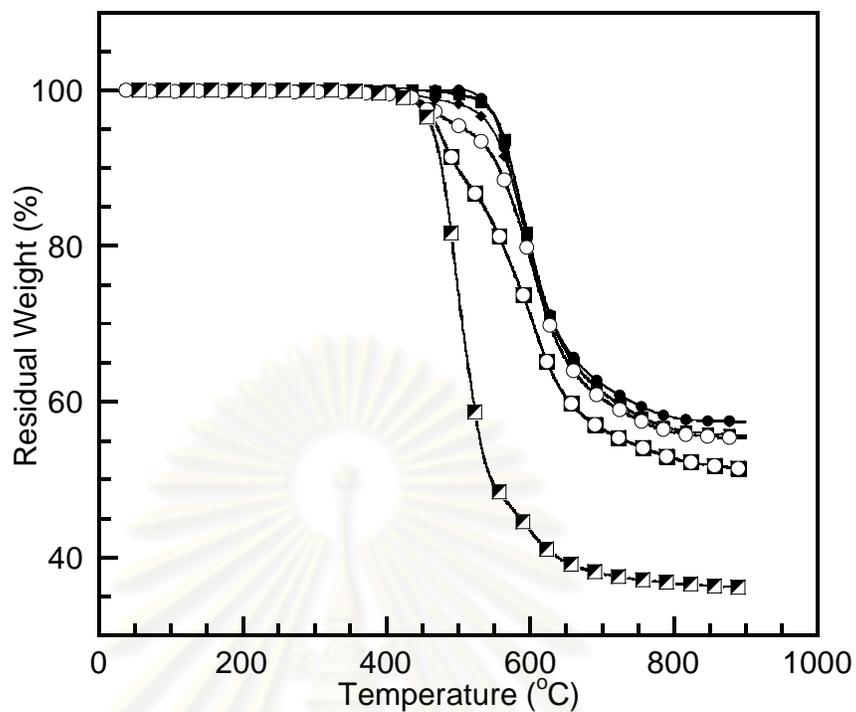
Figure 5.23a: TGA thermograms of ODPA/ODA blends at various BSF30 contents:

(●) ODPA/ODA, (■) 1 phr, (♦) 3 phr, (□) 10 phr, (▣) 30 phr, (◪) BSF30.

Figure 5.23b: TGA thermograms of s-BPDA/ODA blends at various BSF30

contents: (●) s-BPDA/ODA, (■) 1 phr, (♦) 3 phr, (□) 10 phr,

(▣) 30 phr, (◩) BSF30.

Figure 5.23c: TGA thermograms of PMDA/ODA blends at various BSF30 contents:

(●) PMDA/ODA, (■) 1 phr, (♦) 3 phr, (□) 10 phr, (▣) 30 phr,

(◪) BSF30.

Figure 5.24a: Appearance of ODPA/ODA-BSF30 Films.
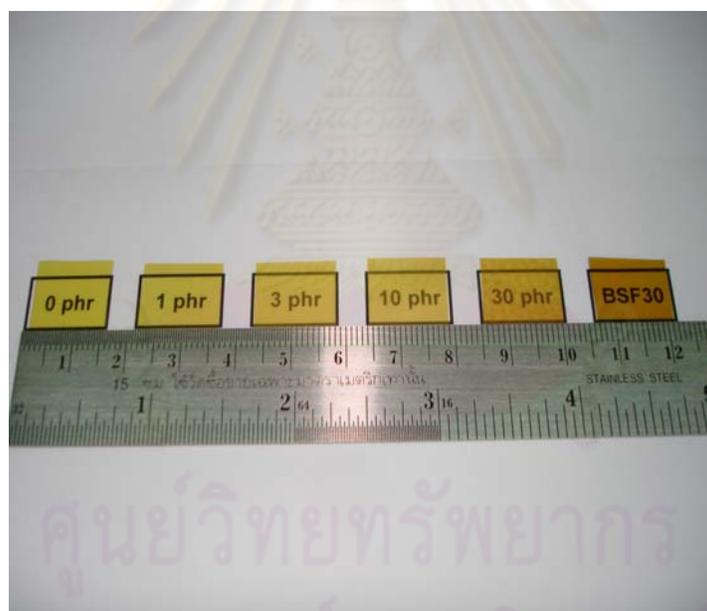
Figure 5.24b: Appearance of s-BPDA/ODA-BSF30 Films.

Figure 5.24c: Appearance of PMDA/ODA-BSF30 Films.
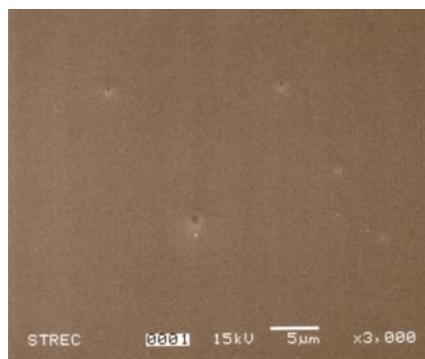
a) ODPA/ODA + 30 phr BSF30
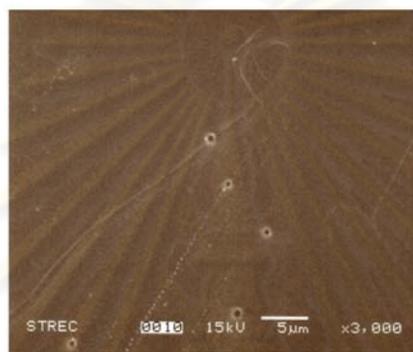
b) s-BPDA/ODA + 30 phr BSF30
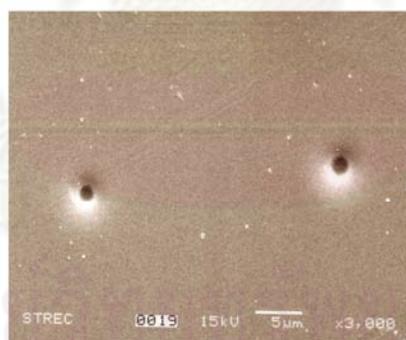
c) PMDA/ODA + 30 phr BSF30

Figure 5.25: SEM micrographs of the polyimide-BSF30 blends at 30 phr (hill zone).

CHAPTER VI

CONCLUSIONS

The surface segregation behavior of the blends between BSF30 and three polyimides (ODPA/ODA, s-BPDA/ODA, and PMDA/ODA) with different chain flexibility was investigated by using various measurement techniques, i.e. from contact angle, surface profilometer, ATR-FTIR, and ATR microscope. Because of the lower surface tension of the BSF30 fraction compared to the three polyimide fraction, surface segregation of the BSF30 was found in all blend compositions. These results are attributed to the low surface tension of the siloxane moieties in the BSF30 (21-22 dyne/cm), which tended to migrate to the air-polymer interface and form a siloxane-enriched surface. In comparison among the surface tension values on glass-exposed surface of the blends, the ODPA/ODA system renders the lowest value (29.3 dyne/cm) which is close to that of the s-BPDA/ODA blend (29.9 dyne/cm), while the PMDA/ODA blend possesses the highest values (32.8 dyne/cm). The difference between polyimide and BSF30 indicates the degree of segregation, i.e. the blends between PMDA/ODA and BSF30 possibly provides the greatest degree of segregation. This hypothesis was proven by the results of surface profilometer that showed the greatest roughness of the surface of PMDA/ODA blend at 30 phr. Furthermore, the results from ATR microscope indicate that a large difference between silicone content on the hill area and valley area on the air-exposed surface of PMDA/ODA blends at 30 phr was found, while that difference for the ODPA/ODA blends is lower than that of s-BPDA/ODA blends. The degree of segregation can be shown as follows: PMDA/ODA blends > s-BPDA/ODA blends > ODPDA/ODA blends. From the results from surface profilometer, it can be additionally concluded that the more content of BSF30 leads to the greater degree of segregation.

REFERENCES

Andre, S.; Guida-Pietrasanta, F.; Rousseau, A.; and Boutevin , B. Novel synthesis of polyimide-polyhybridsiloxane block copolymers via polyhydrosilylation: Characterization and physical properties. J. Polym. Sci., Part A: Polym. Chem. 39 (2001): 2414-2425.

Arnold, C. A., Summers, J. D., Chen, Y. P., Yoon, T. H., McGrath, B. E., Chen, D., and McGrath, J.E., Polyimides: Materials, Chemistry and Characterization. Amsterdam: Elsevier Science Publishers B.V., 1989.

Banks, B. A. and Denko, R. Proc. SAMPE 2002, May 12-16, 2002, Long Beach, California.

Bowens, A. D. Synthesis and Characterization of Poly(siloxane imide) Block Copolymers and End-Functional Polyimides for Interphase Applications. Doctoral dissertation, Chemistry, Virginia Polytechnic Institute and State University, 1999.

Chen, J. and Gardella. J. A. Solvent Effects on the Surface Composition of Poly(dimethylsiloxane) – co – Polystyrene / Polystyrene Blends. Macromolecules 31 (1998): 9328-9336.

Chen, X. and Gardella, J. A. Surface Modification of Polymers by Blending Siloxane Block Copolymers. Macromolecules 27 (1994): 3363-3369.

Chen, X.; Gardella, J. A.; and Kumler, P. L. Surface Morphology Studies of Multiblock and Starblock Copolymers of Poly(α-methy1styrene) and Poly(dimethylsi1oxane). Macromolecules 26 (1993): 3778-3783.

Cho, S. H.; Kim, S. H.; Lee, J. G.; and Lee, N. E. Micro-scale Metallization of High Aspect-ratio Cu and Au Lines on Flexible Polyimide Substrate by Electroplating Using SU-8 Photoresist Mask. Microelectron. Eng. 77 (2005): 116-124.

Cowie, J. M. G. and Lath, D., " Miscibility mapping in some blends involving poly(styrene-co-acrylonitrile)", Makromol. Chem., Macromol. Symp., 16 (1988): 103-112.

Dunson, D. L. Synthesis and Characterization of Thermosetting Polyimide Oligomers for Microelectronics Packaging. Doctoral dissertation, Chemistry, Virginia Polytechnic Institute and State University, 2000.

Furukawa, N.; Yamada, Y.; Furukawa, M.; Yuasa, M.; and Kimura, Y. Surface and Morphological Characterization of Polysiloxane-Block-Polyimide. J. Polym. Sci., Part A: Polym. Chem. 35 (1997): 2239-2251.

Ghosh, M. K., and Mittal, K. L., eds. Polyimides Fundamentals and Applications. New York: Marcel Dekker, 1996.

Hayashi, M.; Ribbe, A.; Hashimoto, T.; Weber, M.; and Heckmann, W. The Influence of Wettability on the Morphology of Blends of Polysulfones and Polyamides. Polymer 39 (1998): 299-308.

Hergenrother, P. M.; Watson, K.A.; Smith, J. G.; Connell, J. W.; and Yokota, R. Polyimides from 2,3,3',4'-Biphenyltetracarboxylic Dianhydride and Aromatic Diamines. Polymer 43 (2002): 5077-5093.

Hsiao, S. H. and Chen, Y. J. Structure–Property Study of Polyimides Derived from PMDA and BPDA Dianhydrides with Structurally Different Diamines. European Polymer Journal 38 (2002): 815-828.

Inoue, H.; Matsumoto, A.; Matsukawa, K.; Ueda, A.; and Nagai, S. J. Appl. Polym. Sci. 41 (1990); 1815. Cite in Spanos, C. G.; Ebbens, S. J.; Badyal, J. P. S.; Goodwin, A. J.; and Merlin, P. J. Surface Segregation and Plasma Oxidation of Polyethylene-Poly(dimethylsiloxane) Copolymer Doped Polyethylene Films. Macromolecules 36 (2003): 368-372.

Jeffry, A.H.; James F.D.; Feuz L.; Klinedinst D., Technical Memorandum of NASA Langley Research Center Hampton, 10 (1999).

Kano, Y.; Inoue, M.; Akiba, I.; Akiyama, S.; Sano, H.; and Fujita, Y. Effect of Substrate on Gradient Domain Morphology Formed in Acrylate Copolymer/Fluoro-copolymer Blends. Polymer 39 (1998): 6747-6745.

Kealbe, D. H. Phsical Chemistry of Adhesion. n.p.: John Wiley and Sons, 1971.

Kim, Y. S.; Yang, J.; Wang, S.; Banthia, A. K.; and McGrath, J. E. Surface and Wear Behavior of Bis-(4-hydroxyphenyl) Cyclohexane (bis-Z) Polycarbonate/Polycarbonate–Polydimethylsiloxane Block Copolymer Alloys. Polymer 43 (2002): 7207-7217.

Kinloch, A. J. Adhesion and adhesives: science and technology, London: Chapman and Hall, 1987.

Li, X.; Han, Y.; and An, L. Surface Morphology Control of ImmisciblePolymer-blend Thin Films. Polymer 44 (2003): 8155-8165.

Licari, J. J., and Hughes, L. A. Handbook of Polymer Coatings for Electronics Chemistry, Technology and Applications, New Jersey: Noyes Publications, 1990.

Ohya, H.; Kudryavtsev, V. V.; and Semenova, S. I. Polyimide Membranes. Tokyo: Kodanaha, 1996.

Olabisi, O., Handbook of Thermoplastics. New York: Marcel Dekker Inc., 1997.

Owen, M. J. Surface Chemistry and Applications. In Clarson, S. J. and Semlyen, J. A. (eds.), Siloxane Polymers, pp. 309-372. New Jersey: PRT Prentice Hall, 1993.

Painter, P. C. and Coleman, M. M. Fundamentals of polymer science. Technomic, Lancaster, USA, 1994.

Polk, W. D. Polydimethylsiloxane Containing Block Copolymers: Synthesis and Characterization of Alternating Poly(arylene Ether Phosphene Oxide)-b-Siloxane and Segmented Nylon 6,6–b-Siloxane Copolymers. Doctoral dissertation, Chemistry, Virginia Polytechnic Institute and State University, 2001.

Rimdusit, S.; Benjapan, W.; Assabumrungrat, S.; Takeichi, T.; Yokota, R. P Surface segregation of siloxane containing component in polysiloxane-*block*-polyimide and *s*-BPDA/ODA polyimide blends Polymer Engineering and Science., 47 (2007): 489 - 498.

Rimdusit, S. and Yokota, R. Atomic Oxygen Protections in Polymeric Systems: A Review. J. Space Techn. Sci. 18 (2002): 34-48.

Silverman, E.M. Environmental Effects on Spacecraft: LEO Materials Selection Guide NASA Contractor Report 4661 Part 1 and Part 2 (1995).

Smith, B. C, Fundamentals of Fourier Transform Infrared Spectroscopy, CRC Press, Washington, D.C, 1999.

Smith, G. L.; DeSimone, S. D.; Huang, J. M.; York, H.; Dwight, G.; Wilkes, D. W.; and McGrath, J. E. Synthesis and Characterization of Poly(methyl methacrylate)-g-poly(dimethylsiloxane) Copolymers. 1.

Bulk and Surface Characterization. Macromolecules 25 (1992): 2575-2581.

Spanos, C. G.; Ebbens, S. J.; Badyal, J. P. S.; Goodwin, A. J.; and Merlin, P. J. Surface Segregation and Plasma Oxidation of Polyethylene-Poly(dimethylsiloxane) Copolymer Doped Polyethylene Films. Macromolecules 36 (2003): 368-372.

Strobl, G. R. The Physics of Polymers: concepts for understanding their structures and behaviours. Berlin: Springer Verlag, 1997.

Tanaka, K.; Takahara, A.; and kajiyama, T. Film Thickness Dependence of the Surface Structure of Immiscible Polystyrene/Poly(methyl methacrylate) Blends. Macromolecules 29 (1996): 3232-3239.

Tsujita, Y. Gas sorption and permeation of glassy polymers with microvoids. Prog. Polym. Sci. 28 (2003) 1377-1401.

Tiptipakorn, S.; Damrongsakkul, S.; Ando, S.; Hemvichian, K., and Rimdusit, S. Thermal degradation behaviors of polybenzoxazine and silicon-containing polyimide blends. Polym Degrad Stab 92, 7 (2007): 1265-1278.

Tiwari, A. and Nema, S. K. Synthesis, Characterization, Physicochemical and Dielectric Properties of Siloxane, Polyimide and Their Blends. Mat. Res. Innovant 7 (2003): 133-143.

Tiwari, A.; Nema, S. K.; Das, C. K.; and Nema, S. K. Thermal Analysis of Polysiloxanes, Aromatic Polyimide and Their Blends. Thermochimica Acta 417, (2004): 133-142.

Ton-That, C.; Shard, A. G.; Teare, D. O. H.; and Bradley, R. H. XPS and AFM surface studies of solvent-cast PS/PMMA blends. Polymer 42 (2001): 1121-1129.

Walheim, S.; Boltau, M.; Mlynek, J.; Krausch, G.; and Steiner, U. Structure Formation via Polymer Demixing in Spin-Cast Films. Macromolecules 30 (1997): 4995-5003.

Wen, J.; Somorjai, G.; Lim, F.; and Ward, R. XPS Study of Surface Composition of a Segmented Polyurethane Block Copolymer Modified by PDMS End

Groups and Its Blends with Phenoxy. <u>Macromolecules</u> 30 (1997): 7206-7213.

Willson, D., Stenzenberger, H. D., and Hergenrother, P. M., eds. <u>Polyimides</u>. London: Blackie & Son Ltd, 1990.

Winesett, D. A.; Ade, H.; Sokolov, J.; Rafailovich, M.; and Zhu, S. Substrate Dependence of Morphology in Thin Film Polymer Blends of Polystyrene and Poly(methyl methacrylate). <u>Polym. Inter.</u> 49 (2000): 458-462.

Wu, S. <u>Polymer Interface and Adhesion</u>, New York: Marcel Dekker, 1982.

Yamada,Y. Siloxane Modified Polyimides for Microelectronics Coating Applications. <u>High Perform. Polym</u> 10 (1998): 69-80.

Yokota, R. J. Recent Trends and Space Applications of Polyimides. <u>Journal of Photopolymer Science and Technology</u> 12 (1999): 209-216.

Zisman, W. A., Jarvis, N. L., and Fox, R. B. <u>Contact Angle, Wettability and Adhesion. Advances in chemistry series 43</u>. Washington D.C.: American Chemical Society, 1964, p. 317. Cite in Bowens, A. D. <u>Synthesis and Characterization of Poly(siloxane imide) Block Copolymers and End-Functional Polyimides for Interphase Applications</u>. Doctoral dissertation, Chemistry, Virginia Polytechnic Institute and State University, 1999.

APPENDICES

Appendix A

Beer-Lambert's Law

In addition to chemical structures, infrared spectra can provide quantitative information as well, such as the concentration of a molecule in a sample. the basis of all quantitative analyses in FTIR is Beer's law, which relates concentration to absorbance, and has the following form [Smith, 1999]:

$$A = \varepsilon\, l\, c$$

where:

A = Absorbance

ε = Absorptivity (the proportionality constant)

l = Pathlength

c = Concentration
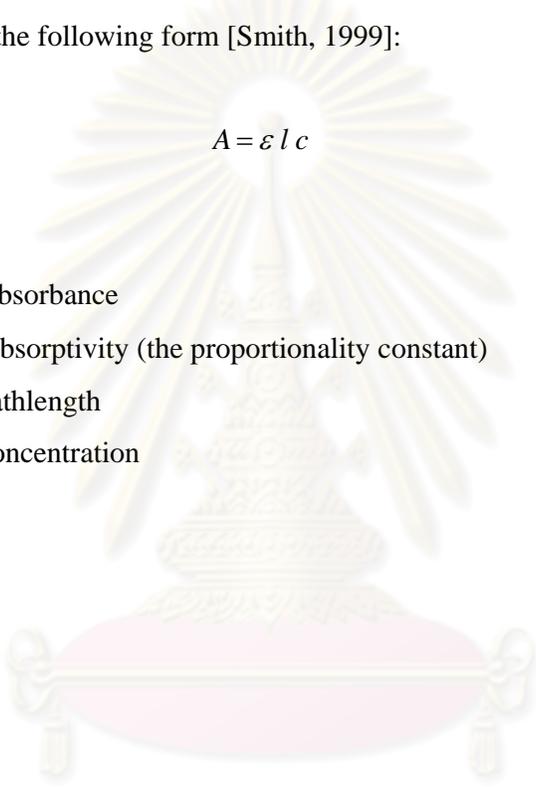
Appendix B

Thermal Degradation Behaviors of Polybenzoxazine and Silicon-containing Polyimide Blends

The blending of BSF30 and polybenzoxazine has been a topic of interesting because the system possesses some synergistic behaviors such as char yield. The thermal degradation behavior of BSF30 was studied and reported in this appendix [Tiptipakorn et al., 2007].

Thermal degradation behaviors of polybenzoxazine and silicon-containing polyimide blends

Sunan Tiptipakorn [a], Siriporn Damrongsakkul [a], Shinji Ando [b], Kasinee Hemvichian [c], Sarawut Rimdusit [a],*

[a] *Department of Chemical Engineering, Faculty of Engineering, Chulalongkorn University, Pathumwon, Bangkok 10330, Thailand*
[b] *Department of Chemistry and Material Sciences, Graduate School of Science and Engineering, Tokyo Institute of Technology, Ookayama, Meguro-ku, Tokyo 152-8552, Japan*
[c] *Chemistry and Material Science Research Program, Office of Atoms for Peace, 16 Vibhavadi Rangsit Road, Chatuchak, Bangkok 10900, Thailand*

Abstract

Thermal behaviors of polymer blends between common-type polybenzoxazine (PBA-a) and polysiloxane-*block*-polyimide (SPI) were studied using Dynamic Mechanical Analysis (DMA) and Thermogravimetric Analysis (TGA). The polymer blends showed only one glass-transition temperature (T_g) that increased as the content of SPI increased. Synergistic behavior in the char formation of the alloys was clearly observed. The DTG curves showed three stages and two stages of decomposition reaction in neat PBA-a and SPI, respectively. For the blending systems with 25 wt%, 50 wt%, and 75 wt% of SPI, the DTG thermograms of the blends exhibited four stages of thermal decomposition reaction. The apparent activation energies (E_a) of each step were determined using Kissinger method, Flynn–Wall–Ozawa method and Coats–Redfern method. The type of solid state mechanism was determined by Criado method. From the calculation, the solid state thermal degradation mechanism is proposed to be F1 (random nucleation with one nucleus on the individual particle) type for PBA-a, SPI, and their blends.
© 2007 Elsevier Ltd. All rights reserved.

Keywords: Polybenzoxazine; Silicon-containing polyimide; Kinetics; Degradation; Char yield

1. Introduction

Polymer blends between polybenzoxazines and other polymers have been a subject of many current investigations, which aim to utilize some outstanding properties of polybenzoxazines. Polybenzoxazines are particularly applied to improve the processability, mechanical, and adhesion properties of the resulting resin mixtures. They can be synthesized via a simple and cost-competitive solventless technology [1]. Moreover, their molecular design flexibility provides wide range of properties that can be tailor-made. The polymers have been reported to possess many intriguing properties such as high mechanical properties, high char yield, near zero shrinkage, low water absorption, excellent electrical properties, low melt viscosity, self-polymerized upon heating, and no by-products during curing [2].

Although there were many studies about this family of the polymers, little is known about the thermal degradation of polybenzoxazine. Hemvichian et al. [3] studied the degradation process of polybenzoxazine in common type (PBA-a) by using TGA and GC–MS. They identified the structures of pyrolysis products. However, the solid state thermal degradation mechanism and kinetics study of PBA-a have not been studied before.

In general, the approaches for improving the performance of polybenzoxazine can be classified into two ways. One is

* Corresponding author. Tel.: +66 2 218 6862; fax: +66 2 218 6877.
E-mail address: sarawut.r@chula.ac.th (S. Rimdusit).

the structure modification of benzoxazine monomers; the other is the formation of composites or blends with other high-temperature polymers like polyimide [4] as well as with inorganic fillers such as clay [5] and metal oxide [6]. The blend of poly-siloxane-*block*-polyimide (SPI) is proposed to enhance the PBA-a properties in this study.

Many researches [7–9] revealed that polysiloxane-*block*-polyimide (SPI) has a number of attractive characteristics, i.e. low moisture sorption, excellent thermal stability, and lower dielectric constant. Furthermore, this kind of block co-polymer is reported to increase the flexibility of the materials. Therefore, the thermal degradation of the blends between polybenzoxazine and polysiloxane-*block*-polyimide (SPI) is worthy to investigate.

In this research, we prepared polymer blends of PBA-a and SPI. The glass-transition temperatures and thermal characteristic were determined by Differential Scanning Calorimetry (DSC), Dynamic Mechanical Analysis (DMA), and Thermal Gravimetric Analysis (TGA). The thermal degradation kinetic parameters, activation energy (E_a) and pre-exponential factor (A), were evaluated by using three well-known methods, i.e. Kissinger method, Flynn–Wall–Ozawa method, and Coats–Redfern method. Kissinger method and Flynn–Wall–Ozawa method were used in this study because they are mostly used in the literatures and can be used without prior knowledge of reaction mechanism. Additionally, Coats and Redfern method was used because it renders the degradation parameters such as E_a, A, and possible reaction mechanism. The thermal degradation mechanism of PBA-a, SPI, and the blend was also evaluated by using Criado method.

2. Theoretical consideration

Generally for polymer degradation, it is assumed that the rates of conversion are proportional to the concentration of reacted material. The rate of conversion can be expressed by the following basic rate equation

$$\frac{d\alpha}{dt} = kf(\alpha) \tag{1}$$

For thermogravimetric analysis, the fraction of decomposition (α) is defined as the ratio of weight loss at time t to total weight loss at complete decomposition temperature as shown in Eq. (2).

$$\alpha = \frac{(M_o - M_t)}{(M_o - M_f)} \tag{2}$$

where M_t is the weight of the sample at time t; M_o is the initial weight of the sample and; M_f is the final weight of the completely decomposed sample.

It is assumed that k follows the Arrhenius equation.

$$k = A \exp(- E_a/RT) \tag{3}$$

Substituting "k" from Eq. (3) into Eq. (1) one obtains:

$$\frac{d\alpha}{dt} = A \exp(- E_a/RT)f(\alpha) \tag{4}$$

According to non-isothermal kinetic theory, thermal degradation at a constant heating rate, β

$$\beta = dT/dt \tag{5}$$

can be expressed by Eq. (6)

$$\frac{d\alpha}{dT} = \frac{A}{\beta} \exp(- E_a/RT)f(\alpha) \tag{6}$$

where $f(\alpha)$ is the differential expression of a kinetic model function, α is the conversion, β is the heating rate (K min^{-1}), E_a and A are the so-called activation energy (kJ/mol) and pre-exponential factor (min^{-1}) for the decomposition reaction, respectively. R is the gas constant (8.314 J mol^{-1} K^{-1}).

Generally, E_a can be calculated by using three well-known methods for dynamic heating experiment, i.e. Kissinger method, Flynn–Wall–Ozawa method, and Coats–Redfern method [10–12].

2.1. Kissinger method (differential method) [12–15]

Kissinger method uses Eq. (7) to determine the E_a of solid state reactions.

$$\ln\left(\frac{\beta}{T_P^2}\right) = \ln\frac{AR}{E_a} + \ln\left[n\left(1 - \alpha_p\right)^{n-1}\right] - \frac{E_a}{RT_p} \tag{7}$$

where T_p and α_p are the absolute temperature and weight loss at maximum weight-loss rate $(d\alpha/dt)_p$, respectively, and n is the reaction order. From the slope of the straight line $\ln(\beta/T_p^2)$ versus $1/T_p$, the E_a can be obtained. The advantage of the Kissinger model is that the E_a can be obtained without the knowledge of any thermal degradation reaction mechanism in advance.

2.2. Flynn–Wall–Ozawa method (integration method) [11–16]

Flynn–Wall–Ozawa method can be employed to quantify E_a without any knowledge of the reaction mechanisms. The main advantage of this method is that it is not based on any assumption concerning the temperature integral, giving, thus, a higher degree of precision to the results.

From Eq. (6), it can be integrated using the Doyle approximation [17,18]. The result of the integration after taking logarithms is

$$\log \beta = \log \frac{AE_a}{g(\alpha)R} - 2.315 - \frac{0.457E_a}{RT} \tag{8}$$

The E_a of the thermal degradation process of the blending system was determined from the slope of the straight line $\log \beta$ versus $1/T$.

2.3. Coats−Redfern method [10,11,23]

Besides the above two methods, Coats−Redfern method is often used in kinetic analysis of solid state processes. Coats−Redfern method is presented in Eq. (9).

$$\ln\frac{g(\alpha)}{T^2} = \ln\left(\frac{AR}{\beta E_a}\right) - \frac{E_a}{RT} \tag{9}$$

From the slope of the straight line $\ln[(g(\alpha))/T^2]$ versus $1/T$, E_a can be calculated and A can be obtained from the intercept, i.e. from $\ln(AR/\beta E_a)$.

2.4. Criado method [19−21]

The degradation reaction mechanism can be determined using Criado method [19]. Criado et al. [19] proposed a method which can accurately determine the reaction mechanism in the solid reaction process.

Criado et al. defined a type of $Z(\alpha)$ function

$$Z(\alpha) = \frac{\left(\dfrac{d\alpha}{dt}\right)}{\beta}\pi(x)T \tag{10}$$

where $x = E_a/RT$ and $\pi(x)$ is an approximate expression obtained by integration against temperature, which cannot be expressed by simple analysis formulas, Paterson [22] proposed a reasonable relationship between $\pi(x)$ and $P(x)$ as shown in Eq. (11).

$$\pi(x) = x\,e^x P(x) \tag{11}$$

Senum and Yang [23] proposed the fourth rational expression of $P(x)$

$$P(x) = \frac{e^{-x}}{x}\frac{x^3 + 18x^2 + 86x + 96}{x^4 + 20x^3 + 120x^2 + 240x + 120} \tag{12}$$

when $x > 20$, the error of Eq. (15) is less than $10^{-5}\%$, which is the basis we use in this paper.

Combining Eqs. (1), (10) and (11), we can obtain:

$$Z(\alpha) = f(\alpha)g(\alpha) \tag{13}$$

From Eqs. (1), (10) and (11), the following relationship can be derived:

$$Z(\alpha) = \frac{d\alpha}{dT}\frac{E_a}{R}e^{E_a/RT}P(x) \tag{14}$$

Eq. (13) is used to plot the master $Z(\alpha)−\alpha$ curves for different models listed in Table 1 [24], whereas Eq. (14) is used for representing the experimental curve. By comparing these two curves, the mechanism type of the thermal degradation can be identified.

3. Experimental

3.1. Materials

The benzoxazine monomer bis(3-phenyl-3,4-dihydro-2H-1,3-benoxzinyl) isopropane (BA-a) as shown in Fig. 1a was prepared from 2,2′-bis(4-hydroxyphenyl)-propane (Bisphenol-A) with aniline and formaldehyde according to the reported method [25]. Bisphenol-A (commercial grade) provided by Thai Polycarbonate Co., Ltd. (TPCC) was used as received. Para-formaldehyde (AR grade) and aniline (AR grade) were purchased from Merck and APS Finechem Companies. As shown in Fig. 1b, polysiloxane-block-polyimide (SPI) under the trademark of ''BSF30'' with molecular weight of 167,720 was obtained from Nippon Steel Chemical. The ratio of the block components (polysiloxane/polyimide) is 36.8 mol%.

3.2. Synthesis of blends

Polysiloxane-block-polyimide (SPI) was blended with benzoxazine monomers at various weight ratios, i.e. 100:0, 75:25, 50:50, 25:75, and 0:100. The blends were formed in a Teflon mould and dried at 60 °C for 18 h. After that, the thermal treatment was performed at 100 °C (for 1 h), 150 °C (for 1 h), and 200 °C (for 4 h) in a vacuum oven.

Table 1
Algebraic expressions for $g(\alpha)$ and $f(\alpha)$ for the most frequently used mechanisms of solid state processes

Mechanism	$g(\alpha)$	$f(\alpha)$
A$_2$, Nucleation and growth (Avrami equation (1))	$[-\ln(1-\alpha)]^{1/2}$	$2(1-\alpha)[-\ln(1-\alpha)]^{1/2}$
A$_3$, Nucleation and growth (Avrami equation (2))	$[-\ln(1-\alpha)]^{1/3}$	$3(1-\alpha)[-\ln(1-\alpha)]^{2/3}$
A$_4$, Nucleation and growth (Avrami equation (3))	$[-\ln(1-\alpha)]^{1/4}$	$4(1-\alpha)[-\ln(1-\alpha)]^{3/4}$
R$_1$, Phase boundary controlled reaction (one-dimensional movement)	α	1
R$_2$, Phase boundary controlled reaction (contracting area)	$[1-(1-\alpha)^{1/2}]$	$2(1-\alpha)^{1/2}$
R$_3$, Phase boundary controlled reaction (contracting volume)	$[1-(1-\alpha)^{1/3}]$	$3(1-\alpha)^{2/3}$
D$_1$, One-dimensional diffusion	α^2	$(1/2)\alpha^{-1}$
D$_2$, Two-dimensional diffusion (Valensi equation)	$(1-\alpha)\ln(1-\alpha)+\alpha$	$-[\ln(1-\alpha)]^{-1}$
D$_3$, Three-dimensional diffusion (Jander equation)	$[1-(1-\alpha)^{1/3}]^2$	$(3/2)[1-(1-\alpha)^{1/3}]^{-1}(1-\alpha)^{2/3}$
D$_4$, Three-dimensional diffusion (Ginstling Brounshtein equation)	$[1-(2/3)\alpha]-(1-\alpha)^{2/3}$	$(3/2)[1-(1-\alpha)^{1/3}]^{-1}$
F$_1$, Random nucleation with one nucleus on the individual particle	$-\ln(1-\alpha)$	$1-\alpha$
F$_2$, Random nucleation with two nuclei on the individual particle	$1/(1-\alpha)$	$(1-\alpha)^2$
F$_3$, Random nucleation with three nuclei on the individual particle	$1/(1-\alpha)^2$	$(1/2)(1-\alpha)^3$
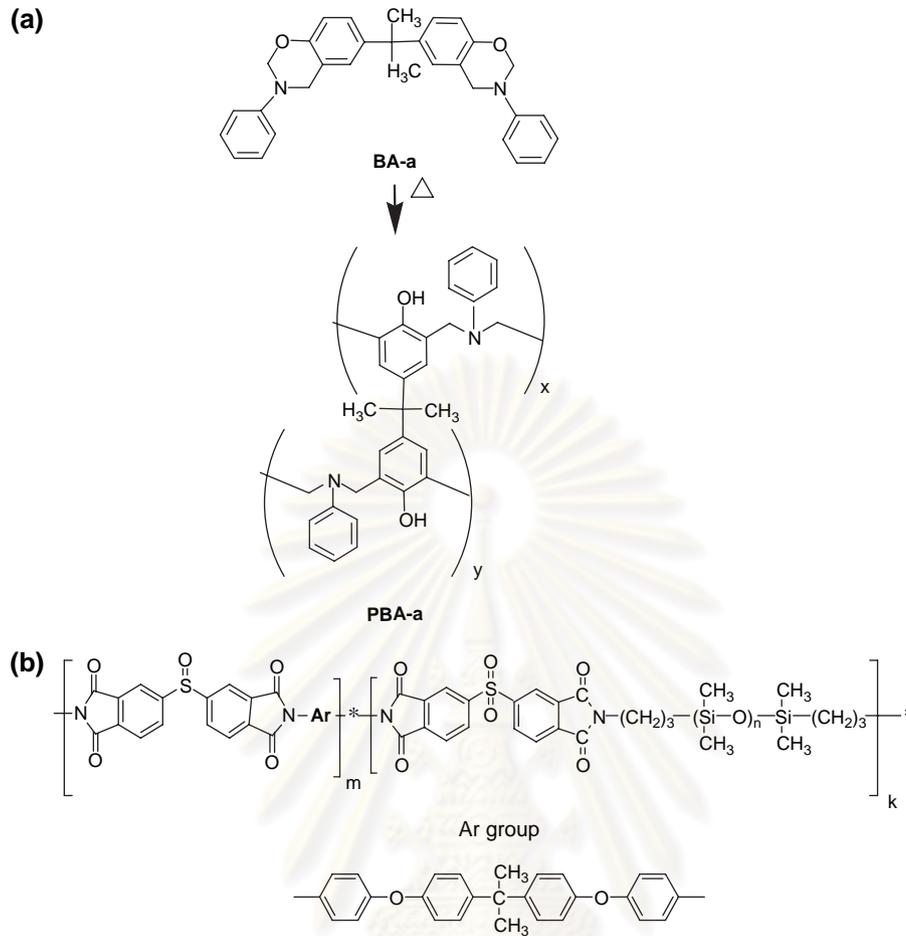
Fig. 1. (a) Benzoxazine monomer and polybenzoxazine; (b) polysiloxane-*block*-polyimide (SPI).

4. Measurements

4.1. Thermal analysis

Differential Scanning Calorimeter (DSC) of TA instruments (model DSC2910), calibrated with Indium standard, was used. A sample of about 10 mg was used for each test. In order to erase any thermal history, the samples were heated at 10 °C/min. Then, they were cooled to the ambient temperature, and scanned again using the same heating rate as before.
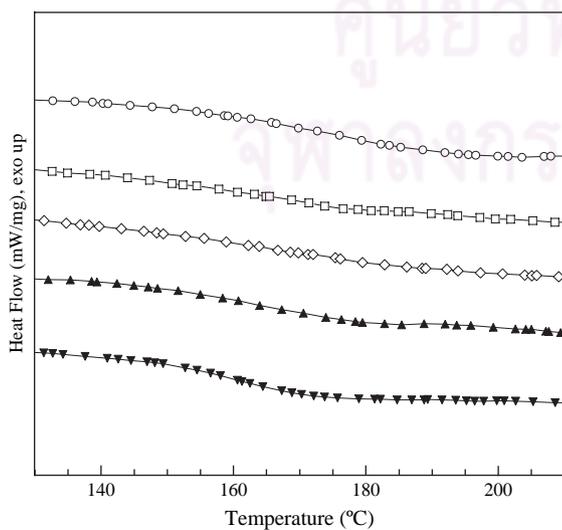
Fig. 2. DSC thermograms of PBA-a, SPI and their blends at various SPI contents: (○) SPI, (□) 75 wt%, (◇) 50 wt%, (▲) 25 wt%, and (▼) PBA-a.
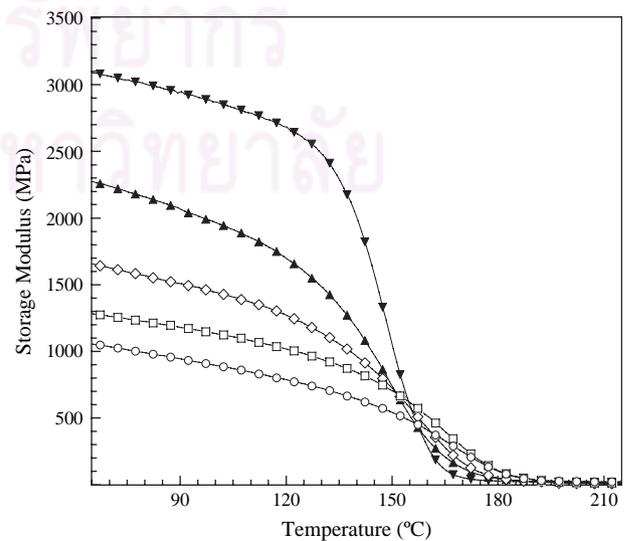
Fig. 3. Storage moduli of PBA-a, SPI and their blends at various SPI contents: (○) SPI, (□) 75 wt%, (◇) 50 wt%, (▲) 25 wt%, and (▼) PBA-a.
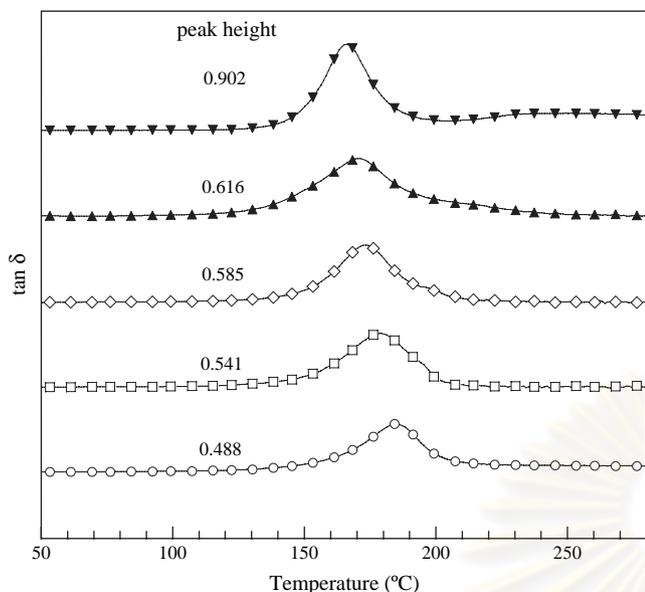
Fig. 4. Loss tangent of PBA-a, SPI and their blends at various SPI contents: (○) SPI, (□) 75 wt%, (◇) 50 wt%, (▲) 25 wt%, and (▼) PBA-a.

The glass-transition temperatures (T_g) of the blends were measured.

Dynamic mechanical properties of the blends were tested using the NETZSCH Model DMA242. The experiment is done in a tension mode using the dimension of the specimens of approximately 23.7 mm (length) × 5 mm (width) × 0.5 mm (thickness). The applied strain amplitude was 0.3% at the deformation frequency of 1 Hz. The specimens were heated using a temperature ramp rate of 3 °C/min from 40 to 250 °C.

4.2. Thermal gravimetric analysis (TGA)

The decomposition temperature (T_d) and char yield of the blends were studied using TGA Instruments (model TGA/
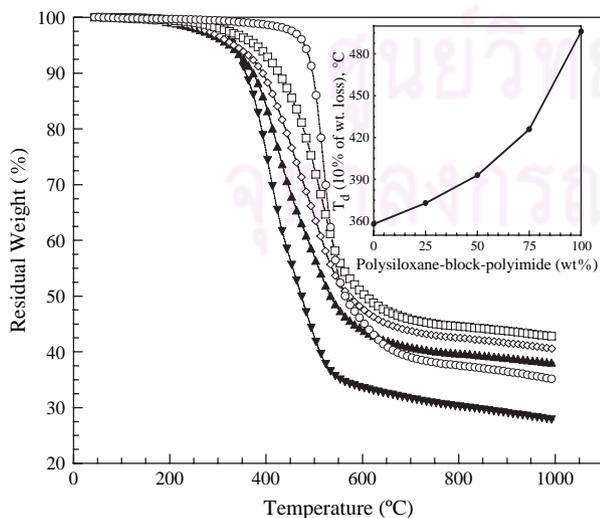
Fig. 5. Thermogravimetric curves of PBA-a, SPI and their blends at various SPI contents: (○) SPI, (□) 75 wt%, (◇) 50 wt%, (▲) 25 wt%, and (▼) PBA-a. Inset: decomposition temperatures (T_d at 10% weight loss) at various SPI contents.
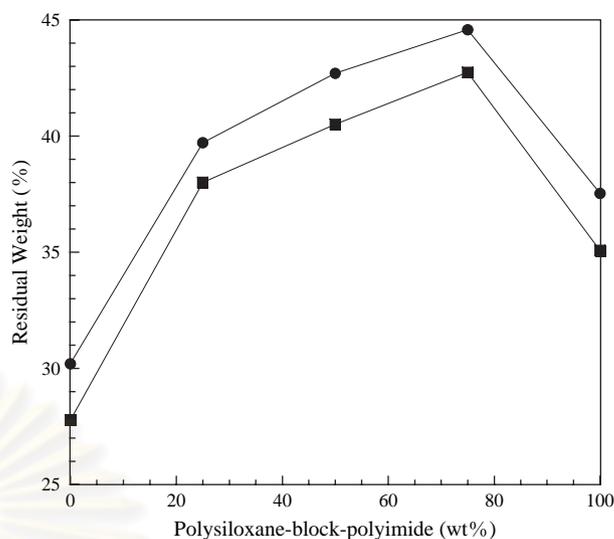
Fig. 6. Char yield of PBA-a, SPI and their blends at various temperatures: (●) 1000 °C, (■) 800 °C.

SDTA 851^e). The experiments were performed using a heating rate of 20 °C/min from 40 to 1000 °C under nitrogen atmosphere. The flow of purging nitrogen was kept at 80 ml/min. The sample mass was approximately 20 mg.

Kinetics analysis via Kissinger method, Flynn–Wall–Ozawa method, and Coats–Redfern method was carried out at various heating rates, i.e. 5, 10, 20, and 25 °C/min.

5. Results and discussion

5.1. Effect of SPI content on glass-transition temperature

Fig. 2 shows the DSC thermograms depicting the glass-transition temperature (T_g) of PBA-a, SPI, and their blends. At heating rate of 10 °C/min, the T_g of the neat polybenzoxazine (PBA-a) was determined to be 160 °C. The T_gs of all blends were slightly higher than that of neat PBA-a ranging from 163 to 169 °C, while the T_g of the SPI was 173 °C. It is found that SPI was able to elevate the T_gs of the blends. In these systems, there was only one broad T_g in all blend compositions. However, the systems exhibit partial miscibility [26] as evidenced by a transformation of transparent PBA-a and SPI to opaque appearance with orange color of the blends.

Storage moduli of the PBA-a, SPI, and their blends in the temperature range of 40–220 °C are illustrated in Fig. 3. The thermograms revealed the glassy state moduli, reported at 40 °C of PBA-a to be approximately 3.1 GPa and that of SPI to be around 1.1 GPa. Therefore, the SPI is much less stiff than PBA-a due to the presence soft silicone segments in its molecular structure. The stability of the polymer can be seen from the slope of the glassy state moduli in the DMA thermograms. The lower the slope of the glassy state modulus, the greater is the thermal stability of the polymer. As a result, DMA thermograms suggested that SPI was more thermally stable than PBA-a. The presence of the SPI fraction thus helps improving thermal stability of the resulting blends.
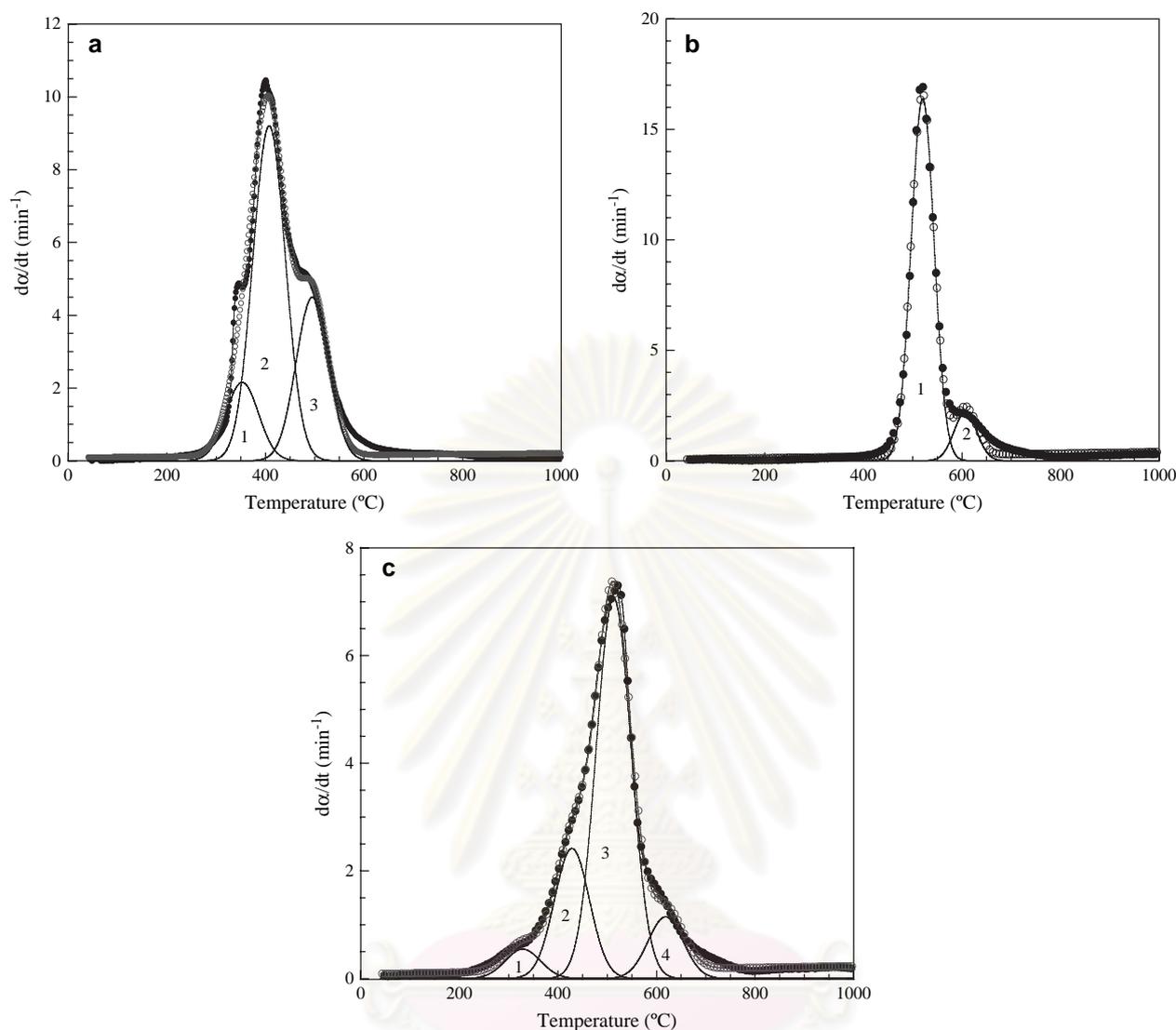
Fig. 7. DTG curve and individual contributions of (a) PBA-a (20 °C/min), $R^2 = 0.9918$; (b) SPI (20 °C/min), $R^2 = 0.9958$; (c) blends with 75 wt% of SPI (20 °C/min), $R^2 = 0.9968$; (●) experimental data, (○) simulated curve.

In addition, the tan δ of the polyimides and their blends is depicted in Fig. 4. Generally, the magnitude of tan δ peaks reflects the large scale mobility associated with α relaxation process, whereas the width of the tan δ relates to the homogeneity of the materials. The peak at lower temperature of 166 °C could be attributed to that of PBA-a and the peak at higher temperature of 184 °C was attributed to that of SPI. It can be noticed that only one single and broad peak was observed in all blend systems. Furthermore, the peaks of the blends were found to shift to higher temperature with increasing SPI content, which corresponds to the DSC results.

5.2. Thermogravimetric analysis of the blends and degradation kinetics

TGA thermograms of PBA-a, SPI, and their blends at various weight ratios of SPI are presented in Fig. 5. From the figure, it can be observed that the addition of SPI was able to enhance the decomposition temperature of the PBA-a. The

inset of Fig. 5 explains the relationship between the decomposition temperatures at 10% weight loss and the SPI content in the blends. It clearly shows that the decomposition temperatures of the blends increase from about 360 °C (for 0 wt% of SPI) to about 500 °C (for 100 wt% of SPI) with the increase of the SPI fraction.

Interestingly, the char yields of the blended systems exhibited the synergistic behavior as shown in Fig. 6. The char yields of the blends were higher than those of neat PBA-a and SPI. The highest char value at 800 °C of about 45% was found at 75 wt% of the SPI fraction, while the value of pure PBA-a was only 30%. Theoretically, the possible reason for synergism in the char formation is due to a large amount of aromatic ring in the blends with some additional chemical bonding between the PBA-a and the SPI. This synergy in the char formation was also observed in the systems of polybenzoxazine alloyed with other types of polyimides [27].

From these results, we selected the blend at 75 wt% of SPI for further kinetic studies of the blending systems since it

Table 2

Initial temperature, final temperature, and peak temperature of small curves for polybenzoxazine, SPI and their blends at 20 °C/min in N_2 atmosphere

Polysiloxane-*block*-polyimide (wt% in PBA-a)

		0			25	50	75			100
Stage 1	T_i	280	Stage 1	T_i	213	198	227	Stage 1	T_i	422
	T_{peak}	353		T_{peak}	323	313	328		T_{peak}	521
	T_f	426		T_f	432	427	429		T_f	618
	% Area	14		% Area	9	8	5		% Area	88
Stage 2	T_i	316	Stage 2	T_i	292	294	310	Stage 2	T_i	521
	T_{peak}	408		T_{peak}	420	429	428		T_{peak}	607
	T_f	499		T_f	548	563	546		T_f	694
	% Area	58		% Area	51	40	22		% Area	12
Stage 3	T_i	413	Stage 3	T_i	386	375	384	R^2		0.9958
	T_{peak}	496		T_{peak}	509	511	513			
	T_f	577		T_f	634	645	642			
	% Area	28		% Area	34	44	63			
R^2		0.9918	Stage 4	T_i	504	501	508			
				T_{peak}	609	616	618			
				T_f	714	730	728			
				% Area	6	8	10			
			R^2		0.9976	0.9974	0.9968			

Note: T_i = initial temperature and T_f = final temperature.

provides maximum char yield. After obtaining the TGA and DTG curves, we used Peakfit program to separate the DTG curves of the blends at 0 wt%, 75 wt%, and 100 wt%. After resolving the curves by using the computer software, it can be noticed that the DTG curve of the PBA-a, presented in Fig. 7a, composes of a three-stage weight-loss process. This result is in good agreement with the study of Hemvichian et al., which reports that this degradation process was observed with the middle peak having the highest maximum rate of weight loss. In addition, the degradation products were identified into eight categories as follows: benzene derivatives, amines, phenolic compounds, 2,3-benzofuran derivatives, iso-quinoline derivatives, biphenyl compounds, Mannich base compounds, and phenanthridine derivatives [3]. Moreover for the pure SPI, the DTG curve can also be resolved

into two main loss processes as shown in Fig. 7b. These results correspond to the degradation study in the system of siloxane-containing polyimide with the molecular weight of 1300 [28], which reported at least two overlapping stages. Moreover, our results also reveal the same phenomenon as found in the similar system of polydimethylsiloxane (PDMS). It is well known that the thermal degradation of PDMS in nitrogen atmosphere results in depolymerization over the range of 400—650 °C to produce cyclic oligomers [29,30]. In the degradation of PDMS, the most abundant product is reported to be the trimer of hexamethylcyclotrisiloxane with decreasing amounts of tetramer, and higher oligomers [29]. For the blend system with 75 wt% of SPI as shown in Fig. 7c, the DTG can be resolved into four curves, which represent the four main stages of degradation in the blend. The determination of the areas under the resolved peaks (% area) and the peak positions (T_{peak}) was useful to make us understand more about the degradation process of the blend system. All these data including initial decomposition temperatures (T_i) and final decomposition temperatures (T_f) of pure PBA-a, SPI, and their blends are exhibited in Table 2. In comparison of peak positions, it can be observed that the T_{peak}s of stage 1 and stage 2 in the blends for all SPI compositions are similar to that of stage 1 in pure PBA-a, while the T_{peak}s of stage 4 in the blends for are close to that of stage 2 in pure SPI. Additionally, the T_{peak}s of stage 3 in the blends are the values between the T_{peak} of stage 3 in pure PBA-a and that of stage 1 in pure SPI. In the determination of the areas
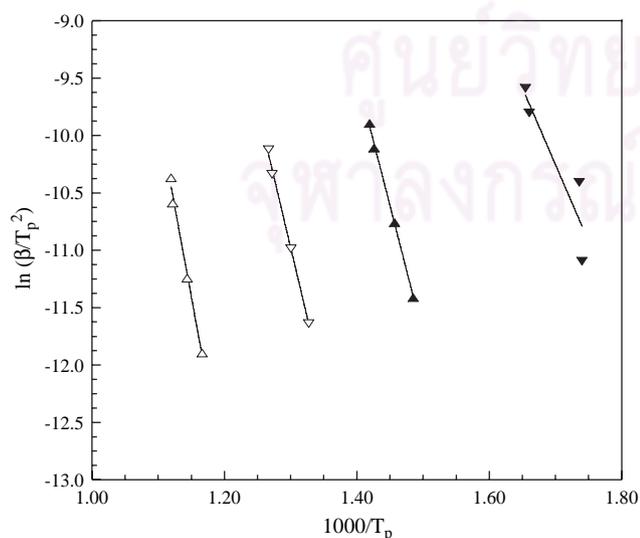
Fig. 8. Plots of ln β/T_p^2 versus $1000/T_p$ at different heating rates according to Kissinger method for the blends (75 wt% of SPI): (▼) peak 1, (▲) peak 2, (□) peak 3, (△) peak 4.

Table 3

Activation energies obtained by using Kissinger method for the blend (75 wt% of SPI)

Peak 1		Peak 2		Peak 3		Peak 4	
E_a (kJ/mol)	R^{2a}	E_a (kJ/mol)	R^{2a}	E_a (kJ/mol)	R^{2a}	E_a (kJ/mol)	R^{2a}
111	0.9204	187	0.9983	202	0.9972	260	0.9919

[a] Correlation coefficient.

S. Tiptipakorn et al. / Polymer Degradation and Stability 92 (2007) 1265–1278
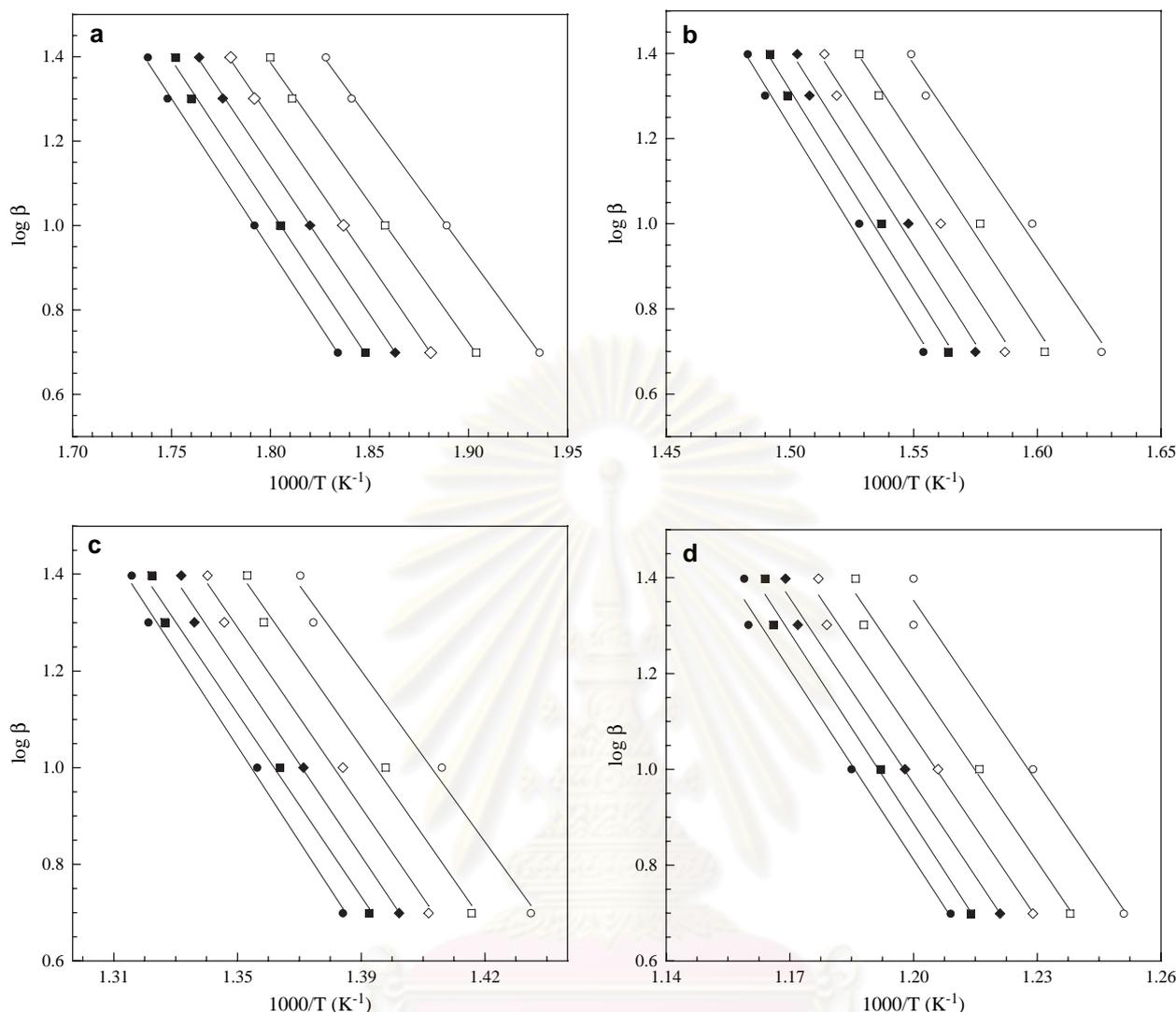
Fig. 9. Plots of log β versus 1000/*T* according to Flynn–Wall–Ozawa method for the blend (75 wt% of SPI) with weight loss from 5% to 20% conversion for (a) peak 1; (b) peak 2; (c) peak 3; (d) peak 4: (○) 5%, (□) 8%, (◇) 11%, (◆) 14%, (■) 17%, and (●) 20%.

under the resolved curves, the values of all degradation stages of the blends are related to the contents of PBA-a and SPI. It can be seen that the addition of SPI led to the decrease of the % area values in stages 1 and 2 and the increase of the values in stages 3 and 4. These results confirm that that stages 1 and 2 of the degradation in the blends are mainly from the degradation of PBA-a, while stage 4 of the degradation in the blends is from the degradation of SPI. For the stage 3 of degradation, it is proposed to be the degradation of some additional chemical bonding between the PBA-a and the SPI.

After the four overlapped curves were resolved, the conversions were calculated from the areas under the curves by using Simpson's 3/8 rule. Then, the E_a of each one was obtained via three mentioned methods.

5.3. Calculation of the thermal degradation kinetics parameters

The E_a of the thermal degradation process of this blend was determined using three well-known methods for dynamic

heating experiment i.e., the Kissinger method, Flynn–Wall–Ozawa method, and Coats–Redfern method.

By using Kissinger method, the E_a can be calculated from the slope of the plot of $\ln(\beta/T_p^2)$ versus $1000/T_p$ (T_p is the temperature at the maximum weight-loss rate) as presented in Fig. 8. The calculated values are shown in Table 3. The obtained E_a values of stages 1, 2, 3, and 4 are 111, 187, 202, 260 kJ/mol, respectively. From the literature [12,31], the Kissinger's method was reported to provide highly reliable values of E_a with an error of less than 5% independent of reaction mechanism, provided that $E/RT > 10$.

The E_a of the blends can also be determined using the method of Flynn–Wall–Ozawa from a linear fitting of ln β versus 1000/ *T* at different conversions (Fig. 9a–d). Owing to the fact that this equation was derived using the Doyle approximation only conversion values in the low range can be used. In this study, the conversion values of 5%, 8%, 11%, 14%, 17% and 20% were used. Fig. 9a–d shows that the fitting straight lines are nearly parallel. Using Flynn–Wall–Ozawa method, the E_a values corresponding to the different conversions are listed in Table 4. The

Table 4
Activation energies obtained by using Flynn−Wall−Ozawa method for the blend (75 wt% of SPI)

Conversion (%)	E_a (kJ/mol)	R^{2a}	E_a (kJ/mol)	R^{2a}
	Peak 1		Peak 2	
5	117	0.9996	157	0.9895
8	120	0.9992	161	0.9905
11	125	0.9996	164	0.9882
14	127	0.9996	168	0.9917
17	130	0.9970	170	0.9935
20	130	0.9985	173	0.9933
Average	125		166	
	Peak 3		Peak 4	
5	172	0.9900	231	0.9856
8	178	0.9940	231	0.9904
11	181	0.9928	233	0.9912
14	186	0.9954	236	0.9943
17	184	0.9925	239	0.9909
20	190	0.9946	241	0.9898
Average	182		235	

[a] Correlation coefficient.

calculated E_a from this method are 125, 166, 182, and 235 kJ/mol for peaks 1, 2, 3, and 4, respectively.

The method by Coats−Redfern is one of the most widely used procedure for the determination of the reaction processes [10,19,21]. From Eq. (9), proposed by Coats and Redfern, the E_a for all $g(\alpha)$ functions listed in Table 1 can be obtained at constant heating rate. In this study, the same conversion values have been used as those used in the Flynn−Wall−Ozawa

methods. Table 5 shows E_a, A, and correlations for conversions in the range 5−20% at constant heating rate of 20 °C/min. It was found that the solid state thermal degradation mechanism of the blends with 75 wt% of SPI is likely to be of F1 type, because this mechanism presents the E_a that is similar to the value obtained by isoconvensional methods. Furthermore in comparison with other mechanisms, this mechanism renders the lowest E_a to start the degradation stage [32]. The type of degradation mechanism is confirmed by Criado method in the next determination.

As presented in Table 6, Coats−Redfern method was applied at the heating rate of 25, 20, 10, and 5 °C/min to determine the average values of the E_a, A, and the degradation mechanism. The E_a calculated by Coats−Redfern method are 116, 174, 223, and 281 kJ/mol. It is clearly shown that the E_a of each degradation stage increases with the increase of the heating rates. In addition, the results suggest F1 type of solid state thermal degradation mechanism for all four stages and all heating rates. The possible reason that the increase of the amount of SPI led to the increase of area under the curve of stage 3 of the blends is that stage 3 correlates with SPI structure. The E_a of this peak was around 218 kJ/mol, which was lower than the bond dissociation energy of Si−C bond (360 kJ/mol), the weakest bond of the base polymers [33]. Hence, the decomposition of the blends could be governed mainly by the molecular structure and kinetic consideration and not by bond energies for stage 3.

By using Coats−Redfern method, the calculated E_a at 20 °C of PBA-a for stages 1, 2, and 3 are 172, 209, and

Table 5
Activation energies obtained by using Coats−Redfern method for several solid state processes at a heating rate of 20 °C/min for the blend (75 wt% of SPI)

Type	E_a (kJ/mol)	ln A (min^{-1})	R^2	Type	E_a (kJ/mol)	ln A (min^{-1})	R^2
Peak 1				Peak 2			
A2	57	10.46	0.9976	A2	82	13.07	0.9976
A3	35	5.55	0.9971	A3	51	7.31	0.9972
A4	24	2.95	0.9965	A4	35	4.30	0.9967
R1	116	22.76	0.9971	R1	164	27.67	0.9971
R2	120	22.93	0.9976	R2	169	27.97	0.9975
R3	121	22.82	0.9977	R3	171	27.90	0.9976
D1	247	48.78	0.9974	D1	339	58.15	0.9973
D2	247	48.78	0.9976	D2	346	58.75	0.9975
D3	252	48.43	0.9979	D3	353	58.58	0.9978
D4	249	47.66	0.9977	D4	348	57.69	0.9976
F1	124	24.50	0.9980	F1	174	29.68	0.9979
F2	6	−1.64	0.8542	F2	10	−0.88	0.9040
F3	21	3.05	0.9470	F3	31	4.23	0.9561
Peak 3				Peak 4			
A2	105	15.23	0.9975	A2	139	34.94	0.9976
A3	66	8.76	0.9972	A3	88	34.48	0.9973
A4	47	5.41	0.9968	A4	63	34.14	0.9969
R1	210	31.70	0.9970	R1	275	35.62	0.9969
R2	217	32.14	0.9975	R2	284	35.65	0.9974
R3	219	32.11	0.9976	R3	287	35.66	0.9975
D1	432	66.21	0.9972	D1	565	36.34	0.9971
D2	441	66.99	0.9975	D2	576	36.36	0.9974
D3	450	66.99	0.9770	D3	588	36.38	0.9977
D4	444	65.99	0.9976	D4	580	36.36	0.9975
F1	223	33.98	0.9978	F1	293	35.68	0.9978
F2	15	−0.20	0.9245	F2	22	33.08	0.9347
F3	42	5.38	0.9603	F3	57	34.05	0.9613

Table 6
Average activation energies obtained by using Coats–Redfern method at 25, 20, 10, 5 °C/min for the blend (75 wt% of SPI)

Heating rate (°C/min)	E_a (kJ/mol)	ln A (min^{-1})	Possible mechanism
Peak 1			
5	113	23.35	F1
10	108	22.21	F1
20	124	24.50	F1
25	119	23.87	F1
Average	116		
Peak 2			
5	161	28.51	F1
10	168	29.10	F1
20	174	29.68	F1
25	175	28.51	F1
Average	170		
Peak 3			
5	206	32.66	F1
10	217	34.14	F1
20	223	33.98	F1
25	252	39.25	F1
Average	225		
Peak 4			
5	287	39.73	F1
10	272	37.24	F1
20	293	35.68	F1
25	270	36.12	F1
Average	281		

263 kJ/mol, respectively (Table 7). The solid state thermal degradation mechanism of PBA-a is proposed to be of F1 type. The PBA-a thermal degradation of this study is in agreement with the results in the literature [34], which reveals the phenolic cleavage at the maximum derivative of peak temperature at around 400 °C.

With the Coats–Redfern method, the calculated E_a at 20 °C of neat SPI for peaks 1 and 2 are 369 and 460 kJ/mol, respectively (Table 8). These calculation results coincide with the bonding energy of Si–C (360 kJ/mol) [33], the weakest bond in PDMS, and that of Si–O (454 kJ/mol) [35]. Hence, the degradation of SPI could possibly be governed mainly by the breaking of Si–C bond and Si–O bond.

Table 8
Activation energies obtained by using Coats–Redfern method for several solid state processes at a heating rate of 20 °C/min of BSF30

Type	Peak 1			Peak 2		
	E_a (kJ/mol)	ln A (min^{-1})	R^2	E_a (kJ/mol)	ln A (min^{-1})	R^2
A2	178	26.64	0.9959	223	30.14	0.9957
A3	115	16.55	0.9956	144	18.89	0.9955
A4	83	11.40	0.9952	104	13.16	0.9951
R1	348	52.80	0.9953	434	59.44	0.9952
R2	358	53.85	0.9958	447	60.66	0.9956
R3	362	54.04	0.9959	452	60.90	0.9958
D1	708	107.96	0.9954	882	121.23	0.9953
D2	722	109.54	0.9958	899	123.04	0.9956
D3	737	110.39	0.9961	917	124.10	0.9959
D4	727	108.82	0.9952	905	122.38	0.9957
F1	369	56.33	0.9962	460	63.30	0.9960
F2	31	3.03	0.9502	40	3.73	0.9569
F3	76	10.99	0.9648	94	12.33	0.9684

From the calculation in the system of SPI, the solid state thermal degradation mechanism is proposed to be of F1 type. In this study, the degradation phenomenon of SPI coincides with that of the literature [35], which reported that the thermal degradation of PDMS in inert atmosphere results in degradation over the range of 400–650 °C.

In comparison of PBA-a, SPI and the blend with 75 wt% of SPI, the E_a of the blend was found to be lower than those of both pure components. This phenomenon corresponds to the research of Nandan et al. [36], who studied the blending system of poly(ether ether ketone)/poly(aryl ether sulphone). They reported that the E_a of the blends were lower than that of the pure components because of different factors that concurrently effect the process of degradation. Firstly, interactions are possible among the different components in the blend during degradation and among the products of degradation. These chemical reactions can lead to an acceleration of the degradation rate with respect to that of pure components. These reactions can be grouped into following processes [37,38].

– Reactions between macromolecules and small molecules,
– reactions between macromolcules and small radicals,

Table 7
Activation energies obtained by using Coats–Redfern method for several solid state processes at a heating rate of 20 °C/min of BA-a

Type	Peak 1			Peak 2			Peak 3		
	E_a (kJ/mol)	ln A (min^{-1})	R^2	E_a (kJ/mol)	ln A (min^{-1})	R^2	E_a (kJ/mol)	ln A (min^{-1})	R^2
A2	81	14.82	0.9969	99	16.67	0.9969	126	19.13	0.9970
A3	51	8.55	0.9964	62	9.80	0.9965	80	11.45	0.9966
A4	36	5.29	0.9959	44	6.24	0.9960	57	7.49	0.9962
R1	162	30.76	0.9964	196	34.27	0.9964	248	38.89	0.9963
R2	167	31.16	0.9969	202	34.76	0.9968	256	39.52	0.9968
R3	169	31.12	0.9970	204	34.75	0.9970	258	39.56	0.9970
D1	333	64.13	0.9966	403	71.15	0.9966	508	80.38	0.9965
D2	340	64.86	0.9969	411	71.99	0.9969	518	81.41	0.9968
D3	347	64.82	0.9972	420	72.07	0.9971	529	81.68	0.9971
D4	342	63.84	0.9970	414	71.01	0.9970	522	80.50	0.9969
F1	172	32.97	0.9972	209	36.66	0.9972	263	41.56	0.9972
F2	11	−0.17	0.9191	14	0.24	0.9283	19	0.91	0.9348
F3	32	5.28	0.9587	39	6.00	0.9606	51	7.22	0.9606

− reactions between macroradicals and small molecules,
− reactions between two small molecules,
− reaction between two macroradicals,
− reaction between macromolecules and macroradicals.

In addition, reactions with small molecules or small radicals can give rise to faster breakage of the macromolecules and to chemical structures that act as stabilizer groups.

These above reasons can explain the phenomenon that the E_a of the blends in many systems [38−40] are not close to the predicted values on the basis of linear additive behaviour, using following equation,

$$E_a = E_{a1}w_1 + E_{a2}w_2 \tag{15}$$

where E_{a1} and E_{a2} are activation energies of the homopolymers, and w_1 and w_2 are the weight fraction of components 1 and 2, respectively [36].

5.4. Determination of the reaction mechanism using Criado method

The $Z(\alpha)−\alpha$ master curves can be plotted using Eq. (13) according to different reaction mechanisms shown in Table 1. The experimental data at 20 °C/min obtained by Flynn−Wall−Ozawa method (Table 4) were substituted into Eq. (14). Fig. 10a−d shows the $Z(\alpha)−\alpha$ master and experimental curve of the blend with 75 wt% of PSI. The results show that the experimental curves of all four steps of degradation belong to F1 reaction mechanism (random nucleation having one nucleus on individual particle) with rate-controlling step of the nucleation process. Figs. 11a−c and 12a,b exhibit the comparison of the experimental curves of pure PBA-a and PSI, respectively. It can be observed that the degradation of pure PBA-a and PSI was proved to obey the F1 mechanism. That means random nucleation with one nucleus on the individual particle. The degradation
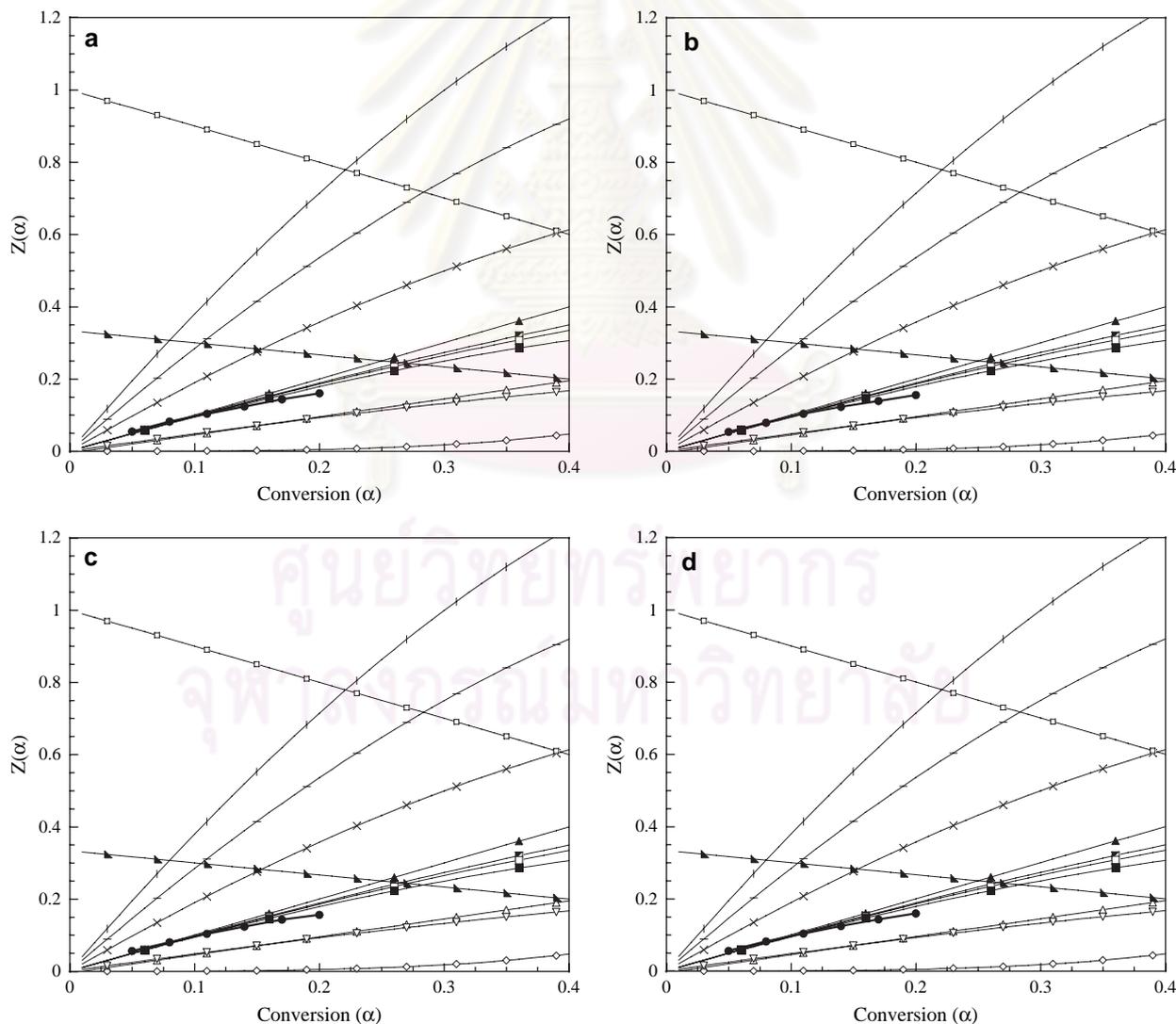

Fig. 10. Plots of $Z(\alpha)$ versus α of the blend (75 wt% of SPI) compared between experimental curve and master curve at different mechanisms for (a) peak 1; (b) peak 2; (c) peak 3; (d) peak 4: (×) A2, (|) A3, (−) A4, (▲) R1, (◪) R2, (□) R3, (△) D1, (◇) D2, (▽) D3, (◆) D4, (■) F1, (▫) F2, (◣) F3, (●) experimental data.

S. Tiptipakorn et al. / Polymer Degradation and Stability 92 (2007) 1265–1278
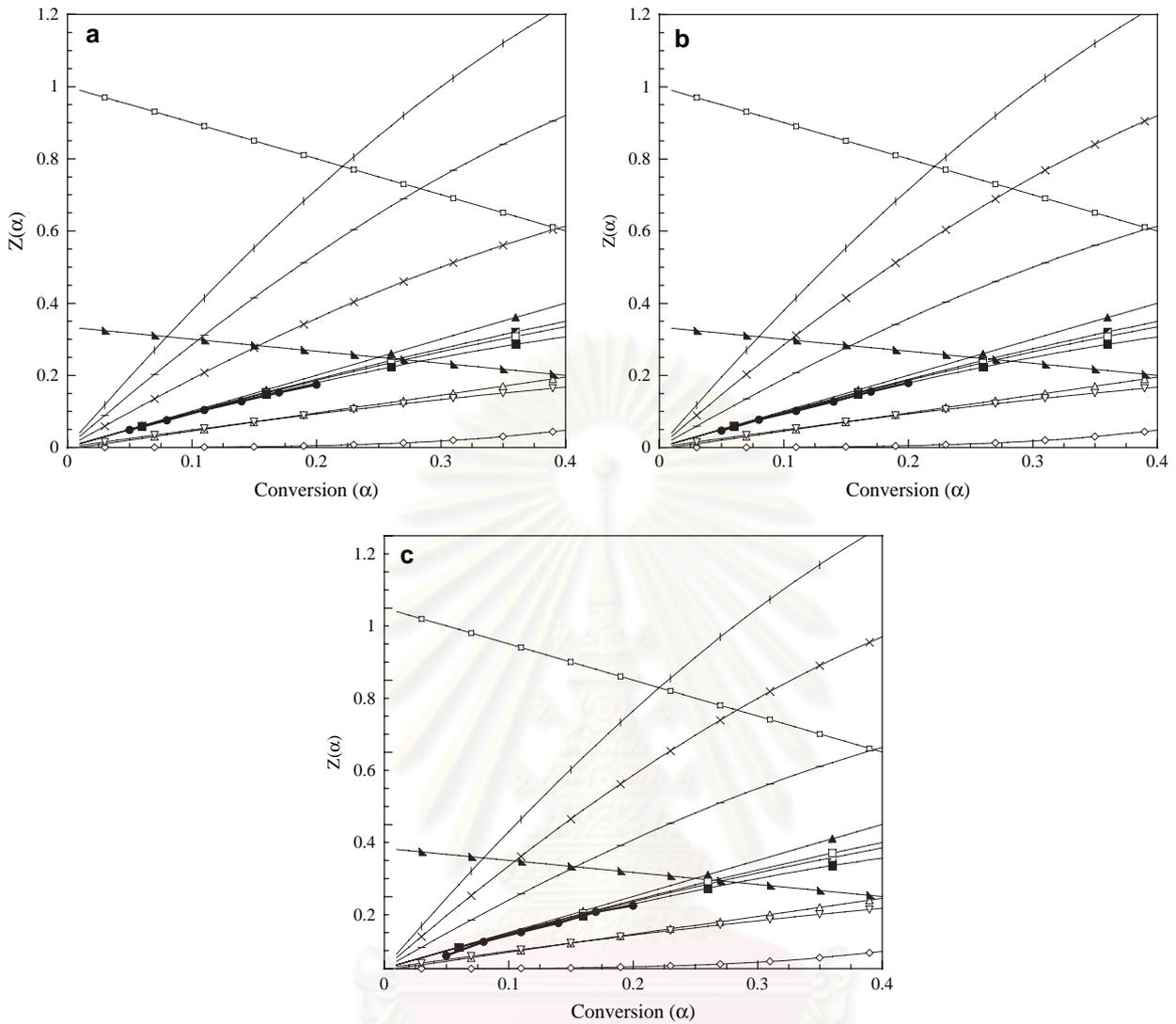
Fig. 11. Plots of $Z(\alpha)$ versus α of PBA-a compared between experimental curve and master curve at different mechanisms for (a) peak 1; (b) peak 2; (c) peak 3; (d) peak 4: (×) A2, (|) A3, (−) A4, (▲) R1, (◪) R2, (□) R3, (△) D1, (◇) D2, (▽) D3, (◆) D4, (■) F1, (▫) F2, (◣) F3, (●) experimental data.
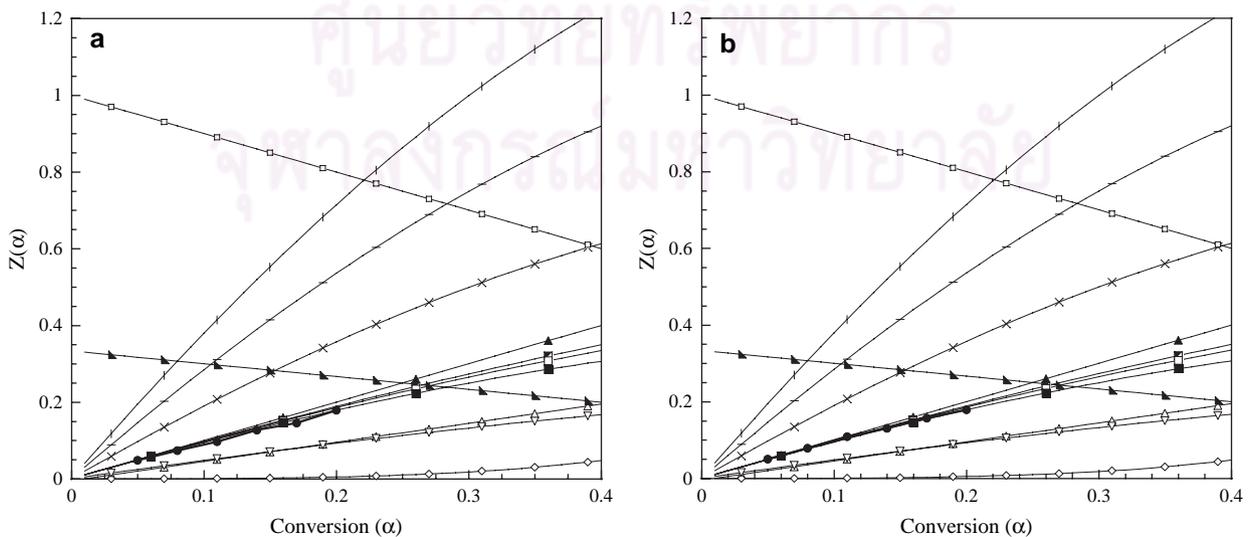

Fig. 12. Plots of $Z(\alpha)$ versus α of BSF30 compared between experimental curve and master curve at different mechanisms for (a) peak 1; (b) peak 2: (×) A2, (|) A3, (−) A4, (▲) R1, (◪) R2, (□) R3, (△) D1, (◇) D2, (▽) D3, (◆) D4, (■) F1, (▫) F2, (◣) F3, (●) experimental data.

was initiated from one random point acting as growth center, which follows unimolecular decay law with first order reaction [41,42].

6. Conclusions

In the blending systems of BA-a monomer and SPI, synergistic behavior of char yield was observed. The possible reason for the increase of char yield is that there was higher cross-link density in the blend than both neat polybenzoxazine and SPI. PBA-a and SPI showed three-stage weight-loss process and two-stage weight-loss process, respectively. The degradation of the blends between benzoxazine monomer and SPI was found to be a complex process composed of at least four overlapping stages, of which the E_a can be calculated. The study of separated curves from Criado method indicates that PBA-a, SPI and their blending systems follow F1 thermal degradation mechanism in the conversion range considered.

Acknowledgements

References

[1] Ishida H. US Patent 5,543,516; 1996.
[2] Nair CPR. Advances in addition-cure phenolic resins. Prog Polym Sci 2004;29:401–98.
[3] Hemvichian K, Ishida H. Thermal decomposition process in aromatic amine-based polybenzoxazine investigated by TGA and GC–MS. Polymer 2002;43:4391–402.
[4] Takeichi T, Agag T, Zeidam R. Preparation and properties of polybenzoxazine/poly(imide siloxane) alloys: in situ ring-opening polymerization of benzoxazine in the presence of soluble poly(imide-siloxane)s. J Polym Sci Part A Polym Chem 2001;39:2633–41.
[5] Agag T, Takeichi T. Polybenzoxazine–montmorillonite hybrid nanocomposites: synthesis and characterization. Polymer 2000;41:7083–90.
[6] Agag T, Takeichi T. Synthesis and properties of silica-modified polybenzoxazine. Mater Sci Forum 2004;449–452:1157–60.
[7] Furukawa N, Yamada Y, Kimura Y. Preparation and stress relaxation properties of thermoplastic polysiloxane-block-polyimides. High Perform Polym 1996;8:617–30.
[8] Yamada Y. Siloxane modified polyimides for microelectronics coating applications. High Perform Polym 1998;10:69–80.
[9] Furukawa N, Yuasa M, Kimura Y. Structure analysis of a soluble polysiloxane-block-polyimide and kinetic analysis of the solution imidization of the relavant polyamic acid. J Polym Sci Part A Polym Chem 1998;36:2237–45.
[10] Coats AW, Redfern JP. Kinetic parameters from thermogravimetric data. Nature 1964;201:68–9.
[11] Nam JD, Seferis JC. A composition methodology for multistage degradation of polymers. J Polym Sci Part B Polym Phys 1991;30:601–8.
[12] Barral L, Cano J, Lopez J, Lopez-Bueno I, Nogueira P, Ramirez C, et al. Thermogravimetric study of tetrafunctional/phenol novolac epoxy mixtures cured with a diamine. J Therm Anal Calorim 1998;51:489–501.
[13] Kissinger HE. Reaction kinetics in differential thermal analysis. Anal Chem 1957;29:1702–6.
[14] Ozawa T. A new method of analyzing thermogravimetric data. Bull Chem Soc Jpn 1965;38:1881–6.
[15] Liaw DJ, Shen WC. Curing of acrylated epoxy-resin based on bisphenols. Polym Eng Sci 1994;34:1297–303.
[16] Nam JD, Seferis JC. Generalized composite degradation kinetics for polymeric systems under isothermal and nonisothermal conditions. J Polym Sci Part B Polym Phys 1992;30:455–63.
[17] Flynn JH. The 'temperature integral' – its use and abuse. Thermochim Acta 1997;300:83–92.
[18] Doyle CD. Kinetic analysis of thermogravimetric data. J Appl Polym Sci 1961;5:285–92.
[19] Criado JM, Malek J, Ortega A. Applicability of the master plots in kinetic analysis of a non-isothermal rate. Thermochim Acta 1989;147:377–85.
[20] Criado JM, Perez-Maqueda LA, Gotor FJ, Malek J, Koga N. A unified theory for the kinetic analysis of solid state reactions under any thermal pathway. J Therm Anal Calorim 2003;72:901–6.
[21] Pérez-Maqueda LA, Criado JM, Gotor FJ, Malek J. Advantages of combined kinetic analysis of experimental data obtained under any heating profile. J Phys Chem A 2002;106:2862–8.
[22] Paterson WL. Computation of the exponential trap population integral of glow curve theory. J Comput Phys 1971;7(1):187–90.
[23] Pérez-Maqueda LA, Criado JM. The accuracy of Senum and Yang's approximations to the Arrhenius integral. J Therm Anal Calorim 2000;60:909–15.
[24] Urbanovici E, Popescu C, Seqal E. Improved iterative version of the Coats–Redfern method to evaluate non-isothermal kinetic parameters. J Therm Anal Calorim 1999;58:683–700.
[25] Low HY, Ishida H. Structural effects of phenols on the thermal and thermo-oxidative degradation of polybenzoxazines. Polymer 1999;40:4365–76.
[26] Sperling LH, Hu R. In: Utracki LA, editor. Polymer blends handbook, vol. 1; 2002. p. 426.
[27] Takeichi T, Guo Y, Rimdusit S. Performance improvement of polybenzoxazine by alloying with polyimide: effect of preparation method on the properties. Polymer 2005;46:4909–16.
[28] Chang TC, Wu KH, Liao CL, Lin ST, Wang GP. Thermo-oxidative degradation of siloxane-containing polyimide and unmodified polyimide. Polym Degrad Stab 1998;62:299–305.
[29] Thomas TH, Kendrick TC. Thermal analysis of polydimethylsiloxanes. I. Thermal degradation in controlled atmospheres. J Polym Sci 1969;7:537–49.
[30] Grassie N, MacFarlane IG. The thermal degradation of polysiloxanes [polydimethylsiloxane]. Eur Polym J 1978;14:875–84.
[31] Criado JM, Ortega A. Non-isothermal transformation kinetics: remarks on the Kissinger method. J Non-Cryst Solids 1986;87:302–11.
[32] Albano C, Freitas ED. Thermogravimetric evaluation of the kinetics of decomposition of polyolefin blends. Polym Degrad Stab 1998;61:289–95.
[33] Korshak VV. The chemical structure and thermal characteristics of polymers. Jerusalem: Keter Press; 1971.
[34] Hemvichian K, Kim DH, Ishida H. Identification of volatile products and determination of thermal degradation mechanisms of polybenzoxazine model oligomers by GC–MS. Polym Degrad Stab 2005;87:213–24.
[35] Camino G, Lomakin SM, Lazzari M. Polydimethylsiloxane thermal degradation. Part 1. Kinetic aspects. Polymer 2001;42:2395–402.
[36] Nandan B, Kandpal LD, Mathur GN. Poly(ether ether ketone)/poly(aryl ether sulphone) blends: thermal degradation behaviour. Eur Polym J 2003;39:193–8.
[37] Hamid SH, Amin MB, Maadhah AG. Handbook of polymer degradation. New York: Marcel Dekker; 1992.

[38] Remiro PM, Cortazar MM, Calahorra ME. A study of the degradation of uncured DGEBA/PVP blends by thermogravimetry and their miscibility state. J Mater Sci 1999;34:2627–33.

[39] Erceg M, Kovacic T, Klaric I. Dynamic thermogravimetric degradation of poly(3-hydroxybutyrate)/aliphatic-aromatic copolyester blends. Polym Degrad Stab 2005;90:86–94.

[40] Mohanty S, Mukunda PG, Nando GB. Kinetics of thermal degradation and related changes in the structure of blends of poly(ethylene-*co*-acrylic acid) (PEA) and epoxidized natural rubber (ENR). Polym Degrad Stab 1996;52:235–44.

[41] Moguet F, Bordére S, Tressaud A, Rouquerol F, Llewellyn P. Deintercalation process of fluorinated carbon fibres – II. Kinetic study and reaction mechanisms. Carbon 1998;36:1199–205.

[42] Dinh LN, Cecala CM, Leckey JH, Balooch M. The effects of moisture on LiD single crystals studied by temperature-programmed decomposition. J Nucl Mater 2001;295:193–204.

VITA

Mr. Sunan Tiptipakorn was born in Bangkok, Thailand. After graduation from Triamudomsuksa Pattanakarn school, he attained the Bachelor's degree from Chulalongkorn University. He had an experience as a process engineer at HMC Polymer Co., Ltd., Rayong, before taking a Master's degree program and Ph.D. program, at Chulalongkorn University, respectively. During Oct 19, 2006 to Jan 18, 2007, he got the scholarship from the foundation for the international exchange of the faculty of engineering, Tokyo Institute of Technology to do a research in Japan. When he was a Ph.D. candidate, he had published five international papers, for two of which he was the main author. Additionally, he had some international proceeding papers, and took part in some international conferences. His works were mainly focused on the polymer blends and polymer alloys including thermal degradation kinetics of polymers.